Universität Bremen

RECONSTRUCTION OF EDIACARAN TO EARLY CAMBRIAN OCEAN pH AND WEATHERING CONDITIONS

Dissertation

zur Erlangung des Doktorgrades der Naturwissenschaften

- Doctor rerum naturalium -

(Dr. rer. nat.)

im Fachbereich Geowissenschaften

der Universität Bremen

vorgelegt von

Frank Ohnemüller

Bremen, Juni 2014

Erstgutachter: Prof. Dr. Simone Kasemann
Universität Bremen
FB 5 Geowissenschaften
Isotopengeochemie
Leobenerstr.
28359 Bremen
Deutschland

Zweitgutachter: Dr. Anthony Prave
University of St. Andrews
School of Geography & Geosciences
Department of Earth Sciences
St Andrews KY16 9AL
Schottland, Großbritannien

Tag der mündlichen Prüfung: 08.08.2014

"Not everything that can be counted counts.

Not everything that counts can be counted."

William Bruce Cameron

EHRENWÖRTLICHE ERKLÄRUNG

Ehrenwörtliche Erklärung zu meiner Dissertation mit dem Titel: „Reconstruction of Ediacaran to Early Cambrian ocean pH and weathering conditions"

Sehr geehrte Damen und Herren,

hiermit versichere ich, Frank Ohnemüller, dass ich die vorliegende Arbeit selbständig verfasst und keine anderen als die angegebenen Hilfsmittel benutzt habe. Die Stellen der Arbeit, die anderen Werken wörtlich und inhaltlich entnommen sind, wurden durch entsprechende Angaben der Quellen kenntlich gemacht.
Diese Arbeit hat in gleicher oder ähnlicher Form noch keiner Prüfungsbehörde vorgelegen.

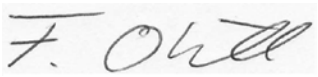

Bremen, den 26.06.2014

DECLARATION

Declaration of dissertation: „Reconstruction of Ediacaran to Early Cambrian ocean pH and weathering conditions"

I, Frank Ohnemüller declare that this dissertation is the product of my own work and that all the sources I have used or quoted have been indicated and acknowledged as complete references.
This dissertation has not been submitted before for any degree or examination in any other university.

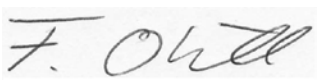

Bremen, 26th of June 2014

ACKNOWLEDGEMENTS

Without the help and support of many kind people around me, of whom I can only thank some here in particular, it would not have been possible to write this PhD thesis.

First and foremost, I would like to express my sincere gratitude to my advisor Simone Kasemann for her continuous support, motivation and enthusiasm. She introduced me patiently into the exciting field of Isotope Geochemistry and I appreciate all her help and contributions of time and ideas, as well as her encouraging and contagious can-do attitude that made my PhD experience as productive and stimulating as possible. I also would like to thank my co-advisor Tony Prave for his willingness to participate in my PhD project on short notice although he was initially not part of it. He was actively interested in my work and provided helpful assistance during the final phase.

Besides my advisors, I want to thank all members of our small but impressive working group. I am very grateful to Anette and Friedrich for helping me getting started in Isotope Geochemistry. Thanks for the enormous amount of time and effort you spent teaching me patiently, all your useful advices and continuous assistance not only professionally but also personally. Additionally, I like to acknowledge Barbara for many nice conversations and making my office life easier.

Special thanks goes to Antonia for being such a close friend since almost ten years. I appreciate all your help and support to finish this thesis, no matter if it was work-related or emotional in all circumstances and life situations. I would like to thank my office mates Basti, Timo, Michel, Lera and Ricarda for three great years and a lot of fun at work. I always enjoyed our chats, coffee- and lunch-breaks, after work and weekend activities and I highly appreciate your helpful ideas and assistance concerning my PhD project. It means a lot to me, that we are not only colleagues but also friends. My sincere thanks also go to my co-workers of the DFG FOR 736, especially the other PhD students, and all MARUM and FB 5 colleagues involved in my PhD project. I gratefully acknowledge funding by the Deutsche Forschungsgemeinschaft (KA3192/1-1), within the DFG FOR 736 *"The Precambrian-Cambrian Biosphere (R)evolution: Insights from Chinese Microcontinents"*.

For the non-scientific part, Karen is thanked for many nice evenings, BBQs and plenty of interesting conversations as well as being a very good friend since my settling-in phase in Bremen. I am grateful to my closest friend Wolf for his daily support, advice and listing on the phone. Thanks for caring, buddy! Now it's also time to thank two very special and close friends, Laura and Toni. I have been extremely lucky to get to know you and I want to thank you for the awesome time we had together! Moreover, I want to acknowledge all of my 'new' friends from Bremen for making my time here very enjoyable, especially Beppo is thanked for many nice football afternoons and evenings. I am grateful to my cousin Patrick and my best friends from Berlin: Limbo, Barthel, Daniel, Conny, Nina, Matze, Julian, Juri, Marina and Miao who visited me several times here in Bremen.

Last but by no means least, I would like to sincerely thank my family and in particular my parents, Ilona and Lutz, for their never-ending support, care and faith throughout my life.

SUMMARY

The Neoproterozoic era is one of the most decisive periods in Earth's history. Its strata sheds light on global-scale ice ages, step-wise oxygenation events, significant changes to (bio-)geochemical cycling and climate as well as extensive modifications to the atmosphere-ocean-continent interactions. All of these factors contribute in a pivotal way to one of the most essential transformations of organism body plans and even to the evolution of novel organisms culminating in the Precambrian-Cambrian (PCC) revolution.

This thesis was conducted in the context of the interdisciplinary, Sino-German DFG Research Unit 736 "*The Precambrian-Cambrian Biosphere (R)evolution: Insights from Chinese Microcontinents*". The objective was the reconstruction of ocean pH conditions and the quantification of weathering rates with the utilization of boron and strontium isotope analyzes on Ediacaran and Early Cambrian marine carbonate rocks. In order to compare local signals and specific features with global patterns, I examined a variety of sections on two different palaeo continents (South China, Kazakhstan).

The Earliest Ediacaran (635 Ma) represents the deglacial phase after a suspected Snowball Earth event. At this time, a global ocean acidification event occurred, which was apparently associated with highly enhanced atmospheric pCO_2 levels during the ice age. The magnitude and duration of this acidification event not only varies considerably between different palaeo continents, but also within distinct facies environments of a single craton. Moreover, the entire Ediacaran is characterized by minor to major ocean pH fluctuations and a general increase in weathering rates and fluxes to the ocean. Southern Chinese and Kazakh boron isotope data corresponding to the Ediacaran-Cambrian transition indicate a temporary ocean acidification for this crucial time period, too. In addition, strontium isotope data from South China and Kazakhstan hint towards increasing weathering rates during the terminal Ediacaran. Both effects had a significant influence on ocean geochemistry and may have decisively contributed to the creation of new ecological niches, possibly enabling the appearance of multicellular animals and reinforcing their radiation.

ZUSAMMENFASSUNG

Das Neoproterozoikum ist eines der richtungsweisenden Zeitalter der Erdgeschichte. Seine Schichtenfolge gibt Aufschluss über globale Eiszeiten, stufenweise erfolgende Oxygenierungsereignisse, maßgebliche Veränderungen innerhalb der biologisch-geochemischen Stoffkreisläufe und des Klimas sowie umfassende Modifikationen der Wechselwirkungen zwischen Atmosphäre, Ozean und Kontinent. Sämtliche Faktoren tragen ausschlaggebend zur essentiellen Neuentwicklung und Umgestaltung von Organismenbauplänen bei, die in der kambrischen Artenexplosion münden.

Diese Dissertation wurde im Rahmen der interdisziplinären, chinesisch-deutschen DFG Forschergruppe 736 *„The Precambrian-Cambrian Biosphere (R)evolution: Insights from Chinese Microcontinents"* angefertigt. Das Ziel war die Rekonstruktion von Meerwasser pH-Werten und die Quantifizierung von Verwitterungsbedingungen mit Hilfe von Bor- und Strontiumisotopenmessungen mariner Karbonate des Ediakariums und frühen Kambriums. Um lokale Signale und Besonderheiten mit globalen Mustern vergleichen zu können, untersuchte ich eine Vielzahl von Sektionen auf zwei verschiedenen Paläokontinenten (Südchina und Kasachstan).

Das frühe Ediakarium (635 Ma) spiegelt die Abtauphase nach einem vermuteten Schneeball-Erde Ereignis wieder. Zu diesem Zeitpunkt ereignete sich eine globale Ozeanversauerung, die vermutlich mit erhöhten atmosphärischen CO_2-Konzentrationen während der Eiszeit verbunden war. Die Ausprägung und Dauer dieses Versauerungs-Events variiert nicht nur beträchtlich zwischen den Paläokontinenten, sondern auch innerhalb verschiedener Faziszonen eines einzelnen Kratons. Das gesamte Ediakarium ist durch weitere pH-Wert Fluktuationen und einen generellen Anstieg des Verwitterungseintrags in den Ozean geprägt. In der entscheidenden Übergangsphase vom Ediakarium zum Kambrium deuten die Borisotopendaten aus Südchina und Kasachstan darauf hin, dass auch in dieser Zeitspanne die Ozeane temporär versauerten. Zudem zeigen Strontiumisotopendaten aus Südchina und Kasachstan ansteigende Verwitterungsraten am Ende des Ediakariums. Diese beiden Effekte hatten maßgeblichen Einfluss auf die Meerwasserchemie und könnten somit ausschlaggebend zur Entstehung neuer ökologischer Nischen und dem möglicherweise daraus resultierendem verstärkten Auftreten vielzelliger Tiere und ihrer Radiation beigetragen haben.

FOREWORD

This cumulative PhD thesis is structured in form of a compilation of three manuscripts dealing with the key topic of ocean pH and weathering reconstruction within the Ediacaran and the Early Cambrian. The individual manuscripts have been either submitted for review or are in final preparation for submission. The present dissertation is composed of five chapters in total:

- **Chapter 1:** The first chapter of the PhD thesis provides an introduction into the Precambrian-Cambrian biosphere (R)evolution including an overview about the time period, the stratigraphic framework and geological setting of the study area and explains the research goals.
- **Chapter 2:** The second chapter includes the first manuscript "*Ocean acidification in the aftermath of the Marinoan*" that is currently under review at *Geology*. It elucidates the global ocean pH conditions immediately after the suspected terminal Cryogenian Snowball Earth event at ~635 Ma. Literature boron isotope data from Namibia are compared to newly investigated cap dolomite sections of the Malyi Karatau Range (Southern Kazakhstan) and the Yangtze Platform (South China).
- **Chapter 3:** This chapter introduces the second manuscript "*Ocean pH and weathering conditions during the upper Ediacaran: Insights from the Chinese Gaojiashan Section*" that is in final preparation for submission to *Earth and Planetary Science Letters*. It has a strong focus on the ocean geochemical evolution of the terminal Ediacaran and Precambrian-Cambrian transition at the Chinese Yangtze Platform and includes new boron, strontium and lithium isotope data.
- **Chapter 4:** The fourth chapter includes the third manuscript "*Ediacaran to Cambrian ocean pH and continental weathering conditions: Implications from Southern Kazakhstan*" that is in final preparation for submission to *Precambrian Research*. The manuscript sheds light on the geochemical ocean evolution of the Karatau microcontinent during the entire Ediacaran and Early Cambrian. Ocean

pH fluctuations and variations in weathering conditions are revealed by the first available strontium and boron isotope dataset of the Kazakh microcontinent.

- **Chapter 5:** The final chapter summarizes the overall results and new discoveries concerning ocean pH states and changing weathering conditions of the Ediacaran-Cambrian time. It is evaluated if these changes and fluctuations can serve as trigger mechanisms for the advent and radiation of metazoa. Additionally, perspectives for future studies are introduced.
- **Appendices:** Within the appendices a summary of all measured reference and standard materials is given. It mentions co-authorships and conference contributions resulting from the PhD project.

TABLE OF CONTENS

List of Figures:

List of Tables:

CHAPTER 1:

INTRODUCTION INTO THE PRECAMBRIAN-CAMBRIAN BIOSPHERE (R)EVOLUTION

1.1 The Ediacaran to Cambrian Period

The Ediacaran represents the youngest period of the Neoproterozoic Era and therefore ends the Proterozoic Eon. The beginning of this decisive time in Earth's history is defined by a Global Stratotype Section and Point (GSSP) which is placed directly at the base of Nuccaleena Formation cap carbonates (Flinders Ranges, South Australia, Knoll et al., 2006). These globally observable cap carbonates (Halverson et al., 2005; Hoffman et al., 1998; Hoffman and Schrag, 2002; Jiang et al., 2006) are deposited in the direct aftermath of the late Cryogenian (Marinoan) glaciation, which is dated ~635 Ma (Condon et al., 2005; Hoffmann et al., 2004). The upper boundary is defined by the first appearance date (FAD) of *Trichophycus/Treptichnus pedum* (Narbonne and Hoffman, 1987; Seilacher, 1955) the earliest complex and wide-spread trace fossil and the extinction of *Cloudina* and *Namacalathus* (Amthor et al., 2003) at the Precambrian-Cambrian (PCC) boundary, ~541 Ma.

The Ediacaran period is characterized by tremendous perturbations to the carbon cycle, hosts a step-wise oxygenation of the ocean and a steep rise in seawater $^{87}Sr/^{86}Sr$ being indicative for globally increasing weathering rates (Bjerrum and Canfield, 2011; Fike et al., 2006; Halverson et al., 2007; Jacobsen and Kaufman, 1999; Shields, 2007). Besides, major changes in ocean redox chemistry occurred within the Ediacaran. A transition from predominantly sulfidic (H_2S) to ferruginous (Fe^{2+}) and in the latest Ediacaran even oxic (O_2) conditions is discussed as well as a variety of models trying to explain changes to the stratification and mixing of the Ediacaran seawater (Canfield et al., 2007; Johnston et al., 2012; Li et al., 2010; Planavsky et al., 2010; Wang et al., 2012). Within the middle Ediacaran time (~560-551 Ma) one of the most pronounced negative $\delta^{13}C$ excursions (down to -12‰) ever encountered in Earth's history is present. Yet, the origin of the so called Shuram-Wonoka $\delta^{13}C$ negative excursion (Le Guerroué, 2010; Le Guerroué et al., 2006) is still under debate (Macdonald et al., 2013). Explanations include: A diagenetic origin (Derry, 2010), large Neoproterozoic DOC (dissolved organic carbon) pools that are periodically remineralized (Fike et al., 2006), authigenic carbonate formation (Schrag et al., 2013), methane release (Bjerrum and Canfield, 2011) or as recently suggested a non-snowball glaciation (Wang et al., 2014).

The terminal Cryogenian and the Ediacaran also record severe ice ages of which at least the late-Cryogenian Marinoan glaciation was of global extend and represents

a Snowball Earth event (Hoffman et al., 1998; Kirschvink, 1992). Together with the Gaskiers glaciation (~582 Ma, Bowring et al., 2003; Hoffman and Li, 2009) and the above mentioned changes in ocean geochemistry, significant modifications in Earth's ocean-atmosphere-continent interaction occurred and served as potential triggers for the Cambrian explosion. The term "Cambrian explosion" or "Cambrian (R)evolution", respectively, is understood as the transition from complex macroscopic, mostly sessile organisms represented by the Ediacaran fauna to the appearance of the very first multi-cellular, biomineralizing and complex animals (metazoa) and their radiation during the Early Cambrian.

1.2 Research goals

The overall objective of the DFG FOR 736 is the recognition of essential environmental changes and evolutionary innovations that have contributed to the appearance and radiation of metazoa - The Precambrian-Cambrian (R)evolution.

This PhD thesis focuses on the reconstruction of ocean pH states and the quantification of weathering fluxes to the ocean within the Ediacaran and Early Cambrian. These analyses allow us to draw conclusions on the nutrient availability and alkalinity supply into the ocean. In combination with seawater pH estimations, it will be possible to get more profound insights into habitable marine environments and ecological niches on a small scale and on continent-ocean-atmosphere interactions on a global scale. Furthermore, a major intention of this PhD thesis is the evaluation of similarities and differences between global inter-craton correlations and intra-continental, local and facies specific varieties in ocean pH and weathering patterns.

In order to elucidate these significant issues we conducted nontraditional stable boron ($\delta^{11}B$) and radiometric strontium ($^{87}Sr/^{86}Sr$) isotope TIMS (Thermal ionization mass spectrometry) measurements of Kazakh and Chinese marine carbonate rocks and compared their results to literature data of Namibia. The entire dataset comprises rock records and isotope analyses of various facies environments (shallow-water platform to slope-break settings) on different palaeo continents to shed light on unique and common features of local, regional and global extent.

To achieve both, obtaining profound and comprehensive insights into the significantly changing palaeo environment of the Ediacaran and Early Cambrian, the

boron and strontium datasets were combined with additional data records. For the Chinese Gaojiashan dataset (manuscript 2, chapter 3) we extended the dataset by δ^7Li isotope measurements to improve our understanding of the prevailing weathering regime and short-term variations in silicate weathering intensities. Further geochemical proxy-data, palaeo-biological fossil information and sedimentary records were provided by co-workers of the DFG FOR 736. In detail, δ^{15}N, δ^{13}C, δ^{18}O and TOC (total organic carbon) data were provided by subproject 2 (A. Gamper and U. Struck), REE (rare earth element) data by subproject 4 (S. Hohl and H. Becker), sedimentary data by subproject 1 (C. Heubeck) and fossil data by subproject 3 (C. Seidig and M. Steiner). This crosscutting collaboration is essential to understand global patterns and triggering mechanisms for the Cambrian (R)evolution.

1.3 Study areas

Two field campaigns were successfully carried out during the first year of the PhD project. In September 2011 we visited 10 individual sections at the Malyi and Bolshoi Karatau Range, Zhambyl, Kazakhstan and chose 5 of them (all within the Malyi Karatau) for detailed geochemical sampling. A second field trip to South China, Hubei and Hunan Province, was conducted from March to April 2012. Likewise to Kazakhstan, we worked on more than 10 different sections in both provinces and sampled 8 of them in high resolution ($\leq$ 1 m) for later geochemical analyses. In addition to these datasets, samples of the Gaojiashan Section (Shaanxi Province, China) that already existed from a previous field campaign were processed.

During the Ediacaran and Early Cambrian the southern Chinese Yangtze Platform and the Karatau microcontinent were situated at low latitudes (Fig. 1). The precise palaeogeographic position of the Karatau microcontinent is still under debate. For the Early Cambrian a location between the ancient Siberian craton, South China and the Tarim block is suggested based on similar existing ichnofacies, fossil assemblages and depositional regimes (Pradhan et al., 2009; Weber et al., 2013). The position of the Yangtze Platform is far more accurately determined by palaeomagnetic data. One of the latest palaeogeographic reconstructions (Li et al., 2013) is shown in figure 1.

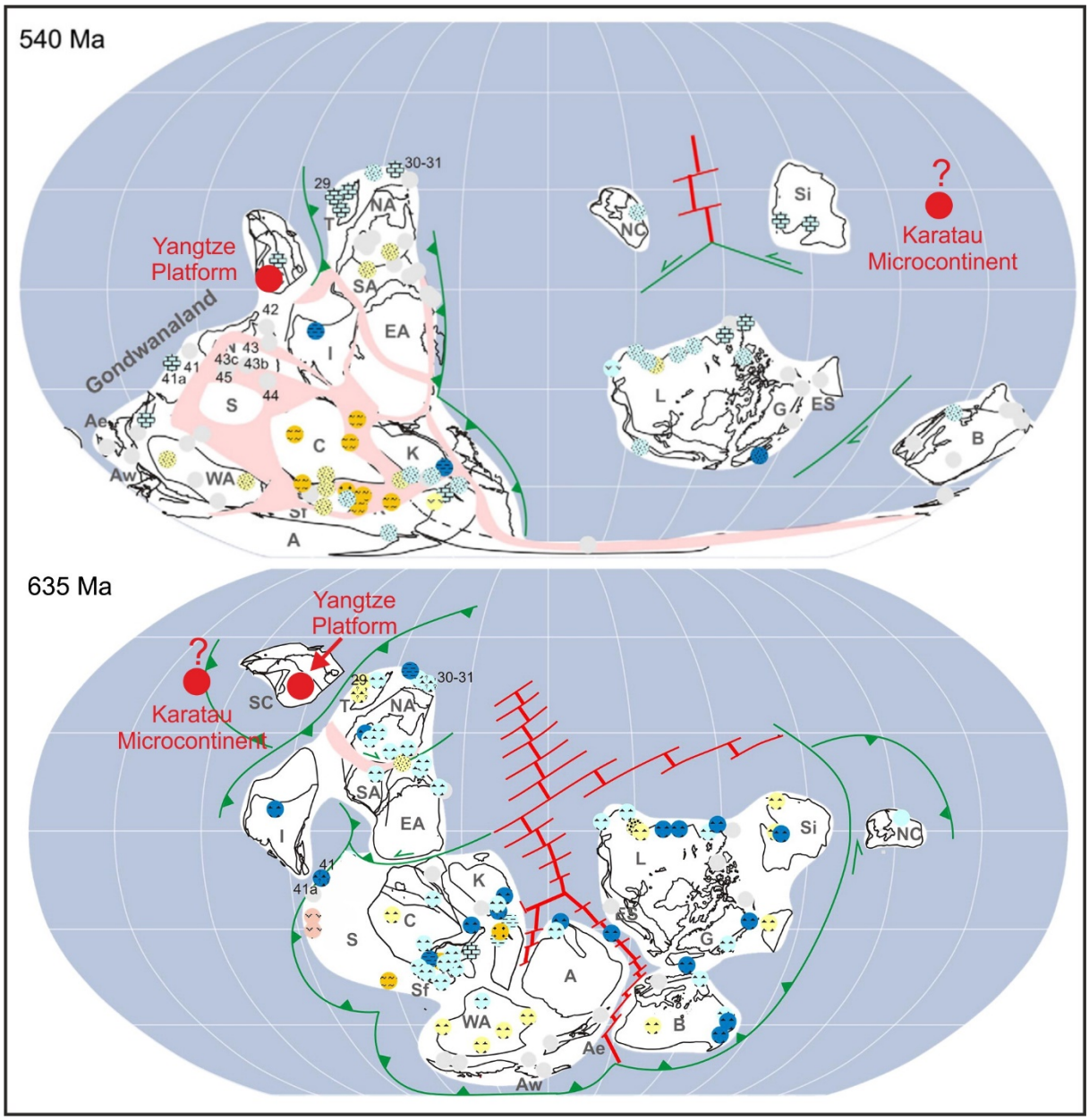

Figure 1: *Palaeogeographic reconstruction (slightly modified) for 635 Ma and 540 Ma by Li et al. (2013). The investigated palaeo continents are indicated by red solid circles. The Karatau microcontinent is suggested to be half-way between Siberia and South China at least for the Early Cambrian (Weber et al., 2013).*

1.3.1 Kazakhstan (Karatau microcontinent)

In southern Kazakhstan closely to the borders of Kyrgyzstan and Uzbekistan, the Karatau mountain chain stretches from NW to SE over ~350 km. The Karatau is part of the Central Asian Orogenic Belt (CAOB) and represents one of several individual microcontinents during the Precambrian, that amalgamated within the Paleozoic (Sengor et al., 1993). More precisely, the Karatau Mountains are forming the foothills of the central Asian Tian Shan orogen and are divided by the main Karatau fault into the Bolshoi (NW) and Malyi (SE) Karatau Range (e.g. Alexeiev et al., 2009 and

references therein, Fig. 2). To the NE the Karatau is surrounded by the Chu Sarysu Basin and to the SW by the Syr Dar'ya Basin (Allen et al., 2001). Our main study area (Fig. 2) is located in the Almaty Province, Zhambyl District, in direct vicinity to the city of Zhanatas. In comparison to the Bolshoi Karatau that underwent major tectonic events until the Triassic (Alexeiev et al., 2009; Allen et al., 2001), the primarily investigated Malyi Karatau is characterized by a far lesser thermal and tectonic history without obvious indices of metamorphic overprint (Weber et al., 2013).

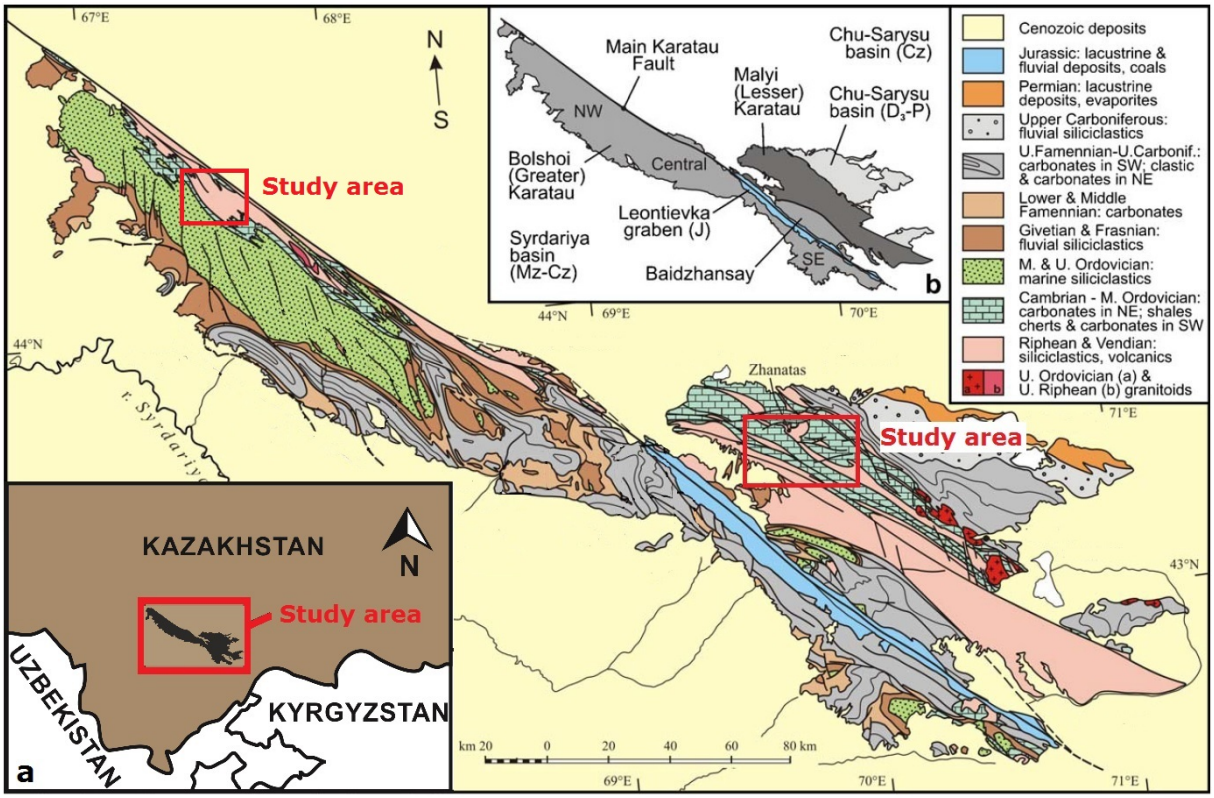

Figure 2: *Geological map of the Bolshoi and Malyi Karatau Range modified after Alexeiev et al. (2009) and Chakabaev (1979) showing the study areas (red rectangle). (a) Inset map displays the geographical position of the study area in southern Kazakhstan. (b) Inset map shows the tectonic setting of the Bolshoi and Malyi Karatau.*

In the whole study area abundant Precambrian-Ordovician strata is directly and very well exposed to the surface. The rocks comprise more than 1000 m of volcanics, siliciclastics and carbonates that dip in moderate to high angles. Concerning the Kazakh dataset the PhD thesis focusses on the Kyrshabakty Section (43°32'2.1''N, 69°57'7.7''E), which is located approximately 18 km E of Zhanatas and provides access to a >500 m thick succession of Precambrian to Ordovician rocks. A detailed stratigraphy as well as additional information with regard to sedimentological features and the fossil records can be found in e.g. Meert et al. (2011) or Heubeck et al. (2013) and in chapter 4 of this thesis. Correlated and also investigated sections in direct

proximity are the Ushbass, Aktugai, Koksu, Kyurdubulake and Berkuty Section. All of them provide access to corresponding Precambrian to Cambrian strata, however only the Kyrshabakty Section obtains a nearly continuous rock record from the earliest Ediacaran to the Early Cambrian, with direct exposure of the Marinoan-age cap dolomites, abundant middle Ediacaran carbonate rocks and the complete PCC interval within one section.

1.3.2 China (Yangtze Platform)

At the Chinese Yangtze Platform (Fig. 3) several Precambrian to Cambrian successions associated with various facies environments are situated. Therefore, the Yangtze Platform is one of the most suitable areas in the world to study the late Neoproterozoic and early Paleozoic. Today, northwards of the Yangtze Platform the North China Block is located. Both palaeo continents collided during the Mesozoic (Hsü and Chen, 1999), whereas the Cathaysia Block to the South was already linked to the platform since the Silurian (Vernhet and Reijmer, 2010).

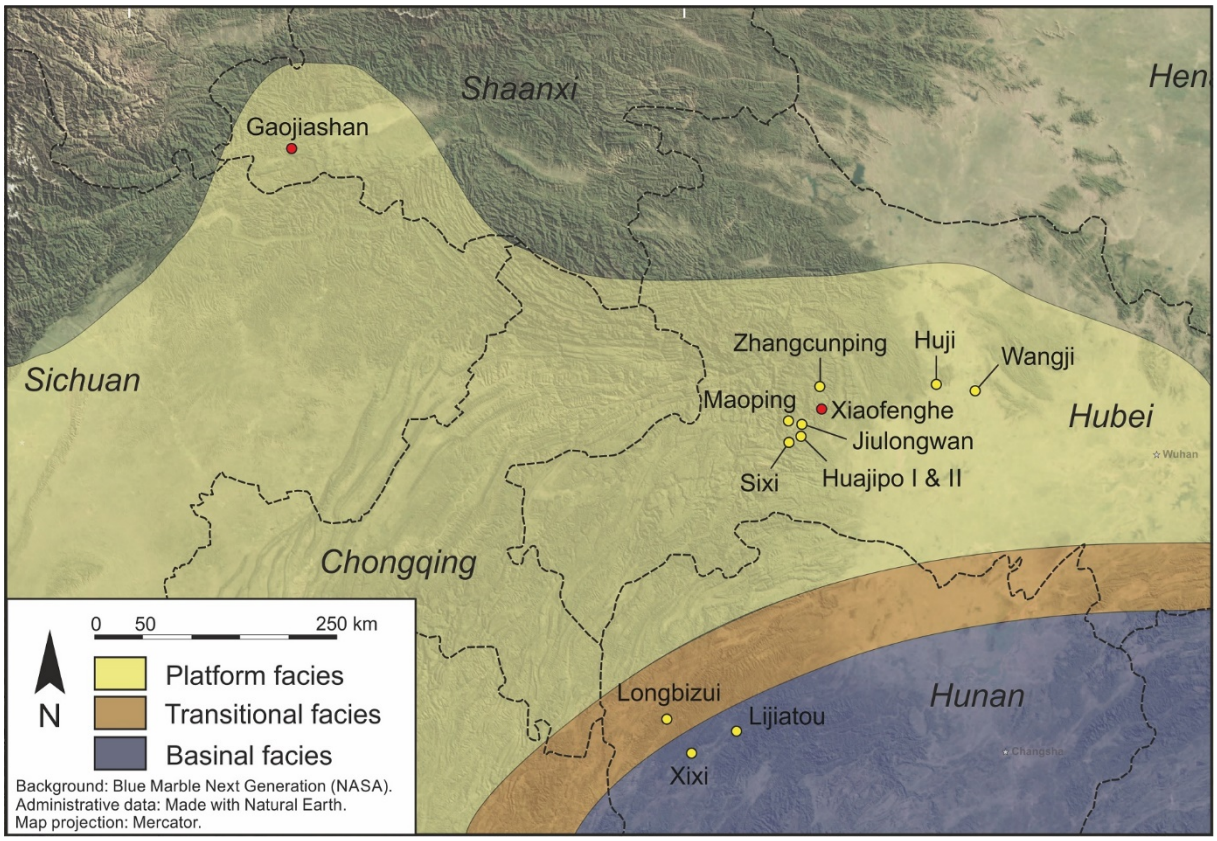

Figure 3: *Geological sketch of the central, northern Yangtze Platform displaying all visited (yellow circles) and studied sections (red circles) of this PhD thesis (modified after Kraus and Scouflaire (2010)). The Yangtze Platform is separated in three parts: Yellowish colors indicate the platform facies, brownish colors indicate the transitional facies and bluish colors show a deeper marine environment.*

One of the first Ediacaran to Cambrian platform-wide correlations and facies reconstructions was done by Zhu et al. (2003) and expanded by Zhu et al. (2007). In general, the Yangtze Platform is divided into three parts: (1) a shallow water platform environment to the NW, (2) a deeper marine, basinal part to the SE and (3) a transitional slope environment in-between (Fig. 3). Formation and Member names vary in different regions of the platform and are also depending on local facies. The Gaojiashan (32°57′29.4′′N, 106°27′33.8′′E) and Xiaofenghe (30°56′31.9′′N, 111°13′57.1′′E) Sections, which were studied in greater detail for further geochemical analyses (Fig 3., marked in red), are both situated within a shallow-marine environment. Yangtze Platform sections are generally comprised of Marinoan-age Nantuo glacial deposits (~635 Ma, Condon et al., 2005), the Ediacaran Doushantuo and Dengying Formations and the Early Cambrian Yanjiahe Formation (Three Gorges region) or Kuanchuanpu Formation (Shaanxi Province), respectively (Ishikawa et al., 2008; Steiner et al., 2004; Zhu et al., 2007). Additionally visited platform facies sections were: Maoping, Zhangcunping, Sixi, Huajipo, Jiulongwan, Wangji and Huji (all Hubei Province, Fig 3). In Hunan we investigated the Longbizui, Xixi and Lijiatuo Section that are all situated in transitional to deeper marine environments (Fig. 3).

1.4 References

Alexeiev, D. V., Cook, H. E., Buvtyshkin, V. M., and Golub, L. Y., 2009, Structural evolution of the Ural-Tian Shan junction: A view from Karatau ridge, South Kazakhstan: Comptes Rendus Geosciences, v. 341, no. 2-3, p. 287-297.

Allen, M. B., Alsop, G. I., and Zhemchuzhnikov, V. G., 2001, Dome and basin refolding and transpressive inversion along the Karatau Fault System, southern Kazakstan: Journal of the Geological Society, v. 158, no. 1, p. 83-95.

Amthor, J. E., Grotzinger, J. P., Schröder, S., Bowring, S. A., Ramezani, J., Martin, M. W., and Matter, A., 2003, Extinction of Cloudina and Namacalathus at the Precambrian-Cambrian boundary in Oman: Geology, v. 31, no. 5, p. 431-434.

Bjerrum, C. J., and Canfield, D. E., 2011, Towards a quantitative understanding of the late Neoproterozoic carbon cycle: Proceedings of the National Academy of Sciences of the United States of America, v. 108, no. 14, p. 5542-5547.

Bowring, S. A., Myrow, P., Landing, E., Ramezani, J., and Grotzinger, J. P., 2003, Geochronological constraints on terminal Neoproterozoic events and the rise of Metazoan: Geophysical Research Abstracts, v. 5, p. 13219.

Canfield, D. E., Poulton, S. W., and Narbonne, G. M., 2007, Late-Neoproterozoic Deep-Ocean Oxygenation and the Rise of Animal Life: Science, v. 315, no. 5808, p. 92-95.

Chakabaev, S. E., 1979, Geological Map of Kazakh SSR, Scale 1:500,000, South Kazakhstan series: Aerogeologiya Map Enterprise, Leningrad, USSR.

Condon, D., Zhu, M., Bowring, S., Wang, W., Yang, A., and Jin, Y., 2005, U-Pb Ages from the Neoproterozoic Doushantuo Formation, China: Science, v. 308, no. 5718, p. 95-98.

Derry, L. A., 2010, A burial diagenesis origin for the Ediacaran Shuram–Wonoka carbon isotope anomaly: Earth and Planetary Science Letters, v. 294, no. 1-2, p. 152-162.

Fike, D. A., Grotzinger, J. P., Pratt, L. M., and Summons, R. E., 2006, Oxidation of the Ediacaran Ocean: Nature, v. 444, no. 7120, p. 744-747.

Halverson, G. P., Dudas, F. O., Maloof, A. C., and Bowring, S. A., 2007, Evolution of the Sr-87/Sr-86 composition of Neoproterozoic seawater: Palaeogeography Palaeoclimatology Palaeoecology, v. 256, no. 3-4, p. 103-129.

Halverson, G. P., Hoffman, P. F., Schrag, D. P., Maloof, A. C., and Rice, A. H. N., 2005, Toward a Neoproterozoic composite carbon-isotope record: Geological Society of America Bulletin, v. 117, no. 9-10, p. 1181-1207.

Heubeck, C., Ergaliev, G., and Evseev, S., 2013, Large-Scale Seismogenic Deformation of A Carbonate Platform Straddling the Precambrian–Cambrian Boundary, Karatau Range, Kazakhstan: Journal of Sedimentary Research, v. 83, no. 11, p. 1004-1024.

Hoffman, P. F., Kaufman, A. J., Halverson, G. P., and Schrag, D. P., 1998, A Neoproterozoic Snowball Earth: Science, v. 281, no. 5381, p. 1342-1346.

Hoffman, P. F., and Li, Z.-X., 2009, A palaeogeographic context for Neoproterozoic glaciation: Palaeogeography, Palaeoclimatology, Palaeoecology, v. 277, no. 3–4, p. 158-172.

Hoffman, P. F., and Schrag, D. P., 2002, The snowball Earth hypothesis: testing the limits of global change: Terra Nova, v. 14, no. 3, p. 129-155.

Hoffmann, K.-H., Condon, D. J., Bowring, S. A., and Crowley, J. L., 2004, U-Pb zircon date from the Neoproterozoic Ghaub Formation, Namibia: Constraints on Marinoan glaciation: Geology, v. 32, no. 9, p. 817-820.

Hsü, K. J., and Chen, H., 1999, Geologic Atlas of China: An Application of the Tectonic Facies Concept to the Geology of China, v. XVI, p. 262.

Ishikawa, T., Ueno, Y., Komiya, T., Sawaki, Y., Han, J., Shu, D., Li, Y., Maruyama, S., and Yoshida, N., 2008, Carbon isotope chemostratigraphy of a Precambrian/Cambrian boundary section in the Three Gorge area, South China: Prominent global-scale isotope excursions just before the Cambrian Explosion: Gondwana Research, v. 14, no. 1-2, p. 193-208.

Jacobsen, S. B., and Kaufman, A. J., 1999, The Sr, C and O isotopic evolution of Neoproterozoic seawater: Chemical Geology, v. 161, no. 1–3, p. 37-57.

Jiang, G., Kennedy, M. J., Christie-Blick, N., Wu, H., and Zhang, S., 2006, Stratigraphy, Sedimentary Structures, and Textures of the Late Neoproterozoic Doushantuo Cap Carbonate in South China: Journal of Sedimentary Research, v. 76, no. 7, p. 978-995.

Johnston, D. T., Poulton, S. W., Goldberg, T., Sergeev, V. N., Podkovyrov, V., Vorob'eva, N. G., Bekker, A., and Knoll, A. H., 2012, Late Ediacaran redox stability and metazoan evolution: Earth and Planetary Science Letters, v. 335–336, no. 0, p. 25-35.

Kirschvink, J. L., 1992, Late Proterozoic Low-Latitude Global Glaciation: The Snowball Earth: Section 2.3 in: J.W. Schopf, C. Klein, & D. Des Maris (eds), The Proterozoic Biosphere: A Multidisciplinary Study, p. 51-52.

Knoll, A. H., Walter, M. R., Narbonne, G. M., and Christie-Blick, N., 2006, The Ediacaran Period: a new addition to the geologic time scale: Lethaia, v. 39, no. 1, p. 13-30.

Kraus, S., and Scouflaire, Q., 2010, Ediacaran / Cambrian sections visited by the Sino-German project, Background: Blue Marble Next Generation (NASA), Natural Earth: Berlin, Freie Universität Berlin.

Le Guerroué, E., 2010, Duration and synchroneity of the largest negative carbon isotope excursion on Earth: The Shuram/Wonoka anomaly: Comptes Rendus Geoscience, v. 342, no. 3, p. 204-214.

Le Guerroué, E., Allen, P. A., and Cozzi, A., 2006, Chemostratigraphic and sedimentological framework of the largest negative carbon isotopic excursion in Earth history: The Neoproterozoic Shuram Formation (Nafun Group, Oman): Precambrian Research, v. 146, no. 1–2, p. 68-92.

Li, C., Love, G. D., Lyons, T. W., Fike, D. A., Sessions, A. L., and Chu, X., 2010, A Stratified Redox Model for the Ediacaran Ocean: Science, v. 328, no. 5974, p. 80-83.

Li, Z.-X., Evans, D. A. D., and Halverson, G. P., 2013, Neoproterozoic glaciations in a revised global palaeogeography from the breakup of Rodinia to the assembly of Gondwanaland: Sedimentary Geology, v. 294, no. 0, p. 219-232.

Macdonald, F. A., Strauss, J. V., Sperling, E. A., Halverson, G. P., Narbonne, G. M., Johnston, D. T., Kunzmann, M., Schrag, D. P., and Higgins, J. A., 2013, The stratigraphic relationship between the Shuram carbon isotope excursion, the oxygenation of Neoproterozoic oceans, and the first appearance of the Ediacara biota and bilaterian trace fossils in northwestern Canada: Chemical Geology, v. 362, no. 0, p. 250-272.

Meert, J. G., Gibsher, A. S., Levashova, N. M., Grice, W. C., Kamenov, G. D., and Ryabinin, A. B., 2011, Glaciation and ~ 770 Ma Ediacara (?) Fossils from the Lesser Karatau Microcontinent, Kazakhstan: Gondwana Research, v. 19, no. 4, p. 867-880.

Narbonne, G. M., and Hoffman, H. J., 1987, Ediacaran biota of the Wernecke Mountains, Yukon, Canada: Palaeontology, v. 30, p. 647–676.

Planavsky, N. J., Rouxel, O. J., Bekker, A., Lalonde, S. V., Konhauser, K. O., Reinhard, C. T., and Lyons, T. W., 2010, The evolution of the marine phosphate reservoir: Nature, v. 467, no. 7319, p. 1088-1090.

Pradhan, V. R., Meert, J., Levashova, N. M., and Gibsher, A. S., 2009, Preliminary paleomagnetic data on late Cambrian to Ordovician carbonate beds of Tamdy Series from the Lesser Karatau microcontinent, South Kazakhstan: Geological Society of America Abstracts with Programs, v. 41, p. 269.

Schrag, D. P., Higgins, J. A., Macdonald, F. A., and Johnston, D. T., 2013, Authigenic Carbonate and the History of the Global Carbon Cycle: Science, v. 339, no. 6119, p. 540-543.

Seilacher, A., 1955, Spuren und Fazies im Unterkambrium; In: Schindewolf, O.H. & Seilacher, A. (eds): Beitrage zur Kenntniss des Kambrium in der Salt Range (Pakistan), v. K1.10, p. 11-143.

Sengor, A. M. C., Natal'in, B. A., and Burtman, V. S., 1993, Evolution of the Altaid tectonic collage and Palaeozoic crustal growth in Eurasia: Nature, v. 364, no. 6435, p. 299-307.

Shields, G., 2007, A normalised seawater strontium isotope curve: possible implications for Neoproterozoic-Cambrian weathering rates and the further oxygenation of the Earth: eEarth Discussion, v. 2, p. 35-42.

Steiner, M., Li, G., Qian, Y., and Zhu, M., 2004, Lower Cambrian Small Shelly Fossils of northern Sichuan and southern Shaanxi (China), and their biostratigraphic importance: Geobios, v. 37, no. 2, p. 259-275.

Vernhet, E., and Reijmer, J. J. G., 2010, Sedimentary evolution of the Ediacaran Yangtze platform shelf (Hubei and Hunan provinces, Central China): Sedimentary Geology, v. 225, no. 3-4, p. 99-115.

Wang, J., Chen, D., Yan, D., Wei, H., and Xiang, L., 2012, Evolution from an anoxic to oxic deep ocean during the Ediacaran–Cambrian transition and implications for bioradiation: Chemical Geology, v. 306–307, no. 0, p. 129-138.

Wang, W., Zhou, C., Guan, C., Yuan, X., Chen, Z., and Wan, B., 2014, An integrated carbon, oxygen, and strontium isotopic studies of the Lantian Formation in South China with implications for the Shuram anomaly: Chemical Geology, v. 373, no. 0, p. 10-26.

Weber, B., Steiner, M., Evseev, S., and Yergaliev, G., 2013, First report of a Meishucun-type early Cambrian (Stage 2) ichnofauna from the Malyi Karatau area (SE Kazakhstan): Palaeoichnological, palaeoecological and palaeogeographical implications: Palaeogeography, Palaeoclimatology, Palaeoecology, v. 392, no. 0, p. 209-231.

Zhu, M., Zhang, J., and Yang, A., 2007, Integrated Ediacaran (Sinian) chronostratigraphy of South China: Palaeogeography, Palaeoclimatology, Palaeoecology, v. 254, no. 1-2, p. 7-61.

Zhu, M. Y., Zhang, J., Steiner, M., Yang, A., Li, G., and Erdtmann, B.-D., 2003, Sinian-Cambrian stratigraphic framework for shallow-to-deep-water environments of the Yangtze Platform: an integrated approach: Progress in Natural Science, v. 13, no. 12, p. 951-960.

CHAPTER 2:

OCEAN ACIDIFICATION IN THE AFTERMATH OF THE MARINOAN GLACIATION

Manuscript was submitted to *Geology* (number: G35937) on the 30th of May 2014 and is currently under review.

Simone Kasemann helped during data interpretation and with comments on the late-stage manuscript versions. Anthony Prave and Anthony Fallick provided helpful comments and feedback on the late-stage manuscript version.

Ocean acidification in the aftermath of the Marinoan glaciation

Frank Ohnemueller[1], Anthony R. Prave[2], Anthony E. Fallick[3], Simone A. Kasemann[1]

[1]*Department of Geosciences and MARUM - Center for Marine Environmental Sciences, University of Bremen, Leobener Str., D-28359 Bremen*
[2]*Department of Earth and Environmental Sciences, University of St Andrews, St Andrews KY16 9AL, UK*
[3]*Scottish Universities Environmental Research Centre, East Kilbride G75 OQF, UK*

2.1 Abstract

Boron isotope patterns preserved in cap carbonates deposited in the aftermath of the younger Cryogenian (Marinoan, ~635 Ma) glaciation confirm a temporary ocean acidification event on the continental margin of the southern Congo craton, Namibia. To test the significance of this acidification event and reconstruct Earth's global seawater pH states at the Cryogenian-Ediacaran transition we present a new boron isotope dataset recorded in cap carbonates deposited on the Yangtze Platform in South China and the Karatau microcontinent in Kazakhstan. Our compiled $\delta^{11}B$ data reveal similar ocean pH pattern for all investigated cratons and confirm the presence of a global ocean acidification event during the Marinoan deglacial period, compatible with elevated postglacial pCO_2 concentrations. Inter- and intracontinental differences in timing and magnitude of the ocean acidification point to regional distinctions in the buffering capacity of the Ediacaran seawater.

2.2 Introduction

During the Neoproterozoic era three major glacial sequences, namely the Sturtian (~716 Ma, Macdonald et al., 2010) the Marinoan (~635 Ma, Condon et al., 2005) and the Gaskiers (~582 Ma, Hoffman and Li, 2009) resulted from modifications of global climate and biogeochemical cycles in response to changes to the ocean-continent-atmosphere interplay (e.g. Higgins and Schrag, 2003; Hoffman et al., 1998; Kirschvink, 1992). Predominant attention was focused on the Marinoan glaciation in efforts to establish global correlations between corresponding strata via comparable

carbonate sequences, sedimentary structures and $\delta^{13}C$ patterns. (Hoffman and Schrag, 2002).

The aftermath of the Marinoan glaciation was associated with a marine transgression and the deposition of carbonate rocks, so-called *cap carbonates* or *cap dolomites*, which immediately overlie glacial deposits (Halverson et al., 2005; Hoffman et al., 1998; Hoffman and Schrag, 2002). These precipitates are interpreted as proxy archive of climatic and environmental changes characterizing the icehouse-greenhouse transition (Hoffman et al., 1998). However, there is still an ongoing discussion about the atmospheric-oceanic conditions under which they were deposited, including ocean pH states (Kasemann et al., 2005; Kasemann et al., 2010) and continental weathering conditions (Higgins and Schrag, 2003; Hoffman et al., 1998; Kasemann et al., 2005; Kasemann et al., 2014; Planavsky et al., 2010; Silva-Tamayo et al., 2010). The significance and global nature of a temporary increase in the continental weathering flux following the demise of the Marinoan glaciation was recently recognized by calcium and magnesium isotope patterns preserved in cap carbonate rocks from Brazil, Canada and Namibia (Kasemann et al., 2014; Silva-Tamayo et al., 2010). To assess whether the proposed post-Marinoan ocean acidification event observed for the Congo craton in Namibia (Kasemann et al., 2010) is also of global extent or merely a regional manifestation, we present ocean pH reconstructions based on new boron ($\delta^{11}B$) isotope data from Marinoan-equivalent cap dolomite records of the Yangtze Platform in South China and the Kazakh Karatau microcontinent. Our new boron (and by deduction ocean pH) data in combination with information on the weathering conditions allow us to draw conclusions on atmospheric pCO_2, ocean-atmosphere CO_2 exchange and ocean alkalinities, and hence provide more profound insights into habitable marine environments and ocean geochemical cycling during the Ediacaran.

2.3 Geological setting

Latest palaeogeographic reconstructions (e.g. Li et al., 2013) suggest that during the Cryogenian-Ediacaran transition all investigated carbonate sections (Fig. 4) were situated at low latitudes. The southern Kazak Kyrshabakty Section (Fig. 4A, Karatau microcontinent) contains shallow-water platform carbonates of the Kyrshabakty Formation from the Tamdy Series (e.g. Eganov et al., 1984). The inner shelf Northern

Xiaofenghe Section (Three Gorges Area, Hubei Province, Fig. 4B) of the early Ediacaran Yangtze Platform contains shallow water carbonates from the Doushantuo II Formation (Ma et al., 1984; Xiao et al., 2012). The stratigraphic framework and sedimentology of the Namibian Keilberg and Maieberg Formations of the Otavi Group in the slope-break Fransfontein Section and shallow-water platform Ombaatjie and Khowarib Sections (Fig. 4C) are described in Kasemann et al. (2014). Details on all geological settings and their associated stratigraphy can be found within the supplement (see chapter 2.9).

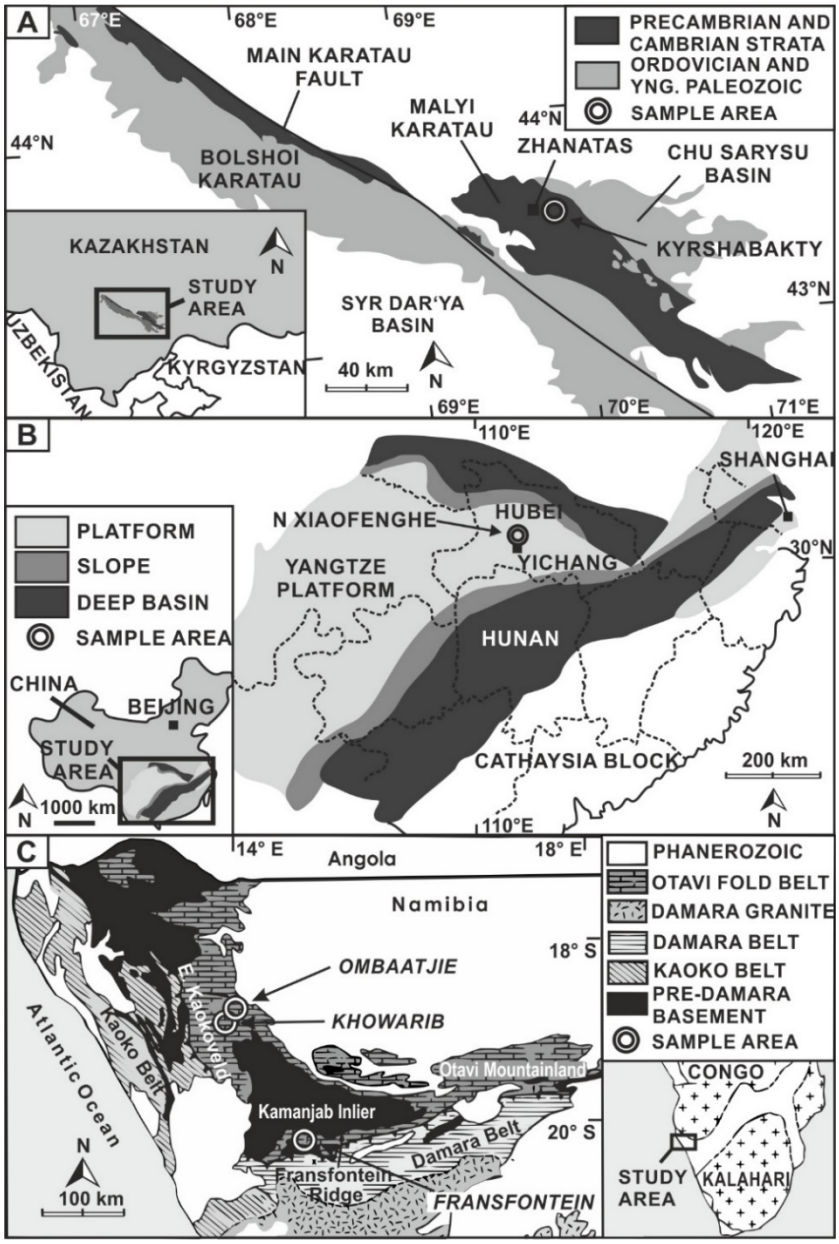

Figure 4: A: Geological sketch of the Malyi and Bolshoi Karatau Range displaying the study area east of Zhanatas (modified after Alexeiev et al., 2009). B: Generalized map of the Chinese Yangtze Platform including the Northern Xiaofenghe Section, Hubei Province (modified after Cremonese et al., 2013). C: Generalized geological map of northern Namibia showing the locations of the Fransfontein, Ombaatjie and Khowarib Sections (modified after Kasemann et al., 2010).

2.4 Sample selection and isotope data

Prior to geochemical analyses, strict sample selection criteria were applied to obtain high-quality samples in which primary isotopic data are likely preserved. Sample selection and stable isotope analyses followed the procedures detailed in Kasemann et al. (2005) and given in the supplement (see chapter 2.9). Carbonate carbon ($\delta^{13}C_{carb}$), boron ($\delta^{11}B$) and oxygen ($\delta^{18}O$) isotope data of the investigated Kyrshabakty and N Xiaofenghe Section together with literature data of the Fransfontein, Khowarib and Ombaatjie Sections (Kasemann et al., 2010), are presented in Figure 5 and Table 1 of the Supplement. Unlike the Namibian sections, those from China and Kazakhstan are more condensed and not continuously exposed. We consequently focus on cap carbonates and the immediately overlying sedimentary units that record the B isotope excursions and the return to climate normalcy.

In detail, the $\delta^{11}B$ values for the Kyrshabakty Section (shallow water; Karatau microcontinent) display a sinusoidal profile and a relative shift of ~12‰. With the onset of cap dolomite deposition a steady decrease in $\delta^{11}B$ composition from 8.7‰ to 1.7‰ is recorded. The nadir of the negative excursion (sample KY 7a) is situated 1.3 m above the glacial contact. Subsequently, the values continuously increase to 14.2‰ through the cap dolostone into the sandy dolostone unit and end with a lighter isotopic composition of 7.8‰ recorded by the uppermost sample (KY 13) at 29.5 m. The Kyrshabakty Section carbonates record the typical negative $\delta^{13}C$ excursion for cap carbonate deposits worldwide (e.g. Halverson et al., 2005) represented by a decline from -0.1‰ to -2.8‰ and return towards positive values of 1.3‰ up section. The minimum value is located at 1.3 m (KY 7b) as for the boron isotopes; oxygen isotope data scatter from -7.8 to -3.4‰. The bow shaped $\delta^{11}B$ profile for the Xiaofenghe Section (shallow-water, inner shelf; Yangtze Platform) starts with a value of 9.6‰ at 20 cm above the glacial deposit, declines to -2.2‰ at 1.6 m and returns to a maximum value of 14.8‰ within the sandy dolomites directly overlying the cap dolomites. $\delta^{13}C_{carb}$ data are in good agreement with literature data (Xiao et al., 2012), scatter around -4.0‰ within the cap carbonates and increase to 1.8‰ in the overlying sediments. Oxygen isotope data show little scatter around -7.3 to -6.5‰. As described by Kasemann et al. (2010) the $\delta^{11}B$ values of the Keilberg-Maieberg Formation (continental margin transect, Congo craton) display a prominent negative excursion, independent of lithology, facies

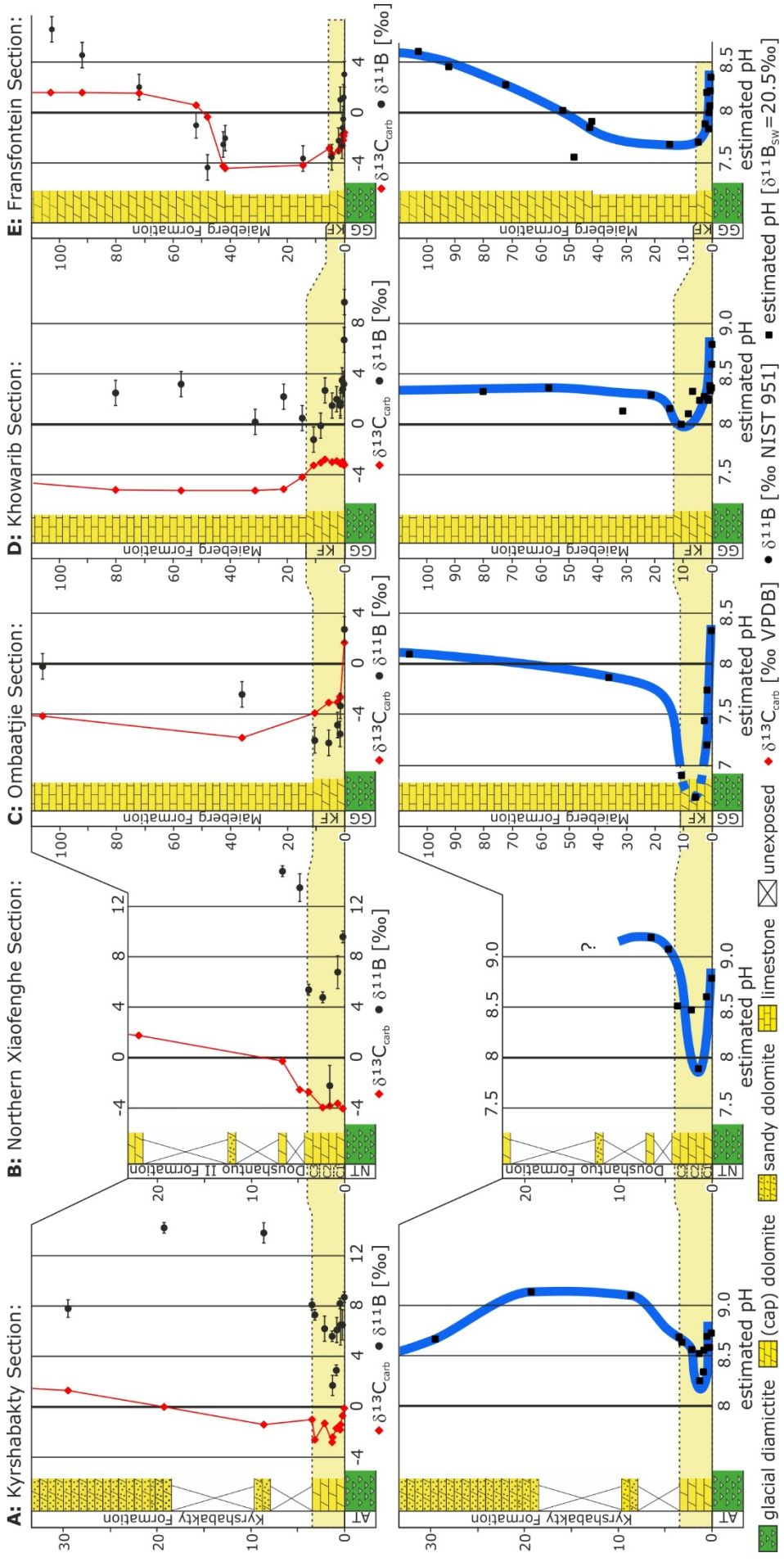

Figure 5: *Stratigraphic column of the investigated sections with corresponding $\delta^{11}B$ (‰, in black) and $\delta^{13}C_{carb}$ (‰, in red) isotope data and estimated ocean pH (in blue). The yellow shaded area marks the cap carbonates. A: Kyrshabakty Section, Malyi Karatau microcontinent, Kazakhstan B: Northern Xiaofenghe Section, Yangtze Platform, South China. C: Ombaatjie Section, Congo craton, Namibia. D: Khowarib Section, Congo craton, Namibia. E: Fransfontein Section, Congo craton, Namibia. AT - Aktas tillite, NT - Nantuo tillite, GG - Ghaub glacial deposit, KF - Keilberg Formation.*

settings or formation boundaries. The shallow-water Khowarib and Ombaatjie Sections show relative $\delta^{11}B$ negative shifts of 11‰ and 9‰, respectively. $\delta^{11}B$ values at Ombaatjie Section start at 2.7‰, 10 cm above the base of the cap carbonates, decline to ~ -6‰ in the Keilberg cap-dolostones and return to positive values (~0‰) up section into the Maieberg limestones and dolostones. At the Khowarib Section $\delta^{11}B$ values start at 9.7‰ with the onset of cap carbonate precipitation, decline to -1.2‰ and return to ~3.2‰ from the Keilberg cap dolostones, through the Maieberg limestones and into the Maieberg dolostones. In contrast, the Fransfontein Section, representing a slope-break palaeo-environment, records a prolonged negative $\delta^{11}B$ anomaly of ~11‰, reaching well above the Keilberg cap dolomites into the Maieberg Formation. The $\delta^{11}B$ profile starts at 3.0‰ when 20 cm into the Keilberg cap carbonates, decreases to -3.5‰ within the cap carbonates, and even to -4.3‰ though the Maieberg limestones into the Maieberg dolostones. Further up section the values climb back to 6.7‰ (sample FF1-37) at the upper Maieberg dolostones. All investigated Namibian sections display the characteristic negative $\delta^{13}C_{carb}$ excursions with values down to -5.8‰. Oxygen isotope data vary widely from -0.9 to -11.4‰.

2.5 Regional ocean pH pattern and global implications

A prerequisite for accurate reconstruction of seawater pH from the B isotope composition of marine carbonates is the knowledge of the seawater B isotope composition ($\delta^{11}B_{sw}$); an unknown parameter for the Neoproterozoic. Modern seawater is taken as homogeneous with a $\delta^{11}B_{sw}$ of 39.6‰ (e.g. Foster et al., 2010). In the past, significant variations in $\delta^{11}B_{sw}$ are likely and attributed to changes in the global boron budget (Joachimski et al., 2005). To gauge ocean pH conditions in the Neoproterozoic, Kasemann et al. (2005) initially explored different pH profiles with basic and acidic end-members. Subsequently, Kasemann et al. (2010) opted for slightly acidic seawater conditions, based on pH models for the Precambrian (Grotzinger and Kasting, 1993; Higgins and Schrag, 2003) and calculated relative ocean pH variation of as much as 1.5 pH units based on $\delta^{11}B_{sw}$ values between 20‰ and 23‰. Our new Chinese and Kazakh boron data are remarkably consistent with the Namibian data and show the same systematic negative $\delta^{11}B$ excursion for the post-glacial carbonates. In analogy to Kasemann et al. (2010) and to infer ocean pH values for the aftermath of the Marinoan,

we performed ocean pH calculations with a $\delta^{11}B_{sw}$ value of 20.5‰, using the empirical relationship between seawater pH and the B isotopic compositions of borate in solution and carbonates ($\alpha_{B3\text{-}B4}$ = 1.0272 at 25 °C from Klochko et al. (2006) and pK_B of 8.579 from Dickson (1990)). A detailed description of the palaeo-pH reconstruction, alternative $\delta^{11}B_{sw}$ assumptions and uncertainties related to variations in e.g. ocean temperature and salinity can be found in the Supplement.

In general, all investigated sections show comparable B isotope and hence ocean pH patterns at the time of the Marinoan deglacial phase, verifying the global extent of the ocean acidification event. The onset of cap carbonate deposition is characterized by positive boron isotope values and thus alkaline seawater with pH ~8.7. Within the cap dolomites, the decrease in $\delta^{11}B$ values and associated ocean pH leads into a temporary acidification event with minimum pH values of ~7 to ~8. Subsequently, the return to positive B isotope values and thus more alkaline seawater conditions further up section is recorded. Enhanced atmospheric pCO_2 levels during the glaciation (Bao et al., 2008; Cao and Bao, 2013; Kasemann et al., 2005) and associated oceanic CO_2 uptake at the earliest meltback most likely triggered the global acidification event after the Marinoan ice age. The recovery from this ocean acidification event to alkaline pH conditions appears to be equally a global phenomenon that was associated with CO_2 drawdown by the globally enhanced continental weathering flux (Kasemann et al., 2014; Silva-Tamayo et al., 2010). The concomitant flux of alkalinity must have also enabled carbonate sedimentation even under acidic ocean conditions (Kasemann et al., 2014).

It is striking that the alkaline pH conditions at the onset of cap carbonate deposition, recognized above as global, are similar to ocean pH states at the incipient Marinoan ice age, as highlighted by Kasemann et al. (2010). They argued that a stable ocean pH during the glaciation is only achievable by a global sea-ice cover preventing ocean-atmosphere gas exchange while atmospheric CO_2 increases until the deglacial. The transition into ocean acidification may then have been triggered by the collapse of the global ice shield enabling the rapid oceanic uptake of CO_2. Another possibility for alkaline pH with the incipient thaw is an intense weathering pulse through highly reactive and quickly dissolving glacial rock flour (Le Hir et al., 2009) which was washed into the ocean, after continuous grinding of continental surfaces by ice sheet dynamics. Each might have buffered the seawater immediately after the glaciation and caused alkaline

seawater conditions. To assess the potential influx and buffering capacity of glacial rock flour for the onset of cap carbonate deposition, additional proxy data that respond to weathering over short timescales are needed.

Apart from the documented similarities in the δ^{11}B-ocean pH relationship at the onset of deglaciation there are significant differences in the acidification magnitude and duration not only between different continents (Fig. 5) but also within different facies along a single continental margin (Kasemann et al., 2010). The smallest drop in pH to a minimum of 8.2 is visible at the Kyrshabakty Section. After cap dolomite deposition an overshoot to alkaline conditions of pH 9.1 is recorded within the directly overlying strata until a return to an assumed ocean pH "normalcy" of ~8.7 takes place. The Xiaofenghe Section comprises a distinct negative peak in ocean pH down to 7.9. Similar to the Kyrshabakty Section, the recovery to a normal pH state takes place within the cap dolomites followed by an alkaline overshoot to pH ~9.1 in the overlying Doushantuo II strata. Compared to the newly investigated sections, an analogous pattern is obvious for the Namibian shallow water sections. The Ombaatjie Section hosts the most prominent ocean acidification of more than 1.6 pH units (nadir below pH 7). After this rapid decrease, a return to far more alkaline pH states of ~8 is seen. At the Khowarib Section, the acidification by 0.8 pH units is less pronounced. The minimum pH is ~8 and the minor turn back to more alkaline seawater, happens shortly after cap dolomite deposition within the lowermost Maieberg Formation. In contrast, the slope break Fransfontein Section shows a distinctly different acidification pattern with an ocean pH as low as 7.6 and no return to more alkaline pH-states until the middle Maieberg Formation, far above cap dolomite deposition.

Variations in seawater pH patterns within a single platform transect and between continents can be driven by several causes. Factors amplifying or reducing the acidification magnitude or duration include varying regional weathering intensities and regimes, palaeo-bathymetries, sedimentation rates and water temperatures. Kasemann et al. (2014) proposed that for the Namibian continental margin, ocean pH is influenced by rising ocean alkalinity through enhanced continental input fluxes, first in shallow water and most proximal, probably restricted, environments, and later at the slope break. Our new shallow-water platform data from South China and Kazakhstan confirm this proposal. All platform sections display a recovery from the acidification within or only shortly after cap dolomite deposition in contrast to the slope environment, where

the recovery is significantly delayed. Furthermore, Namibian data indicate that the continental weathering flux transitioned from being of mixed carbonate and silicate character to a silicate-dominated one. Hence, craton-specific variations in the continental weathering flux together with regional distinctions in the timing of transition from carbonate to silicate weathering and their respective magnitudes at the end of cap dolomite deposition may have led to intercontinental differences in pH patterns. Carbonate weathering would initially increase alkalinity and buffer pH, but only silicate weathering would drastically draw down atmospheric CO_2 (Higgins and Schrag, 2003; Kasemann et al., 2014). Variations in the acidification pattern could also arise from a diachronous ice-cover loss after glaciation (Hoffman and Li, 2009). Continents located near the equator should record the entire ocean acidification event including its recovery, whereas incomplete signals should be present polewards due to a delayed deposition. Instead, our data show a sharp negative $\delta^{11}B$ excursion and acidification pattern on each craton and therefore do not support such a scenario.

2.6 Conclusion

Our new results strongly support the assumption of a global ocean acidification event in the aftermath of the Marinoan glaciation as a potential consequence of oceanic CO_2 uptake. At the incipient glaciation and also at the immediate deglacial phase, similar alkaline ocean pH conditions prevail. Global sea-ice cover preventing CO_2 ocean-atmosphere exchange during the ice age or a massive alkalinity pulse in the direct aftermath of the glaciation by glacial rock flour (Le Hir et al., 2009), could each have been the reason. The subsequently observed ocean acidification was most probably ended by CO_2 drawdown via globally enhanced continental weathering as indicated by Higgins and Schrag (2003) and by Kasemann et al. (2014). While all investigated cratons show similar seawater pH patterns, regional differences in their acidification magnitudes and minimum values as well as acidification durations are recorded. It appears that platform facies display a faster return to normal ocean pH conditions than slope facies as a direct consequence of the massive alkalinity flux to the ocean and hence increased buffer capacity leading to more alkaline seawater.

2.7 Acknowledgements

This work was funded by the DFG to SAK as part of the FOR 736. We thank U. Struck and A. Gamper (Museum für Naturkunde, Berlin) for providing $\delta^{13}C$ and $\delta^{18}O$ data from Kazakhstan and South China. We are grateful to S. Pape (University of Bremen) for trace element measurements, to C. Vogt (University of Bremen), R. Oeser and D. Hippler (TU Berlin) for XRD analyses. Thanks to F. Lucassen and A. Meixner for useful discussions. Fieldwork in South China was supported by the Natural Science Foundation of China (NSFC). Fieldwork in Kazakhstan was guided by G. Ergaliev and S. Zhemzhushnikov (Kazakh Academy of Sciences).

2.8 References

Alexeiev, D. V., Cook, H. E., Buvtyshkin, V. M., and Golub, L. Y., 2009, Structural evolution of the Ural-Tian Shan junction: A view from Karatau ridge, South Kazakhstan: Comptes Rendus Geosciences, v. 341, no. 2-3, p. 287-297.

Bao, H., Lyons, J. R., and Zhou, C., 2008, Triple oxygen isotope evidence for elevated CO2 levels after a Neoproterozoic glaciation: Nature, v. 453, no. 7194, p. 504-506.

Cao, X. B., and Bao, H. M., 2013, Dynamic model constraints on oxygen-17 depletion in atmospheric O-2 after a snowball Earth: Proceedings of the National Academy of Sciences of the United States of America, v. 110, no. 36, p. 14546-14550.

Condon, D., Zhu, M., Bowring, S., Wang, W., Yang, A., and Jin, Y., 2005, U-Pb Ages from the Neoproterozoic Doushantuo Formation, China: Science, v. 308, no. 5718, p. 95-98.

Cremonese, L., Shields-Zhou, G., Struck, U., Ling, H.-F., Och, L., Chen, X., and Li, D., 2013, Marine biogeochemical cycling during the early Cambrian constrained by a nitrogen and organic carbon isotope study of the Xiaotan section, South China: Precambrian Research, v. 225, p. 148-165.

Dickson, A. G., 1990, Thermodynamics of the dissociation of boric acid in synthetic seawater from 273.15 to 318.15 K: Deep Sea Research Part A. Oceanographic Research Papers, v. 37, no. 5, p. 755-766.

Eganov, E. A., Ergaliev, G. K., Ilyin, A. V., and Krasnov, A. A., 1984, Guidebook / International Geological Congress, XXVII Session Kazakhstan: Karatau Phosphorite Basin, Moskau, Nauka.

Foster, G. L., Pogge von Strandmann, P. A. E., and Rae, J. W. B., 2010, Boron and magnesium isotopic composition of seawater: Geochemistry, Geophysics, Geosystems, v. 11.

Grotzinger, J. P., and Kasting, J. F., 1993, New Constraints on Precambrian Ocean Composition: The Journal of Geology, v. 101, no. 2, p. 235-243.

Halverson, G. P., Hoffman, P. F., Schrag, D. P., Maloof, A. C., and Rice, A. H. N., 2005, Toward a Neoproterozoic composite carbon-isotope record: Geological Society of America Bulletin, v. 117, no. 9-10, p. 1181-1207.

Higgins, J. A., and Schrag, D. P., 2003, Aftermath of a snowball Earth: Geochemistry, Geophysics, Geosystems, v. 4, no. 3, p. 1028.

Hoffman, P. F., Kaufman, A. J., Halverson, G. P., and Schrag, D. P., 1998, A Neoproterozoic Snowball Earth: Science, v. 281, no. 5381, p. 1342-1346.

Hoffman, P. F., and Li, Z.-X., 2009, A palaeogeographic context for Neoproterozoic glaciation: Palaeogeography, Palaeoclimatology, Palaeoecology, v. 277, no. 3–4, p. 158-172.

Hoffman, P. F., and Schrag, D. P., 2002, The snowball Earth hypothesis: testing the limits of global change: Terra Nova, v. 14, no. 3, p. 129-155.

Joachimski, M. M., Simon, L., van Geldern, R., and Lécuyer, C., 2005, Boron isotope geochemistry of Paleozoic brachiopod calcite: Implications for a secular change in the boron isotope geochemistry of seawater over the Phanerozoic: Geochimica et Cosmochimica Acta, v. 69, no. 16, p. 4035-4044.

Kasemann, S. A., Hawkesworth, C. J., Prave, A. R., Fallick, A. E., and Pearson, P. N., 2005, Boron and calcium isotope composition in Neoproterozoic carbonate rocks from Namibia: evidence for extreme environmental change: Earth and Planetary Science Letters, v. 231, no. 1-2, p. 73-86.

Kasemann, S. A., Pogge von Strandmann, P. A. E., Prave, A. R., Fallick, A. E., Elliott, T., and Hoffmann, K.-H., 2014, Continental weathering following a Cryogenian glaciation: Evidence from calcium and magnesium isotopes: Earth and Planetary Science Letters, v. 396, no. 0, p. 66-77.

Kasemann, S. A., Prave, A. R., Fallick, A. E., Hawkesworth, C. J., and Hoffmann, K.-H., 2010, Neoproterozoic ice ages, boron isotopes, and ocean acidification: Implications for a snowball Earth: Geology, v. 38, no. 9, p. 775-778.

Kirschvink, J. L., 1992, Late Proterozoic Low-Latitude Global Glaciation: The Snowball Earth: Section 2.3 in: J.W. Schopf, C. Klein, & D. Des Maris (eds), The Proterozoic Biosphere: A Multidisciplinary Study, p. 51-52.

Klochko, K., Kaufman, A. J., Yao, W., Byrne, R. H., and Tossell, J. A., 2006, Experimental measurement of boron isotope fractionation in seawater: Earth and Planetary Science Letters, v. 248, no. 1-2, p. 276-285.

Le Hir, G., Donnadieu, Y., Goddéris, Y., Pierrehumbert, R. T., Halverson, G. P., Macouin, M., Nédélec, A., and Ramstein, G., 2009, The snowball Earth aftermath: Exploring the limits of continental weathering processes: Earth and Planetary Science Letters, v. 277, no. 3–4, p. 453-463.

Li, Z.-X., Evans, D. A. D., and Halverson, G. P., 2013, Neoproterozoic glaciations in a revised global palaeogeography from the breakup of Rodinia to the assembly of Gondwanaland: Sedimentary Geology, v. 294, no. 0, p. 219-232.

Ma, G., Li, H., and Zhang, Z., 1984, An investigation of the age limits of the Sinian System in South China: Bulletin of Yichang Institute of Geology Mineral Resources, v. 8, p. 1-29.

Macdonald, F. A., Schmitz, M. D., Crowley, J. L., Roots, C. F., Jones, D. S., Maloof, A. C., Strauss, J. V., Cohen, P. A., Johnston, D. T., and Schrag, D. P., 2010, Calibrating the Cryogenian: Science, v. 327, no. 5970, p. 1241-1243.

Planavsky, N. J., Rouxel, O. J., Bekker, A., Lalonde, S. V., Konhauser, K. O., Reinhard, C. T., and Lyons, T. W., 2010, The evolution of the marine phosphate reservoir: Nature, v. 467, no. 7319, p. 1088-1090.

Silva-Tamayo, J. C., Nägler, T. F., Sial, A. N., Nogueira, A., Kyser, K., Riccomini, C., James, N. P., Narbonne, G. M., and Villa, I. M., 2010, Global perturbation of the marine Ca isotopic composition in the aftermath of the Marinoan global glaciation: Precambrian Research, v. 182, no. 4, p. 373-381.

Xiao, S., McFadden, K. A., Peek, S., Kaufman, A. J., Zhou, C., Jiang, G., and Hu, J., 2012, Integrated chemostratigraphy of the Doushantuo Formation at the northern Xiaofenghe section (Yangtze Gorges, South China) and its implication for Ediacaran stratigraphic correlation and ocean redox models: Precambrian Research, v. 192-195, no. 0, p. 125-141.

2.9 Supplemental Material

Geological setting

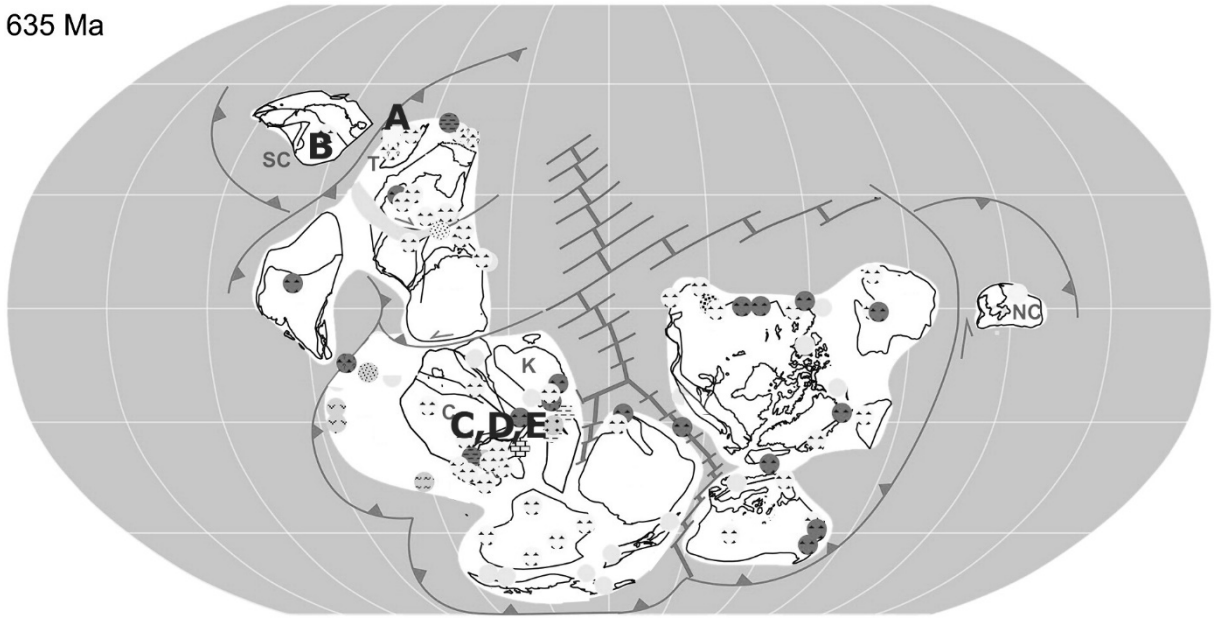

Figure 6: Palaeogeographic reconstruction for 635 Ma (slightly modified from Li et al., 2013). The investigated sections are indicated in black: A: Kyrshabakty Section, Karatau microcontinent. B: N Xiaofenghe Section, South China Block. C: Ombaatjie Section, Congo craton. D: Khowarib Section, Congo craton. E: Fransfontein Section, Congo craton. The geographic position of the Karatau-Naryn terrane is suggested to be close to South China and the Tarim microcontinent. Abbreviations of the terranes: C-Congo; K-Kalahari; NC-North China; SC-South China; T-Tarim.

Yangtze Platform (China)

Precambrian-Cambrian strata are widespread on the Yangtze Platform (Zhang et al., 1997; Zhu et al., 2003). The Three Gorges area is located at the central northern part of the platform, Hubei Province. Platform interior successions are typically comprised of shallow-water carbonates and deep-water shales of Cryogenian to Cambrian age. From oldest to youngest, the Liantuo, Nantuo, Doushantuo, Dengying, Yanjiahe, Shuijingtuo and Shipai Formations (Ma et al., 1984) are exposed in the Three Gorges area. The investigated Xiaofenghe Section (30°56′31.9′′N, 111°13′57.1′′E) is located approximately 28 km N of Yichang, crops out along the northern and southern mountainsides of a small valley and provides access to ~200 m of well exposed strata.

Nantuo Formation glacial diamictites are directly overlain by ~4 m of Doushantuo Formation cap dolomites (Doushantuo I), which can be subdivided by microfacies into C1, C2 and C3 after the classification of Jiang et al. (2003). The lowermost 0.5 m correspond to unit C1 and consist of grey dolostones with minor calcite

veining. Up to ~2.5 m a grey, fine laminated, micritic dolostone (C2) with minor cm-scale chert layers is exposed. The uppermost unit (C3) displays a laminated dolostone layer containing teepee-like fluid-escape structures. On top of the cap dolomite are several meters of grey, micritic dolostones interbedded with chert-nodule-bearing black shales (Doushantuo II Formation). Xiao et al. (2012) suggested that the northern Xiaofenghe Section represents a shallow-water, inner shelf environment.

Karatau microcontinent (Kazakhstan)

The southern Kazakh Karatau Mountains form the foothills of the Tian Shan orogen and consist of the Bolshoi (NW) and Malyi (SE) Karatau Range that are divided by the Main Karatau Fault (Alexeiev et al., 2009 and references therein). The investigated Kyrshabakty Section (43°32'2.1''N, 69°57'7.7''E), located approximately 18 km E of Zhanatas, is part of the Malyi Karatau Range which is surrounded by the Syr Dar'ya Basin to the SW and the Chu Sarysu Basin to the NE (Allen et al., 2001). The complete Precambrian-Cambrian succession is described in detail by Eganov et al. (1984) and Meert et al. (2011). We focused on the lowermost Kyrshabakty Formation which is part of the Tamdy Series and comprises a ~45 m thick diamictite layer (Aktas tillite) overlain by ~3.5-4 m thick cream-to-ivory-colored cap dolomites without any noticeable sedimentary features besides a fine lamination. Up section the succession is marked by an alternation of dolomitic sandstones and sandy dolostones with an increasing trend in dolomite content towards the top. The first ~30 m of the section are defined by a transgressive system tract and the palaeoenvironment is suggested to represent a very shallow water platform setting which is also confirmed by Eganov et al. (1986).

Congo craton (Namibia)

The analyzed marine successions were all situated on the low-latitude (Fig. 6) continental margin of the southern Congo craton and comprise Neoproterozoic to Cambrian rocks. We concentrate on the thick sequence of carbonate rocks corresponding to the Tsumeb Subgroup, being part of the Otavi Group (Hoffmann et al., 2004; Kaufman et al., 1991). In detail, the shallow-marine platform Ombaatjie and Khowarib Sections as well as the fore-slope Fransfontein Section (Fig. 4C) provide access to Ghaub glacial deposits (~635 Ma, Hoffmann et al., 2004) overlain by post-glacial Keilberg cap dolomites transitioning into a >100 m thick succession of Maieberg Formation dolo- and limestones (Hoffman et al., 1996; Kasemann et al., 2010; Kaufman et al., 1991). The

cap carbonates are micritic dolostones, which can be subdivided into a basal laminated unit, a middle unit containing soft-sediment deformations, sheet-cracks and stromatolite structures, and a capping interval of thin-bedded dolostones. The Maieberg Formation is comprised of rhythmite limestones and thin-bedded dolo- and limestones at the Khowarib and Ombaatjie Section and only of thin-bedded dolostones at the Fransfontein Section (Kasemann et al., 2010). A more detailed stratigraphy and overview about the large-scale tectonic situation is provided by e.g. Miller (2008).

Sample selection criteria/alteration evaluation

Sample selection and quality evaluation for the Namibian carbonate dataset is described in Kasemann et al. (2010). Fresh rock hand samples of the Kyrshabakty Formation (Kazakhstan) and the Doushantuo Formation (South China) carbonates were taken in 10-30 cm intervals and selected by their uniformity and absence of any obvious alteration or veining. To assure a good sample quality, we checked the samples macroscopically in the field, afterwards microscopically in the lab (thin section, scanning electron microscopy) and performed geochemical tests (trace element and oxygen isotope analyses). Rock powders were prepared from pre-screened, micritic, cleaned and fresh surface rock chips with an agate vibratory disc mill at the Museum fuer Naturkunde Berlin, Germany.

Clay contamination

To avoid contamination by the dissolution of boron bearing clays during chemical preparation a 1 N HCl (100 µl 1 N HCl for 10 mg of sample powder) is used during the dissolution procedure. Dissolution of B-bearing clays would generally enrich the boron concentrations. Potential contamination in the isotope composition are dependent on the clay source and hence difficult to assess, but expected to be negligible due to a similar fractionation factor between seawater and carbonates as well as seawater and clay (Palmer et al., 1987). To assess the amount of clay in the sample material XRD analyses of Kyrshabakty Formation cap dolomites were performed at the Mineralogy Department of the Technical University Berlin, Germany. A semi quantitative data evaluation after Cook et al. (1975) showed an average clay content of <1%. XRD analyses of the Chinese data set done at the ZEKAM (Zentrallabor für Kristallographie und angewandte Materialwissenschaften), University of Bremen, Germany showed an

average clay content of ~6%. To test for clay contamination in the sample solution, trace element analyses were performed on an Agilent Technologies 700 Series ICP-OES at the inorganic geochemistry group, University of Bremen, Germany. The boron concentration is 2 µg g^{-1} without any obvious correlation to varying clay content. For example, Al concentrations are around 200 ppm and are not correlated to the B concentration; hence boron contamination by clay dissolution can be excluded.

Post-depositional alteration

Post-depositional alteration, especially diagenesis, is thought to decrease the isotopic composition of oxygen, boron and carbon isotopes (Derry et al., 1992; Kaufman et al., 1993; Paris et al., 2010; Veizer et al., 1999). On that account, only samples with $\delta^{18}O$ values > -10‰ are considered to be of primary origin and suitable for further isotope analyses. Doushantuo Formation dolomites show average $\delta^{18}O$ values of -6.8‰ with no $\delta^{18}O$ value smaller than -7.3‰ and without any significant correlation at the 5% significance level (R^2=0.22) to the carbon (Fig. 7) or boron isotopic composition. A similar situation is present with respect to the Kyrshabakty Formation data. The average $\delta^{18}O$ value is -5‰ and as per the Chinese data there is no significant or obvious correlation with $\delta^{13}C$ at the 5% significance level (R^2=0.07, Fig. 7) or with $\delta^{11}B$ data. Further, both the $\delta^{18}O$ and $\delta^{13}C$ are in perfect agreement with literature data of that time (e.g. Jacobsen and Kaufman, 1999). Diagenesis is also thought to cause a correlation between the boron concentration and the $\delta^{11}B$ values (Spivack and You, 1997). However, no relationship is obvious for our data set.

For the Phanerozoic, primary isotopic signals recorded by carbonates are expected to show Mn/Sr ratios below 10. In comparison, Mn/Sr values above 10 are present in China, which could be a result of hydrothermal overprint, as suggested for the Doushantuo Formation (Derkowski et al., 2013). However, enriched Mn/Sr are a common feature of cap dolomites and also reported by e.g. Liu et al. (2013). In general, the reliability of Mn/Sr ratios as an alteration criterion is doubted for Neoproterozoic rocks by many authors. The ratio is strongly dependent on the primary precipitated carbonate mineral phase (Derry, 2010), and high Mn/Sr ratios can also result from precipitation in early diagenetic anoxic waters (Miller et al., 2009), potentially present during the time of cap dolomite deposition. Likewise, increased seawater concentrations of Mn and Fe leading to high Mn/Sr ratios during the Marinoan time interval are likely,

due to the potential absence of abundant oxygen and sulfate necessary for redox reactions (Anbar and Knoll, 2002; Hoffman and Li, 2009; Miller et al., 2009; Raub et al., 2007).

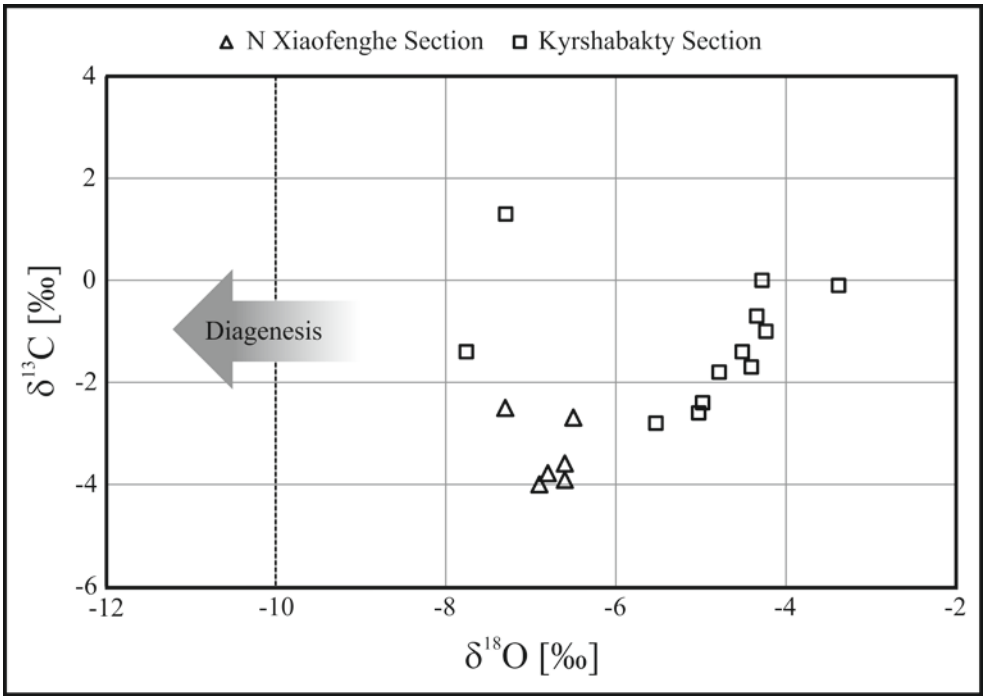

Figure 7: Cross-plot of $\delta^{18}O$ vs. $\delta^{13}C_{carb}$ data of the Northern Xiaofenghe (triangles) and Kyrshabakty Section (squares). None of the data plot in the diagenesis-field and no significant correlation is obvious.

We therefore conclude that our boron isotope data have not been diagenetically compromised. In addition, systematic cyclical isotopic patterns at all measured sections and on different continents further support interpreting the isotopic signatures as primary values.

Constraints on ocean pH reconstruction

In seawater two dominant boron species are present: boric acid ($B(OH)_3$) and borate-ion ($B(OH)_4^-$) (Kakihana et al., 1977; Spivack and Edmond, 1987). Between these two species an isotopic exchange (Hemming and Hanson, 1992) is described by the reaction displayed in equation [1]:

$$^{11}B(OH)_3 + {}^{10}B(OH)_4^- <=> {}^{10}B(OH)_3 + {}^{11}B(OH)_4^- \qquad [1]$$

Due to the fact that the abundance of the species and their isotopic composition is pH dependent and marine carbonates predominantly incorporate the charged, tetrahedral species (Hemming and Hanson, 1992; Sanyal et al., 2000), palaeo pH calculations by boron isotopes measurements are possible (Klochko et al., 2006), with the relationship given in equation [2]:

$$pH = pK_B - \log\left[- \frac{\delta^{11}B_{SW} - \delta^{11}B_{carb}}{\delta^{11}B_{SW} - \alpha_{B3\text{-}B4} \cdot \delta^{11}B_{carb} - 1000 \cdot (\alpha_{B3\text{-}B4} - 1)} \right] \quad [2]$$

To calculate seawater pH, we need the B isotope composition of the carbonate ($\delta^{11}B_{carb}$) and the seawater ($\delta^{11}B_{sw}$) (discussed below), as well as the isotope fractionation factor for boron ($\alpha_{B3\text{-}B4}$) and the dissociation constant of boric acid (pK_B), both of which are temperature dependent. To infer ocean pH values and compare the pH pattern of the different continents, we performed ocean pH calculations with a $\delta^{11}B_{sw}$ value of 20.5‰ using the empirical fractionation factor for seawater pH and the B isotopic compositions of borate in solution and carbonates of $\alpha_{B3\text{-}B4}$ = 1.0272 (Klochko et al., 2006), and a pK_B of 8.579 (Dickson, 1990) both for 25°C seawater temperature. Since exact seawater temperatures for the Early Ediacaran are unknown we have to rely on modelled values. Initial seawater temperatures of -1.5°C rapidly increasing to ~30°C after the deglacial are modelled by Higgins and Schrag (2003). Variations in sea surface temperatures between 15°C and 35°C most likely reflecting the temperatures prevailing during platform carbonate precipitation, would result in a maximum differences of < 0.2 pH. Generally, colder temperatures lead to slightly higher pH conditions, whereas warmer seawater temperatures lead to slightly more acidic conditions. For our dataset, the relative ocean pH pattern including the acidification magnitudes would stay completely the same.

The pK_B also changes with different salinities (Dickson, 1990). However, even if lower salinities (S = ~25 ppt) are assumed due to meltwater influx (Shields, 2005) the associated isotopic variations are negligible for our dataset and a salinity assumption of S = 35 ppt is used for calculations.

The residence time of boron in the modern ocean is ~14-20 Ma (Lemarchand et al., 2000; Spivack, 1986) and should be roughly similar during the Neoproterozoic, but

is in any case far bigger than the maximal assumed duration of cap carbonate deposition (~3 Ma, Condon et al., 2005). Consequently, ocean pH changes instead of variations in seawater $\delta^{11}B$ composition are recorded at the investigated sections. Kasemann et al. (2010) calculated relative ocean pH variation based on $\delta^{11}B_{sw}$ values between 20‰ and 23‰. By combining our new Chinese and Kazakh dataset together with the already published Namibian literature data, we suggest and use a seawater composition of 20.5‰ as our 'best-guess' value. Using a higher isotope composition for seawater, would result in unlikely acidic conditions (< pH 6) for the acidification event for some sections result, while lower $\delta^{11}B_{SW}$ assumptions would lead to highly alkaline seawater conditions (> pH 9.5). In comparison to models and calculations for that time (e.g. Higgins and Schrag, 2003; Kempe and Kazmierczak, 2002), we regard both cases as unlikely. For a better comparison and overview, we nevertheless performed ocean pH calculations for different $\delta^{11}B$ seawater assumptions (A: 20.5‰, B: 21.5‰, and C: 22.5‰) summarized in table 1. The overall acidification pattern observed at all sections is only negligibly affected by changes to the boron isotope seawater composition. For the Ombaatjie Section a pH calculation is only possible with model A, due to its very light boron isotope data (note that the uncertainty of the isotope value is ~1‰ ($2\sigma_f$) for the Ombaatjie Section).

Methods

Boron measurements

Boron ($\delta^{11}B$) isotope analyses were performed by the method detailed in Kasemann et al. (2001). For analyses, 10 mg of the sample powder was dissolved in 100 µl 1 N HCl for 24 h at 20°C and centrifuged afterwards. The $n(^{11}B)/n(^{10}B)$ measurements were performed on a Thermo Fisher Scientific TRITON *Plus* mass spectrometer, using negative thermal ionization mass spectrometry (N-TIMS). 1 µl boron-free seawater emitter was placed on a degassed Re single filament and dried at 0.7 A. Subsequently, 1 µl of the sample solution containing ~1 ng B was added, evaporated to complete dryness at 0.7 A, and afterwards heated at 1.2 A for 30 s. Boron isotopes were registered as BO_2^- complexes on masses 42 and 43, and measurements were carried out at 970°-1050°C with an ion beam intensity of 3-30 pA on mass 43. Each measuring procedure consisted of up to 200 blocks with 10 cycles, taking about 3 hours of data acquisition. To correct

for a CNO^- interference on mass 42 occurring at the beginning of some measurements and for isotopic fractionation during analysis, the extrapolation technique described by Kasemann et al. (2001) was used in the data evaluation.

Boron isotope ratios are given in $\delta^{11}B$-notation relative to the certified reference material NIST SRM 951 that showed an $^{11}B/^{10}B$ ratio of 4.0068±0.0016 (2sd=0.4‰, n=37 over a period of 12 month). In addition to the NIST material, the standard material M93-TB-FC-1, a *Porites* coral with a published value of 24.8±0.4‰ ($2\sigma_{mean}$), as determined by different multicollector techniques (Kasemann et al., 2009), was also regularly analyzed. The coral was reproduced with a $\delta^{11}B$ value of 24.1±0.7‰ (2sd, n=16). Samples were analyzed at least twice and their reproducibility (2sd) is given in table 1.

Carbon and oxygen measurements

The $\delta^{13}C_{carb}$ and $\delta^{18}O$ isotope dataset is based on 14 bulk rock samples of the Kyrshabakty Section and 9 samples of the Xiaofenghe Section, respectively. All measurements were carried out on a Thermo Finnigan GASBENCH II linked online to a Thermo Finnigan DELTA V isotope ratio mass spectrometer at the Museum fuer Naturkunde Berlin, Germany. Isotope ratios are reported in δ-notation in [‰] relative to the Vienna Peedee Belemnite (VPDB). The analytical reproducibility of $\delta^{13}C_{carb}$ and $\delta^{18}O$ values is generally better than ±0.2‰ (2sd) for both isotopic systems.

Trace element analyses

Trace elements analyses of the northern Xiaofenghe Section carbonates were performed on an Agilent Technologies 700 Series ICP-OES at the inorganic geochemistry group of the MARUM, Germany. Three replicates of each dilution/concentration were measured and typically had a relative standard deviation (RSD) of better than 3% (excepting boron, which was <7%).

Assumptions for pH calculations: pK_B = 8.579 Dickson, 1990

α = 1.0272 Klochko *et al.*, 2006

A: 20.5‰ $\delta^{11}B_{sw}$

B: 21.5‰ $\delta^{11}B_{sw}$

C: 22.5‰ $\delta^{11}B_{sw}$

China	Yangtze Platform							
N. Xiaofenghe Section		$\delta^{13}C$	$\delta^{18}O$	$\delta^{11}B$		A	B	C
Sample	meter	[‰]	[‰]	[‰]	2σ	pH	pH	pH
NXF0.2	0.2	-4.0	-6.9	9.6	0.1	8.8	8.7	8.6
NXF0.75	0.8	-3.6	-6.6	6.8	1.3	8.6	8.5	8.5
NXF1.6	1.6	-3.8	-6.8	-2.2	1.6	7.9	7.8	7.6
NXF2.35B	2.4	-3.9	-6.6	4.8	0.2	8.5	8.4	8.3
NXF3.85	3.9	-2.7	-6.5	5.4	0.0	8.5	8.4	8.4
NXF4.8	4.8	-2.5	-7.3	13.5	1.1	9.1	9.0	8.9
NXF6.65	6.7	-0.2	n.a.	14.8	0.1	9.2	9.1	9.0
NXF22	22.0	1.8	n.a.	n.a.				
Kazakhstan	Malyi Karatau Range							
Kyrshabakty Section		$\delta^{13}C$	$\delta^{18}O$	$\delta^{11}B$		A	B	C
Sample	meter	[‰]	[‰]	[‰]	2σ	pH	pH	pH
KY 3	0.0	-0.1	-3.4	8.7	0.2	8.7	8.7	8.6
KY 4	0.2	-0.7	-4.3	6.5	1.2	8.6	8.5	8.4
KY 5a	0.4	-1.4	-4.5	6.5	1.6	8.6	8.5	8.4
KY 5b	0.5	-1.8	-4.8	8.2	0.2	8.7	8.6	8.6
KY 6a	0.8	n.a.	n.a.	6.1	1.0	8.6	8.5	8.4
KY 6b	0.9	-1.7	-4.4	2.9	0.2	8.3	8.3	8.2
KY 7a	1.3	-2.4	-5.0	1.7	0.8	8.2	8.2	8.1
KY 7b	1.3	-2.8	-5.5	5.6	0.3	8.5	8.5	8.4
KY 8	2.1	-1.3	n.a.	6.2	1.0	8.6	8.5	8.4
KY 9	3.2	-2.6	-5.0	7.3	0.0	8.6	8.6	8.5
KY 10	3.5	-1.0	-4.2	8.1	0.3	8.7	8.6	8.6
KY 10a	8.6	-1.4	-7.8	13.8	0.8	9.1	9.0	8.9
KY 11	19.3	0.0	-4.3	14.2	0.2	9.1	9.0	9.0
KY 13	29.5	1.3	-7.3	7.8	0.7	8.7	8.6	8.5

Namibia Congo Craton							
Khowarib Section		$\delta^{13}C$	$\delta^{18}O$	$\delta^{11}B$*	A	B	C
Sample	meter	[‰]	[‰]	[‰]	pH	pH	pH
KW1-10	0.0	-3.2	-7.4	9.7	8.8	8.7	8.7
KW1-11	0.1	-3.2	-7.3	6.7	8.6	8.5	8.5
KW1-12	0.2	-3.2	-6.1	3.2	8.4	8.3	8.2
KW1-14	0.6	-3.0	-7.2	2.8	8.3	8.3	8.2
KW1-15	0.8	n.a.	n.a.	3.5	8.4	8.3	8.2
KW1-18	1.4	-3.1	-7.7	1.7	8.2	8.2	8.1
KW1-18	1.4	-3.1	-7.7	1.5	8.2	8.2	8.1
KW1-21	2.7	-2.9	-7.6	2.0	8.3	8.2	8.1
KW1-24	4.3	-3.0	-7.7	1.5	8.2	8.2	8.1
KW1-29	6.8	-2.8	-7.5	2.7	8.3	8.3	8.2
KW1-32	8.3	-3.0	-7.5	-0.1	8.1	8.0	7.9
KW1-37	10.8	-3.3	-6.9	-1.2	8.0	7.9	7.8
KW1-45	14.8	-4.2	-9.0	0.5	8.2	8.1	8.0
KW1-55	21.3	-5.1	-8.6	2.2	8.3	8.2	8.1
KW1-58	31.3	-5.2	-9.1	0.2	8.1	8.0	7.9
KW1-64	57.3	-5.2	-9.6	3.2	8.4	8.3	8.2
KW1-67	80.3	-5.2	-9.5	2.5	8.3	8.2	8.2

Namibia Congo Craton							
Fransfontein Section		$\delta^{13}C$	$\delta^{18}O$	$\delta^{11}B$*	A	B	C
Sample	meter	[‰]	[‰]	[‰]	pH	pH	pH
FF1-2	0.2	-1.6	-7.0	3.0	8.3	8.3	8.2
FF1-3	0.4	-1.8	-7.0	1.2	8.2	8.1	8.0
FF1-4	0.6	-2.2	-7.3	-0.5	8.1	8.0	7.9
FF1-5	0.8	-1.7	-6.7	-1.2	8.0	7.9	7.8
FF1-6	1.0	-2.6	-7.3	-2.6	7.8	7.7	7.5
FF1-9	1.6	-2.3	-7.4	1.0	8.2	8.1	8.0
FF1-12	2.2	-3.0	-7.5	-2.2	7.9	7.8	7.6
FF1-20	4.6	-3.3	-8.3	-3.5	7.7	7.5	7.2
FF1-22	5.4	-2.8	-8.8	n.a.			
FF1-28	14.7	-4.1	-10.2	-3.6	7.7	7.5	7.2
FF1-29	42.0	-4.4	-9.7	-2.0	7.9	7.8	7.6
FF1-30	42.7	-4.2	-9.4	-2.5	7.9	7.7	7.5
FF1-31	48.2	-0.3	-6.9	-4.3	7.6	7.3	6.6
FF1-32	52.2	0.6	-5.3	-1.0	8.0	7.9	7.8
FF1-34	72.2	1.5	-1.5	2.0	8.3	8.2	8.1
FF1-36	92.2	1.6	-0.9	4.5	8.4	8.4	8.3

FF1-37	102.2	1.6	-5.0	6.7	8.6	8.5	8.5
Namibia	**Congo Craton**						
Ombaatjie Section		$\delta^{13}C$	$\delta^{18}O$	$\delta^{11}B^*$	A	B	C
Sample	meter	[‰]	[‰]	[‰]	pH	pH	pH
OBTJ 43	0.1	1.7	-4.6	2.7	8.3	8.3	8.2
OBTJ 45	1.5	-2.6	-6.3	-3.3	7.7	7.6	7.3
OBTJ 46	1.6	-2.6	-6.9	-5.5	7.2	5.9	-
OBTJ 47	2.5	-3.0	-6.9	-4.8	7.4	7.1	-
OBTJ 52	5.6	-3.0	-6.8	-6.2	6.7	-	-
OBTJ 55	10.5	-3.9	-8.5	-6.0	6.9	-	-
OBTJ 58	36.0	-5.8	-11.4	-2.4	7.9	7.7	7.6
OBTJ 65	106.0	-4.1	-8.9	-0.2	8.1	8.0	7.9

Table 1: *Boron ($\delta^{11}B$ [‰, vs. NIST SRM 951]), carbonate carbon ($\delta^{13}C_{carb}$ [‰, vs. VPDB]) and oxygen ($\delta^{18}O$ [‰, vs. VPDB]) isotope data of all analyzed sections, including Namibia data (Kasemann et al., 2010). Uncertainty for Namibian B isotope data is $\delta^{11}B^*$: ±1‰ $2\sigma_f$. A, B, C are pH estimations based on different $\delta^{11}B_{sw}$ assumptions: pK_B of 8.579 (Dickson, 1990), a fractionation factor α of 1.0272 (Klochko et al., 2006) and a seawater $\delta^{11}B$ composition of A=20.5‰, B=21.5‰ and C=22.5‰ are used. The finally proposed $\delta^{11}B_{sw}$ composition of 20.5‰ is shaded in grey. n.a. = not analyzed.*

References

Alexeiev, D. V., Cook, H. E., Buvtyshkin, V. M., and Golub, L. Y., 2009, Structural evolution of the Ural-Tian Shan junction: A view from Karatau ridge, South Kazakhstan: Comptes Rendus Geosciences, v. 341, no. 2-3, p. 287-297.

Allen, M. B., Alsop, G. I., and Zhemchuzhnikov, V. G., 2001, Dome and basin refolding and transpressive inversion along the Karatau Fault System, southern Kazakstan: Journal of the Geological Society, v. 158, no. 1, p. 83-95.

Anbar, A. D., and Knoll, A. H., 2002, Proterozoic Ocean Chemistry and Evolution: A Bioinorganic Bridge?: Science, v. 297, no. 5584, p. 1137-1142.

Condon, D., Zhu, M., Bowring, S., Wang, W., Yang, A., and Jin, Y., 2005, U-Pb Ages from the Neoproterozoic Doushantuo Formation, China: Science, v. 308, no. 5718, p. 95-98.

Cook, H. E., Johnson, P. D., Matti, J. C., and Zemmels, I., 1975, Methods of sample preparation and X-ray diffraction data analysis, X-ray Mineralogy Laboratory, Deep Sea Drilling Project, University of California, Riverside: In: Hayes, D.E., Frakes, L.A., et al., Init. Repts.

Derkowski, A., Bristow, T. F., Wampler, J. M., Środoń, J., Marynowski, L., Elliott, W. C., and Chamberlain, C. P., 2013, Hydrothermal alteration of the Ediacaran Doushantuo Formation in the Yangtze Gorges area (South China): Geochimica et Cosmochimica Acta, v. 107, no. 0, p. 279-298.

Derry, L. A., 2010, A burial diagenesis origin for the Ediacaran Shuram–Wonoka carbon isotope anomaly: Earth and Planetary Science Letters, v. 294, no. 1-2, p. 152-162.

Derry, L. A., Kaufman, A. J., and Jacobsen, S. B., 1992, Sedimentary cycling and environmental change in the Late Proterozoic: Evidence from stable and radiogenic isotopes: Geochimica et Cosmochimica Acta, v. 56, no. 3, p. 1317-1329.

Dickson, A. G., 1990, Thermodynamics of the dissociation of boric acid in synthetic seawater from 273.15 to 318.15 K: Deep Sea Research Part A. Oceanographic Research Papers, v. 37, no. 5, p. 755-766.

Eganov, E. A., Ergaliev, G. K., Ilyin, A. V., and Krasnov, A. A., 1984, Guidebook / International Geological Congress, XXVII Session Kazakhstan: Karatau Phosphorite Basin, Moskau, Nauka.

Eganov, E. A., Sovetov, Y. K., and Yanshin, A. L., 1986, Proterozoic and Cambrian phosphorite deposits: Karatau, southern Kazakhstan, USSR: In: Cook, P.J., Shergold, J.H. (Eds.), Phosphate Deposits of the World: Volume 1 Proterozoic and Cambrian Phosphorites. Cambridge University Press, Cambridge, UK, p. 175-189.

Hemming, N. G., and Hanson, G. N., 1992, Boron isotopic composition and concentration in modern marine carbonates: Geochimica et Cosmochimica Acta, v. 56, no. 1, p. 537-543.

Higgins, J. A., and Schrag, D. P., 2003, Aftermath of a snowball Earth: Geochemistry, Geophysics, Geosystems, v. 4, no. 3, p. 1028.

Hoffman, P. F., Hawkins, D. P., Isachsen, C. E., and Bowring, S. A., 1996, Precise U-Pb zircon ages for early Damaran magmatism in the Summas Mountains and Welwitschia Inlier, northern Damara Belt, Namibia: Communications of the Geological Survey of Namibia, v. 11, p. 47-52.

Hoffman, P. F., and Li, Z.-X., 2009, A palaeogeographic context for Neoproterozoic glaciation: Palaeogeography, Palaeoclimatology, Palaeoecology, v. 277, no. 3–4, p. 158-172.

Hoffmann, K.-H., Condon, D. J., Bowring, S. A., and Crowley, J. L., 2004, U-Pb zircon date from the Neoproterozoic Ghaub Formation, Namibia: Constraints on Marinoan glaciation: Geology, v. 32, no. 9, p. 817-820.

Jacobsen, S. B., and Kaufman, A. J., 1999, The Sr, C and O isotopic evolution of Neoproterozoic seawater: Chemical Geology, v. 161, no. 1–3, p. 37-57.

Jiang, G., Kennedy, M. J., and Christie-Blick, N., 2003, Stable isotopic evidence for methane seeps in Neoproterozoic postglacial cap carbonates: Nature, v. 426, no. 6968, p. 822-826.

Kakihana, H., Kotaka, M., Satoh, S., Nomura, M., and Okamoto, M., 1977, Fundamental Studies on the Ion-Exchange Separation of Boron Isotopes: Bulletin of the Chemical Society of Japan, v. 50, no. 1, p. pp.158-163.

Kasemann, S. A., Meixner, A., Rocholl, A., Vennemann, T., Rosner, M., Schmitt, A. K., and Wiedenbeck, M., 2001, Boron and Oxygen Isotope Composition of Certified Reference Materials NIST SRM 610/612 and Reference Materials JB-2 and JR-2: Geostandards Newsletter, v. 25, no. 2-3, p. 405-416.

Kasemann, S. A., Prave, A. R., Fallick, A. E., Hawkesworth, C. J., and Hoffmann, K.-H., 2010, Neoproterozoic ice ages, boron isotopes, and ocean acidification: Implications for a snowball Earth: Geology, v. 38, no. 9, p. 775-778.

Kasemann, S. A., Schmidt, D. N., Bijma, J., and Foster, G. L., 2009, In situ boron isotope analysis in marine carbonates and its application for foraminifera and palaeo-pH: Chemical Geology, v. 260, no. 1-2, p. 138-147.

Kaufman, A. J., Hayes, J. M., Knoll, A. H., and Germs, G. J. B., 1991, Isotopic composition of carbonates and organic-carbon from upper Proterozoic successions in Namibia - Stratigraphic variation and the effects of diagenesis and metamorphism: Precambrian Research, v. 49, no. 3-4, p. 301-327.

Kaufman, A. J., Jacobsen, S. B., and Knoll, A. H., 1993, The Vendian record of Sr and C isotopic variations in seawater: Implications for tectonics and paleoclimate: Earth and Planetary Science Letters, v. 120, no. 3–4, p. 409-430.

Kempe, S., and Kazmierczak, J., 2002, Biogenesis and Early Life on Earth and Europa: Favored by an Alkaline Ocean?: Astrobiology, v. 2, no. 1, p. 123-130.

Klochko, K., Kaufman, A. J., Yao, W., Byrne, R. H., and Tossell, J. A., 2006, Experimental measurement of boron isotope fractionation in seawater: Earth and Planetary Science Letters, v. 248, no. 1-2, p. 276-285.

Lemarchand, D., Gaillardet, J., Lewin, E., and Allegre, C. J., 2000, The influence of rivers on marine boron isotopes and implications for reconstructing past ocean pH: Nature, v. 408, no. 6815, p. 951-954.

Li, Z.-X., Evans, D. A. D., and Halverson, G. P., 2013, Neoproterozoic glaciations in a revised global palaeogeography from the breakup of Rodinia to the assembly of Gondwanaland: Sedimentary Geology, v. 294, no. 0, p. 219-232.

Liu, C., Wang, Z., and Raub, T. D., 2013, Geochemical constraints on the origin of Marinoan cap dolostones from Nuccaleena Formation, South Australia: Chemical Geology, v. 351, no. 0, p. 95-104.

Ma, G., Li, H., and Zhang, Z., 1984, An investigation of the age limits of the Sinian System in South China: Bulletin of Yichang Institute of Geology Mineral Resources, v. 8, p. 1-29.

Meert, J. G., Gibsher, A. S., Levashova, N. M., Grice, W. C., Kamenov, G. D., and Ryabinin, A. B., 2011, Glaciation and ~ 770 Ma Ediacara (?) Fossils from the Lesser Karatau Microcontinent, Kazakhstan: Gondwana Research, v. 19, no. 4, p. 867-880.

Miller, N. R., Stern, R. J., Avigad, D., Beyth, M., and Schilman, B., 2009, Cryogenian slate-carbonate sequences of the Tambien Group, Northern Ethiopia (I): Pre-"Sturtian" chemostratigraphy and regional correlations: Precambrian Research, v. 170, no. 3–4, p. 129-156.

Miller, R. M., 2008, The geology of Namibia: Palaeozoic to Cenozoic, Windhoek, Geological Survey, Namibia.

Palmer, M. R., Spivack, A. J., and Edmond, J. M., 1987, Temperature and pH controls over isotopic fractionation during adsorption of boron on marine clay: Geochimica et Cosmochimica Acta, v. 51, no. 9, p. 2319-2323.

Paris, G., Bartolini, A., Donnadieu, Y., Beaumont, V., and Gaillardet, J., 2010, Investigating boron isotopes in a middle Jurassic micritic sequence: Primary vs. diagenetic signal: Chemical Geology, v. 275, no. 3-4, p. 117-126.

Raub, T. D., Evans, D. A. D., and Smirnov, A. V., 2007, Siliciclastic prelude to Elatina–Nuccaleena deglaciation: lithostratigraphy and rock magnetism of the base of the Ediacaran system: Geological Society, London, Special Publications, v. 286, no. 1, p. 53-76.

Sanyal, A., Nugent, M., Reeder, R. J., and Bijma, J., 2000, Seawater pH control on the boron isotopic composition of calcite: evidence from inorganic calcite precipitation experiments: Geochimica et Cosmochimica Acta, v. 64, no. 9, p. 1551-1555.

Shields, G. A., 2005, Neoproterozoic cap carbonates: a critical appraisal of existing models and the plumeworld hypothesis: Terra Nova, v. 17, no. 4, p. 299-310.

Spivack, A. J., 1986, Boron isotope geochemistry [Ph.D.: Massachusetts Institute of Technology], 184 p.

Spivack, A. J., and Edmond, J. M., 1987, Boron isotope exchange between seawater and the oceanic crust: Geochimica et Cosmochimica Acta, v. 51, no. 5, p. 1033-1043.

Spivack, A. J., and You, C.-F., 1997, Boron isotopic geochemistry of carbonates and pore waters, Ocean Drilling Program Site 851: Earth and Planetary Science Letters, v. 152, no. 1–4, p. 113-122.

Veizer, J., Ala, D., Azmy, K., Bruckschen, P., Buhl, D., Bruhn, F., Carden, G. A. F., Diener, A., Ebneth, S., Godderis, Y., Jasper, T., Korte, C., Pawellek, F., Podlaha, O. G., and Strauss, H., 1999, 87Sr/86Sr, δ13C and δ18O evolution of Phanerozoic seawater: Chemical Geology, v. 161, no. 1–3, p. 59-88.

Xiao, S., McFadden, K. A., Peek, S., Kaufman, A. J., Zhou, C., Jiang, G., and Hu, J., 2012, Integrated chemostratigraphy of the Doushantuo Formation at the northern Xiaofenghe section (Yangtze Gorges, South China) and its implication for Ediacaran stratigraphic correlation and ocean redox models: Precambrian Research, v. 192-195, no. 0, p. 125-141.

Zhang, J. M., Li, G., Zhou, C. M., Zhu, M. Y., and Yu, Z., 1997, Carbon isotope profiles and their correlation across the Neoproterozoic-Cambrian boundary interval on the Yangtze Platform, China: Bulletin of National Museum of Natural Science, v. 10, p. 107-116.

Zhu, M. Y., Zhang, J., Steiner, M., Yang, A., Li, G., and Erdtmann, B.-D., 2003, Sinian-Cambrian stratigraphic framework for shallow-to-deep-water environments of the Yangtze Platform: an integrated approach: Progress in Natural Science, v. 13, no. 12, p. 951-960.

CHAPTER 3:

OCEAN PH AND WEATHERING CONDITIONS DURING THE UPPER EDIACARAN: INSIGHTS FROM THE CHINESE GAOJIASHAN SECTION

Manuscript in preparation for submission to *Earth and Planetary Science Letters*.

Antonia Gamper provided $\delta^{13}C_{carb}$ and $\delta^{18}O$ isotope data and helped with the interpretation of biologically related proxy data. Anette Meixner prepared the lithium samples and conducted the $\delta^{7}Li$ isotope measurements. Additionally, she wrote most of the Li methods chapter (see 3.4.2) and assisted with lithium data interpretation. Simone Kasemann helped during data interpretation and supported me with comments on the late-stage manuscript versions.

Ocean pH and weathering conditions during the upper Ediacaran: Insights from the Chinese Gaojiashan Section

Frank Ohnemueller[1], Antonia Gamper[2], Anette Meixner[1], Shao-Yong Jiang[3], Simone A. Kasemann[1]

[1]Department of Geosciences and MARUM - Center for Marine Environmental Sciences, University of Bremen, Leobener Str., D-28359 Bremen
[2]Museum für Naturkunde Berlin, Invalidenstr. 43, D-10115 Berlin
[3]State Key Laboratory for Mineral Deposits Research, Department of Earth Sciences, Nanjing University, CN-210093 Nanjing

3.1 Abstract

The Ediacaran to Cambrian transition was a decisive time in Earth's history since substantial changes in ocean-atmosphere interactions, climate, tectonics and biogeochemical processes presumably catalyzed the advent and radiation of metazoa.

In this study, we investigate the boron, lithium and strontium isotope records at the Gaojiashan Section (551-542 Ma) in southwestern Shaanxi, South China to get detailed insights into changing ocean pH and weathering conditions. The 75 m thick, carbonate-siliciclastic section is located at the northwestern margin of the Ediacaran Yangtze Platform and displays a near shore shallow water setting. A pronounced negative $\delta^{13}C_{carb}$ excursion to -6‰ similar to the global Precambrian-Cambrian (PCC) boundary peak is observed in the upper part of the Gaojiashan Member. This isotope pattern is matched by a negative $\delta^{11}B$ excursion with a relative shift of -14‰, interpreted as a temporarily ocean acidification event of ~1.5 pH units. At the same time, Sr isotopes display a positive excursion ($^{87}Sr/^{86}Sr$ 0.7085 to 0.7110) indicating a time of enhanced weathering in times of relative sea-level fall. Further evidence for silicate weathering in a transport-limited regime is given by a corresponding short-lived negative excursion of -11‰ in $\delta^{7}Li_{carb}$.

Keywords: ocean pH, weathering, boron, strontium, lithium, Ediacaran

Highlights

- We investigate the B, Li and Sr isotope record of the Precambrian-Cambrian (PCC) boundary.
- We present a multi-proxy geochemical dataset of the Gaojiashan Section, South China.
- The isotope record indicates a temporary and large-magnitude decrease in ocean pH.
- A simultaneous increase in weathering input to the ocean during the terminal Ediacaran is observed.
- The PCC boundary interval is characterized by temporary acidic, euxinic to anoxic shallow water conditions.

3.2. Introduction

The terminal Ediacaran was a crucial time in Earth's history. A more complex ecosystem and significant changes in ocean (redox-) geochemistry, climate, tectonics and biogeochemical processes as well as major perturbations in the carbon cycle and successive oxygenation of the oceans likely triggered the advent and radiation of metazoa during the early Cambrian (Bjerrum and Canfield, 2011; Canfield et al., 2007; Halverson and Hurtgen, 2007; Halverson et al., 2010; Johnston et al., 2012; Kaufman et al., 1993; Kennedy et al., 2006; Kouchinsky et al., 2012; Peters and Gaines, 2012; Smith and Harper, 2013).

Here we present a multi-proxy geochemical approach to investigate variations in ocean pH conditions by the isotopic system of boron ($\delta^{11}B$), try to quantify weathering fluxes and to distinguish between different kinds and systematics of continental weathering by strontium and lithium isotopes ($^{87}Sr/^{86}Sr$ and $\delta^{7}Li$). To test the linkage between changing ocean conditions and the remarkable bioradiation in the terminal Ediacaran to Early Cambrian transition we have to document the environmental conditions during this time period, which are in turn preserved in the marine carbonates. It is generally known, that ocean pH fluctuations and especially ocean acidification have extensive effects on organisms and habitats (e.g. Raven et al., 2005; Wootton et al., 2008). Organism life cycles and metabolisms as well as shell and skeleton calcification rates are likewise heavily influenced by the acidity of the seawater (Raven et al., 2005)

and major variations in ocean alkalinity serving as ocean pH buffer. Hence, substantial changes in ocean pH and nutrient (e.g. amino acids, carbohydrates, lipids, Si, N, P, Fe, Mg^{++} and Ca^{++}) supply to the ocean induced by enhanced continental weathering rates may be basic prerequisites for the spreading of organisms at the PCC interval (Zhang et al., 2014b and references therein). Moreover, variations in seawater pH could have led to an extinction or at least poisoning of the Ediacaran fauna with a subsequent development of new niches, possibly enabling the advent of metazoa.

Background B, Li, Sr

So far, boron isotope data and associated pH calculations only exist for the Phanerozoic (e.g. Hönisch et al., 2008; Paris et al., 2010a; Pearson and Palmer, 1999) and the lower and middle Neoproterozoic (Kasemann et al., 2005; Kasemann et al., 2010). On that account, our study provides the first boron dataset for the Precambrian-Cambrian interval. Ocean acidification events associated with enhanced atmospheric pCO_2 in ancient times are for example known from the aftermath of the Marinoan glaciation at ~635 Ma (Kasemann et al., 2010; Ohnemueller et al., in review). At that time, an ocean pH decrease of up to 1.5 pH units during cap dolomite deposition happens most probably due to a re-enabled ocean-atmosphere interplay after a time interval of non-exchange during the glacial period.

The degree and kind of weathering with its associated nutrient availability can be constrained by the isotopic system of strontium and lithium. Major modifications in nutrient accessibility could be one of the main causes for the occurrence and spread of metazoans in the earliest Cambrian. During the later Neoproterozoic a general increase in weathering rates and bioproductivity (Jacobsen and Kaufman, 1999; Peters and Gaines, 2012; Shields, 2007) led to a steep rise in seawater $^{87}Sr/^{86}Sr$ with ratios varying between 0.7085-0.7090 (Halverson et al., 2007; Halverson et al., 2010; Kennedy et al., 2006; Shields-Zhou and Zhu, 2013) for the Precambrian-Cambrian transition. Sawaki et al. (2008) and Sawaki et al. (2014) even report a short-lived $^{87}Sr/^{86}Sr$ positive excursion of up to 0.7110 for the PCC boundary at the Yangtze Platform.

In order to assess the role of silicate weathering recently lithium isotopes studies came into attention (e.g. Burton and Vigier, 2012; Kisakurek et al., 2005; Vigier et al., 2008). Since Li datasets of marine carbonates and especially pre-Phanerozoic Li studies are sparse, little is known about the lithium isotopic composition of the Ediacaran

seawater. For the Cenozoic (~60 Ma, Misra and Froelich, 2012) and the Cretaceous (OAE2, Pogge von Strandmann et al., 2013) δ^7Li_{sw} is up to 10‰ lower compared to modern δ^7Li_{sw} of ~31‰. Similar to strontium, lithium is well mixed in the ocean due to a long residence time of ~1.2 Ma (Misra and Froelich, 2012) and thus gives valuable insights into changing weathering conditions. Besides, lithium isotopes are an eminently suitable tracer to reveal silicate weathering rates and to distinguish between congruent and incongruent weathering or transport- versus weathering-limited regimes (Kisakurek et al., 2005; Misra and Froelich, 2012; Pogge von Strandmann et al., 2010; Pogge von Strandmann et al., 2013; Tomascak, 2004).

3.3. Geological setting

In South China, the northwestern margin of the Yangtze Platform comprises largely continuous marine successions of Neoproterozoic to Cambrian rocks. The investigated Gaojiashan Section is located in Ningqiang County, southwestern Shaanxi Province (Fig. 8) and provides access to a widely undisturbed ~75 m thick carbonate-siliciclastic succession (Cai et al., 2013; Lin et al., 1986, Fig. 9).

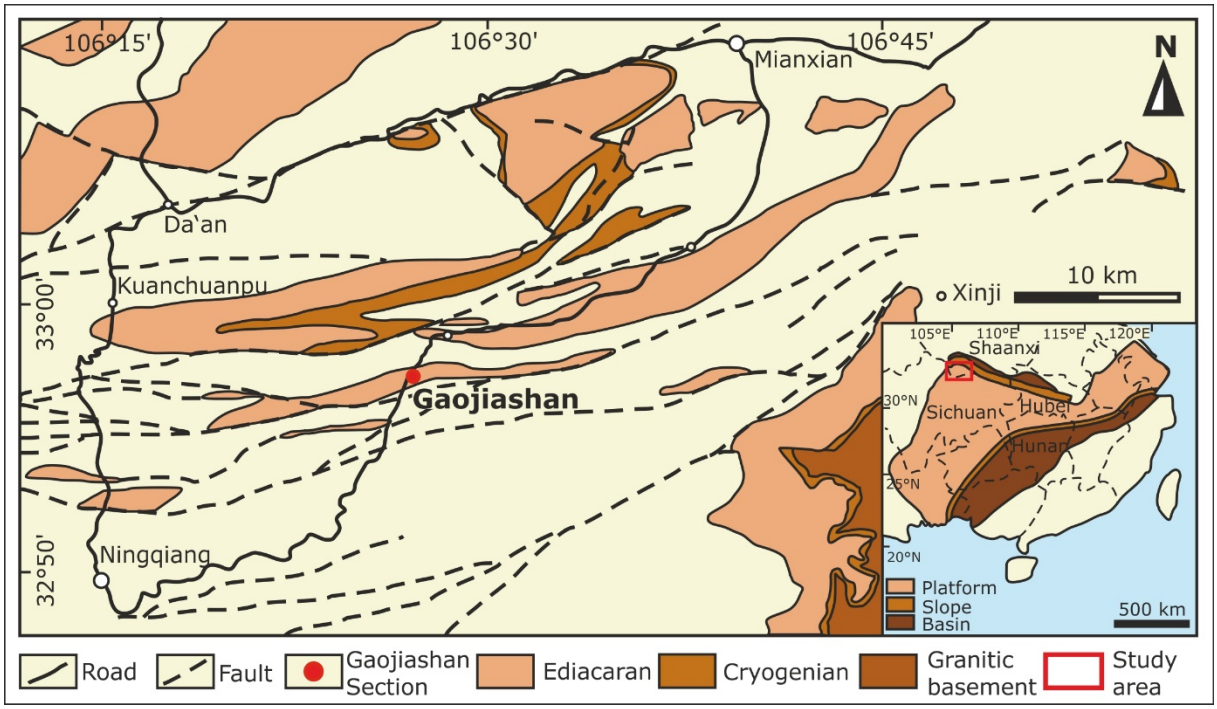

Figure 8: Geological map (modified after Cai et al., 2010) of southern Shaanxi Province. Gaojiashan Section is indicated by the red solid circle. Inset map marks the section's location within the Ediacaran Yangtze Platform.

Due to its unique combination of well-preserved strata, substantial fossil record and only very light tectonic history without obvious strong structural deformation or folding (Cai

et al., 2010), the Gaojiashan Section is one of the most suitable sections to analyze the terminal Neoproterozoic environmental changes leading to the Cambrian (R)evolution.

Generally, the Yangtze Platform possesses a broad facies diversity from shallow-water to deep-basin environments (Zhu et al., 2003). Sedimentary, chemo- and biostratigraphical data indicate a transgressive-regressive cycle with times of enhanced bioactivity in an overall tide- and storm-dominated, temporarily restricted or protected shallow-marine palaeo-environment at the Gaojiashan Section (Scouflaire et al., 2010). Age constraints of northern Yangtze Platform sections are solely based on lithostratigraphical correlations. Yet, it is generally accepted that the Gaojiashan Section hosts ~551-542 Ma old rocks corresponding to the Dengying Formation (Cai et al., 2013; Li, 2008; Meyer et al., 2012). At the carbonate dominated northern platform rim, the total thickness of the Dengying Formation ranges from ~15 m to >400 m. Except for the carbonate-siliciclastic mixture of the Gaojiashan Member, most of the Dengying Formation in Shaanxi is made of monotonous shallow-marine and lagoonal lime- and dolostones. Further to the South, Dengying strata become more condensed and transform to predominantly cherts at the slope and basinal part of the Yangtze Platform (Goldberg et al., 2005). The type locality, Gaojiashan Section, is well exposed on a mountain trail (32°57'29.48"N, 106°27'33.80"E) with strata dipping to the North at 80° angle. In ascending order strata consists of the Algal Dolomite, Gaojiashan, and Beiwan Member (Fig. 9) being reported as equivalents of the Hamajing, Shibantan, and Baimatuo Member of the Three-Gorges-Area (Zhu et al., 2007; Zhu et al., 2003). The Algal Dolomite Member is characterized by thick-bedded, light-grey lagoonal dolomites with increasing cm-scale silt- and sandstone interbeds within the uppermost two meters. The overlaying lowermost 12 m of the Gaojiashan Member host an alternation of dolomitic shales and fine-bedded calcareous clay- to siltstones with increasing coarse-grained sandy dolomite beds within the uppermost 2 m. Up-section an alternation of calcareous sandstones and sandy dolomites is present until 24 m. The middle part of the Gaojiashan Member is comprised of dolomitic clay- to siltstones with abundant cm-scale micritic limestone beds. The upper part shows a transition from predominantly biolaminated calcarenites alternating with micritic limestone beds to a capping well-sorted quartzose sandstone with calcareous cement. All three main fossil assemblages of the Gaojiashan Section (*Shaanxilithes*, *Gaojiashania*, and *Cloudina* biozone) are located within the Gaojiashan Member (Fig. 9) and described in detail by various

authors (Cai et al., 2013; Cai et al., 2010; Hong et al., 2007; Meyer et al., 2012; Weber et al., 2007). The Gaojiashan Member is overlain by the Beiwan Member, which is composed of homogenous white-grey dolostones with only few clay interbeds.

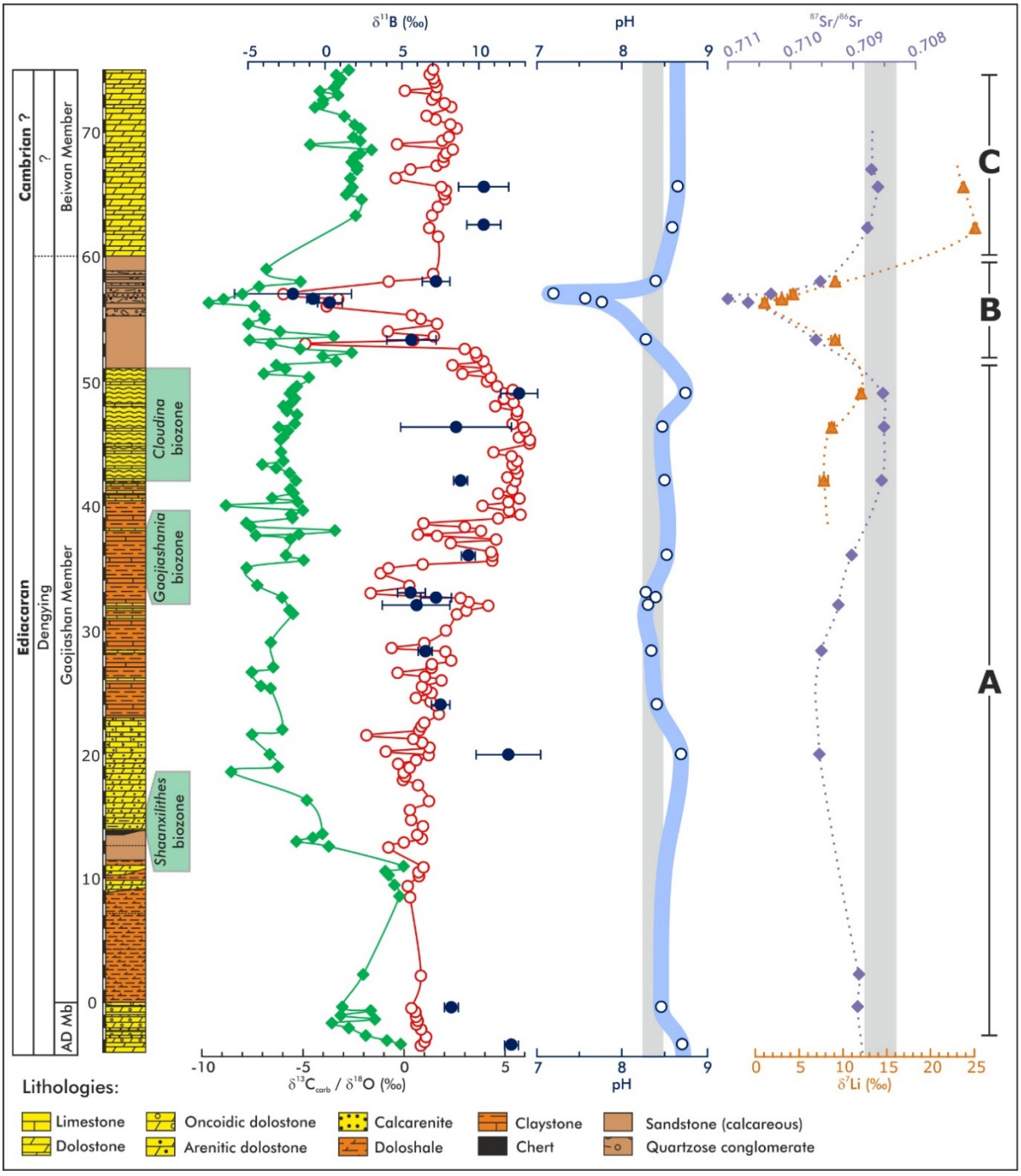

Figure 9: *Stratigraphic column of the Gaojiashan Section after Scouflaire et al. (2010) with corresponding $\delta^{11}B$ (dark blue) $^{87}Sr/^{86}Sr$ (violet), $\delta^{7}Li$ (orange) data. $\delta^{13}C_{carb}$ (red) and $\delta^{18}O$ (green) by Gamper et al. (2012). Inferred ocean pH development is indicated by light blue curve, while grey bars mark average ocean pH composition of supposed Neoproterozoic climate normalcy (Kasemann et al., 2010) and Sr isotopic composition of late Ediacaran open ocean conditions (Halverson et al., 2010) respectively. A, B, C display different palaeo environmental setting shown in figure 11. AD Mb - Algal Dolomite Member*

Recent studies suggest that the central northern margin of the Yangtze Platform represents a north-(east)ward deepening slope transitioning into a small ocean basin instead of a simple shallow carbonate platform setting (e.g. Cai et al., 2013; Cremonese et al., 2013; Wang et al., 2012). Sedimentary data of the Gaojiashan Section are typical for a near-shore, shallow-water setting defined by a pro- and retrograding delta front. Changing relative sea levels led to alternating phases of dominating carbonate precipitation or siliciclastic deposition.

3.4 Methods

3.4.1 Sample selection

Owing to the great age of the studied rocks and the susceptibility of the isotopic systems for diagenesis, a detailed alteration evaluation beginning with the sample selection is necessary. Samples were collected from the Ediacaran Algal Dolomite, Gaojiashan and Beiwan Member. Fresh rock hand specimen carefully selected by their uniformity, e.g. the absence of veins or visible alteration rims, were taken in 20-50 cm intervals along the ~75 m long succession. In order to trace potential diagenetic overprint thin section analyses, cathodoluminescence imaging, trace element concentration and oxygen isotope measurements were performed. Rock powders were prepared from pre-screened, cleaned, fresh surface rock chips with an agate vibratory disc mill at the Museum fuer Naturkunde Berlin, Germany.

Post-depositional alteration

Generally, Mn concentrations are enriched during diagenesis whilst Sr concentrations, $\delta^{13}C$, $\delta^{11}B$, $\delta^{7}Li$ and $\delta^{18}O$ values decrease (e.g. Derry et al., 1992; Kaufman et al., 1993; Paris et al., 2010a; Pogge von Strandmann et al., 2013; Veizer et al., 1999). Thus, high Mn/Sr can indicate secondary alteration, however the liability of this proxy for Neoproterozoic carbonates is doubted by several authors because it is also depending on the primary precipitated carbonate mineral phase (Derry, 2010) and high Mn/Sr ratios can be present for carbonates precipitated in early diagenetic anoxic waters (Miller et al., 2009). Analyzed samples showed an average Mn and Sr concentration of ~400 µg g^{-1} and ~350 µg g^{-1}, respectively. Samples possessing Mn concentrations of >1000 µg g^{-1} together with Mn/Sr ratios >10 were excluded, although increased Mn

and Fe concentrations in seawater can also hint towards absence of abundant oxygen and sulfate necessary for redox reactions (Miller et al., 2009; Raub et al., 2007).

Additionally, all analyzed samples show $\delta^{18}O$ values >-10‰, which is also suggested as alteration criteria (e.g. Bartley et al., 1998; Li et al., 2013; Ling et al., 2007). No obvious correlation between $\delta^{13}C_{carb}$ and $\delta^{18}O$ within the 5% significance level (R^2=0.0003, see Fig. 13 in supplement, chapter 3.10) exists. The lower part of the section was suspected to be possibly influenced by hydrothermal fluids. The manner and intensity in which the primary $\delta^{11}B$ values are changed by this process is strongly depended on the fluid pH and boron concentration, which is typically highly enriched. In our study samples showing a combination of $\delta^{11}B$ >15‰ and high boron concentrations were excluded.

Clay contamination

In general, Gaojiashan Section carbonates comprise minor to major amounts of clay minerals, especially accumulated in pore space. Dissolution of B and Li bearing clays would lead to an enrichment in boron and lithium concentrations. To avoid clay contamination during chemical sample preparation, samples used for isotope analyses were carefully selected after SEM (scanning electron microscopy) imaging performed at the Paleontology Department of the University of Bremen, Germany and XRD (x-ray diffraction) analyses done at the ZEKAM, University of Bremen, Germany. Enriched Al concentrations in combination with enhanced B concentrations can be indicative for the dissolution of clays. However, neither a correlation between Al and B concentrations (R^2=0.18) nor a correlation of B concentration and $\delta^{11}B$ values (R^2=0.04) exist. Additionally, lithium leaching tests and lithium concentration measurements of the carbonate and detrital fraction determined that no clay contamination is obvious (details in supplement, chapter 3.10).

3.4.2 Analytical techniques

The whole carbon and oxygen isotope dataset is based on 150 bulk rock samples measured on a Thermo Finnigan GASBENCH II linked online to a Thermo Finnigan DELTA V isotope ratio mass spectrometer at the Museum fuer Naturkunde Berlin, Germany. Isotopic measurements of B, Li and Sr were conducted in the Isotope Geochemistry Laboratory at the Department of Geosciences and MARUM, University of Bremen.

Boron isotope analyses were performed following the method detailed in Kasemann et al. (2001). For analyses 10 mg of the sample powder were dissolved in 100 µl 1 N HCl for 24 h at 20°C and centrifuged afterwards. The $n(^{11}B)/n(^{10}B)$ measurements were performed on a Thermo Fisher Scientific TRITON *Plus* mass spectrometer, using negative thermal ionization mass spectrometry (N-TIMS). 1 µl boron-free seawater emitter was placed on a degassed Re single filament and dried at 0.7 A. Subsequently, 1 µl of the sample solution containing ~1 ng B was added, evaporated to complete dryness at 0.7 A and afterwards heated at 1.2 A for 30 s. Boron isotopes were registered as BO_2^- complexes on masses 42 and 43, and measurements were carried out at 970°-1050°C typically with an ion beam intensity of 3-30 pA on mass 43. Each measuring process consisted of up to 200 blocks with 10 cycles, taking about 3 hours of data acquisition. To correct for a CNO^- interference on mass 42 occurring at the beginning of some measurements and for isotopic fractionation during analysis, the extrapolation technique described by Kasemann et al. (2001) was used during data evaluation.

Boron isotope ratios are given in $\delta^{11}B$-notation relative to the certified reference material NIST SRM 951 that showed an $^{11}B/^{10}B$ ratio of 4.0065±0.0019 (2sd<0.5‰, n=45 over a period of 15 month). In addition to the NIST material, the standard material M93-TB-FC-1, a *Porites* coral with a published value of 24.8±0.4‰ ($2\sigma_{mean}$), as determined by different multicollector techniques (Kasemann et al., 2009), was also regularly analyzed. The coral was reproduced with a $\delta^{11}B$ value of 24.1±0.7‰ (2sd, n=16). Samples were analyzed at least twice and their reproducibility (2sd) is given in table 2.

Sr separation methods of Pin and Bassin (1992) and Deniel and Pin (2001) were slightly modified and adapted for differing resin-volumes and rock-types used in this study. Isotope measurements were performed on a Thermo Fisher Scientific TRITON *Plus* mass spectrometer on Re single filaments with a Ta emitter (Birck, 1986). The total strontium blank of this procedure is <40 pg. Strontium isotopic ratios are given in $^{87}Sr/^{86}Sr$ notation and were normalized to $^{86}Sr/^{88}Sr$ of 0.1194. The external reproducibility according to the NIST SRM 987 reference material is $^{87}Sr/^{86}Sr$ 0.710247±14 (2sd, n=50; period: January 2012 to September 2012).

Prior to lithium isotope measurements a very accurate sample preparation is necessary. From every sample three fractions were obtained: (1) the water soluble fraction, (2) the carbonate fraction and (3) the silicate fraction in order to explore their

contribution to the Li budget of the sample. About 300 mg of powdered sample material were weighed in a Savillex beaker. First, samples were treated with 3 ml MQ water. Subsequently the samples were centrifuged and their residue washed twice with 0.5 ml MQ water. The collected water soluble fraction was dried and dissolved in 0.15 N HCl. In the second step, 0.5 N HCl was added to the water washed sample until the ongoing reaction has stopped and the carbonate fraction was completely dissolved. Afterwards, the samples were washed twice with MQ water and centrifuged. The collected carbonate fraction was dried and dissolved in 0.15 N HCl. The remainder of the sample is mostly composed of silicates, which were quantitatively digested with HF/HNO_3, dried and dissolved in 4 N HCl. A split of every fraction was used to analyze the Li concentration. The results show that the water soluble fractions contain less than 1% of the total sample Li content, up to 20% of the lithium is fixed in the carbonate phases and most of lithium derives from the silicates.

Lithium must be quantitatively separated from the sample matrix, because the loss of only 1% of Li during column separation as well as the presence of Na can result in significant isotopic shifts (James and Palmer, 2000; Jeffcoate et al., 2004; Moriguti and Nakamura, 1998; Nishio and Nakai, 2002). The best results were attained by the 3 to 4 step separation procedure of Moriguti and Nakamura (1998). Small column sizes and the use of HCl and HCl/EtOH instead of HNO_3/Methanol (e.g. Jeffcoate et al., 2004; Krienitz et al., 2012; Tomascak et al., 1999) allow to handle small sample sizes and minimize blank input. Column separation step 1 and 2 were performed in BioRad Biospin columns, the third step to separate Li from Na was established in Teflon columns (ID 5 mm). All columns were filled with 1 ml of AG-50W-X8 cation exchange resin. Fractions (1) and (2) were passed through the separation steps 2+3 of the column separation procedure. Lithium of the silicate fraction (3) was separated using column steps 1 to 3. Possible loss of lithium during the separation procedures, which could cause isotopic fractionation, was monitored by scanning the Li concentration of the head and the tail of the Li fractions. During the multi-step separation more than 99.7% of Li of the sample were collected. NIST 8545 and a procedural blank or internal seawater standard were processed together with each sample series. Procedural blanks were less than 94 pg Li and without influence on to the isotopic composition of the samples. All isotope analyses where performed on a MC-ICP MS (Thermo Fisher Scientific NEPTUNE *Plus*) equipped with the SIS (stable introduction system: double pass Quartz spray chamber

+ 50 µl PFA nebulizer; TFS) and a high-efficiency X-cone. Matrix and concentration matched samples and standards (dilution in 2% HNO_3 to 25 ± 1.25 ppb Li) where measured repeatedly by standard-sample bracketing with untreated NIST 8545. The solvent was monitored before and after each measurement. The average of these two measurements represents the analytical baseline and was used for correction. Li isotopes are given in delta notation relatively to untreated NIST 8545. The reference material NIST 8545 processed through the whole separation procedure shows a δ^7Li value of 0.03±0.22‰ (2sd, n=13; Jan to Jul 2013). Measured seawater serving as external reproducibility control shows a δ^7Li of 30.90±0.16‰ (2sd, n=2) which agrees very well with published data (James and Palmer, 2000).

Trace element concentration measurements (see table 2 and additional data summarized in table 3 of the supplemental material) were conducted on an Agilent Technologies 700 Series ICP-OES at the inorganic geochemistry group of the MARUM/University of Bremen, Germany. Three replicates of each dilution were measured and typically had a relative standard deviation (RSD) of better than 3% (excepting boron, which was <10%).

REE+Y measurements were carried out on a Thermo Fisher Scientific Element XR ICP-MS with an external calibration to the modern carbonate reference material CAL-S (Yeghicheyan et al., 2003), an internal standardization and an interference correction for Eu at the Geochemistry Group of the Department of Earth Sciences, Freie Universität Berlin, Germany.

3.5 Results

Isotope and trace element data are listed in table 2.

3.5.1 Boron isotopes and concentrations

Trace element analyses (table 2) show an average boron concentration of <3 µg g^{-1} without any obvious relation to the carbonate content of the sample or the Mg/Ca ratio ranging between 0.008 and 0.574. δ^{11}B data generally range from -2.1‰ to 12.6‰. A systematic decrease from 12.2‰ in the Algal Dolomite Member to 5.6‰ in the middle Gaojiashan Member is visible. Subsequently, the values rise again to 12.6‰ in the upper part of the Gaojiashan Member. Afterwards, a prominent negative excursion

down to -2.1‰ is recorded in the uppermost Gaojiashan Member (53.3-57 m). The overlying Beiwan Member dolostones show again positive values of ~10.3-11‰.

Sample n°/[m]	Member	$\delta^{13}C$ (‰)	$\delta^{18}O$ (‰)	$\delta^{11}B$ (‰) (2sd)	pH	$^{87}Sr/^{86}Sr$ (2SE)	$\delta^{7}Li_{carb}$ (‰) (2sd)	B (ppm)	Ca (%)	Mg (%)	Mn (ppm)	Sr (ppm)	Mn/Sr	Mg/Ca
-3.30	Algal Dol. Mb	0.8	-0.1	12.1 ±0.1	8.7	0.709959 ±7	n.a.	6	28	16	232	68	3.4	0.54
-0.30	Algal Dol. Mb	0.3	-3.1	8.2 ±0.2	8.5	0.708928 ±6	n.a.	2	27	16	620	48	12.9	0.57
20.00	Gaojiash. Mb	1.2	-6.7	11.9 ±2.1	8.7	0.709541 ±6	n.a.	2	40	1	1102	348	3.2	0.03
24.00	Gaojiash. Mb	1.5	n.a.	7.5 ±0.6	8.4	n.a.	n.a.	n.a.	n.a.	n.a.	n.a.	n.a.		
28.30	Gaojiash. Mb	2.0	n.a.	6.5 ±0.2	8.3	0.709506 ±40	n.a.	2	40	1	985	362	2.7	0.01
32.00	Gaojiash. Mb	4.1	n.a.	5.9 ±2.2	8.3	0.709235 ±8	n.a.	2	40	0	401	404	1.0	0.01
32.60	Gaojiash. Mb	2.7	-6.1	7.2 ±1.0	8.4	n.a.	n.a.	3	40	0	922	427	2.2	0.01
33.00	Gaojiash. Mb	-1.7	n.a.	5.6 ±0.9	8.3	n.a.	n.a.	6	38	2	193	52	3.7	0.05
36.00	Gaojiash. Mb	4.3	-5.9	9.3 -	8.5	0.709022 ±6	n.a.	2	40	0	447	506	0.9	0.01
42.00	Gaojiash. Mb	5.4	-5.4	8.8 ±0.2	8.5	0.708542 ±10	7.8 ±0.5	3	40	0	248	1292	0.2	0.01
46.30	Gaojiash. Mb	5.9	-6.2	8.5 ±3.6	8.5	0.708505 ±8	8.7 ±0.3	2	40	0	151	1081	0.1	0.01
49.00	Gaojiash. Mb	5.3	-5.7	12.6 ±1.2	8.7	0.708522 ±10	12.1 ±0.3	3	39	2	207	1170	0.2	0.05
53.30	Gaojiash. Mb	0.4	-7.7	5.6 ±1.6	8.3	0.709592 ±8	9.1 ±0.5	1	37	4	184	130	1.4	0.11
56.30	Gaojiash. Mb	-3.8	-9.7	0.3 ±0.8	7.8	0.710678 ±6	1.1 ±0.3	2	38	4	277	138	2.0	0.10
56.60	Gaojiash. Mb	-3.3	-9.0	-0.8 ±0.4	7.6	0.711002 ±8	3.0 ±0.6	3	35	8	261	81	3.2	0.22
57.00	Gaojiash. Mb	-6.0	-8.0	-2.1 ±3.8	7.2	0.710310 ±5	4.3 ±0.3	3	28	15	662	48	13.8	0.53
58.00	Gaojiash. Mb	-0.8	-5.1	7.2 ±0.9	8.4	0.709521 ±8	9.1 ±0.2	6	28	15	24	110	0.2	0.54
62.60	Beiwan Mb	n.a.	n.a.	10.3 ±1.1	8.6	0.708773 ±8	25.1 ±0.2	4	28	15	123	92	1.3	0.56
65.60	Beiwan Mb	1.8	-2.6	10.3 ±1.8	8.7	0.708602 ±8	23.7 ±0.1	5	27	15	95	105	0.9	0.57
67.00	Beiwan Mb	0.3	-2.3	n.a.		0.708704 ±7	n.a.	n.a.	n.a.	n.a.	n.a.	n.a.		

Table 2: *Isotope data, trace element concentrations and ratios of Gaojiashan section carbonates. For complete $\delta^{13}C_{carb}$ and $\delta^{18}O$ isotope data and additional trace element data see supplement (chapter 3.10).Algal Dol. Mb.- Algal Dolomite Member; Gaojiash. Member - Gaojiashan Member.*

3.5.2 Strontium isotopes

Strontium isotopic composition and concentration data of the Gaojiashan Section are in good agreement to previously reported terminal Neoproterozoic values worldwide (e.g. Mongolia: Brasier et al. (1996), Namibia: Halverson et al. (2007), China: Li et al. (2013)). Sr concentrations of the Algal Dolomite and lower Gaojiashan Member vary from 48-427 µg g^{-1} (ø=190 µg g^{-1}). Between 36-49 m (Fig. 9) the Sr concentrations rise up to 1292 µg g^{-1} for sample GJ 42. Associated Mn/Sr ratios are particularly low (<0.2). Sr concentrations in the upper Gaojiashan Member and the overlying strata are similar to those in the lower part of the section, with an average of ~100 µg g^{-1}.

The $^{87}Sr/^{86}Sr$ ratios of the Gaojiashan Section range from 0.7085-0.7110. In the lower part of the succession the Sr values rise slightly from 0.7089 (Algal Dolomite Member) to 0.7095 (middle Gaojiashan Member). Subsequently, the values decrease to 0.7085 until 49 m before a sudden and distinct increase to $^{87}Sr/^{86}Sr$ ratios of 0.7110 takes place. This transient maximum is followed by a rapid decline to values of 0.7086 in the capping Beiwan Member.

3.5.3 Lithium isotopes

Within the upper part of the Gaojiashan Member, the lithium isotopic composition ranges from 1.1-25.1‰ in δ^7Li_{carb} (Fig. 9). Between 42-49 m the lithium values increases from 8 to 12‰ until a pronounced and short-lived negative excursion down to 1.1‰ is recorded. In the uppermost part of the Gaojiashan Member and in the overlying Beiwan Member the values rise again to 23.7‰. The detrital fraction shows a continuous increase in δ^7Li_{det} composition ranging from -0.2‰ to 17.2‰ (table 3, chapter 3.10). δ^7Li_{det} values display a positive excursion from -0.2‰ to 12.8‰ simultaneously to the negative anomaly in δ^7Li_{carb}.

3.5.4 Rare Earth element (REE+Y) data

Samples GJ 56.3, GJ 56.6 and GJ 57 were analyzed for their REE content. PAAS (Post Archean Australian Shale, Nance and Taylor (1976)) normalized REE+Y patterns (Fig. 10) exhibit HREE over LREE enrichment visible in PrN/YbN ratios of 0.35-0.52. Additionally a distinct Y/Ho anomaly of 1.39-1.44 is observed. The conspicuous positive Ce/Ce* anomaly for all three samples only develops under suboxic to euxinic conditions since Ce^{3+} is not oxidized to Ce^{4+}.

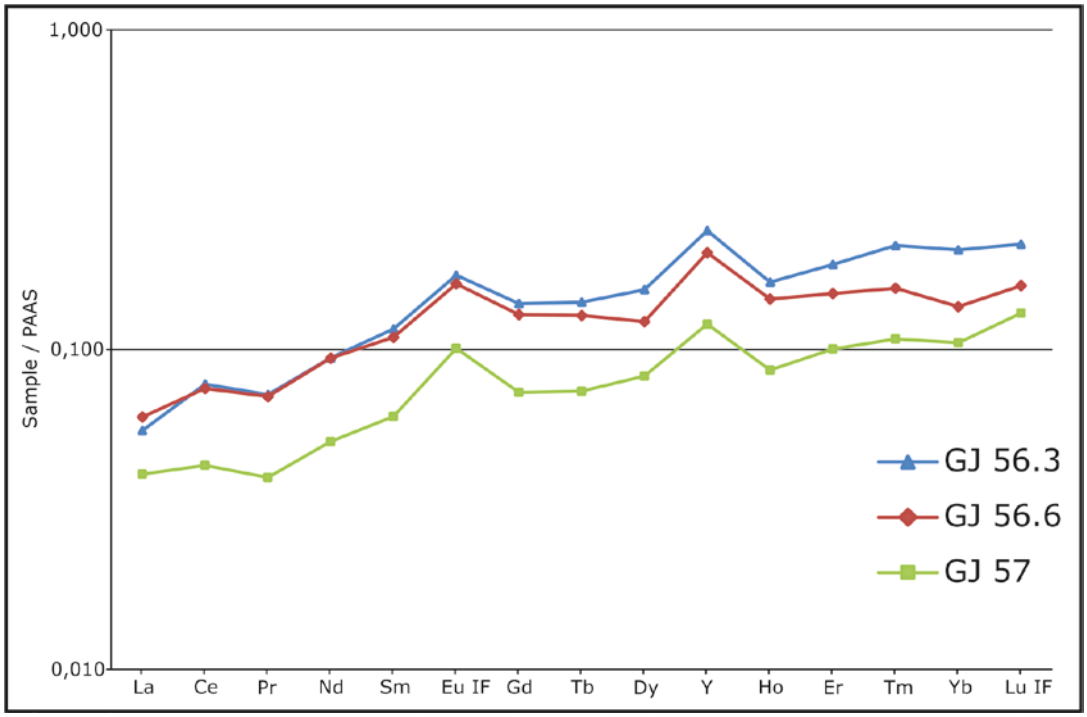

Figure 10: *Diagram shows shale-normalized REE+Y pattern of samples GJ 56.3, GJ 56.6 and GJ 57 within the uppermost Gaojiashan Member using the Post Archean Australian Shale (PAAS) normalization by Nance and Taylor (1976). All three samples show a typical seawater pattern with HREE enriched over LREE. Ce/Ce* (avg.: 1,144 after (Bau and Dulski, 1996)) ratios track the oxidation state of the ocean. A positive Ce anomaly is indicative for suboxic to euxinic conditions (German et al., 1991; Huang et al., 2011).*

3.6. Discussion

3.6.1 Ocean pH evolution

Palaeo pH reconstructions based on boron isotope analyses rely on the isotopic fractionation between the two dissolved boron species in the ocean: boric acid ($B(OH)_3$) and borate-ion ($B(OH)_4^-$) (Hemming and Hanson, 1992; Kakihana et al., 1977; Sanyal et al., 2000; Spivack, 1986). The $^{11}B/^{10}B$ exchange is described by the chemical reaction displayed in equation [1]:

$$^{11}B(OH)_3 + {}^{10}B(OH)_4^- <=> {}^{10}B(OH)_3 + {}^{11}B(OH)_4^- \quad [1]$$

Ocean pH reconstructions by boron isotope analyses are possible due to the pH dependence of the abundance of both species and their isotopic composition as well as the preferential incorporation of the tetrahedral species into carbonates (Hemming and Hanson, 1992). In detail, the relationship of ocean pH and the boron isotopic composition is given in equation [2]:

$$pH = pK_B - \log\left[- \frac{\delta^{11}B_{SW} - \delta^{11}B_{carb}}{\delta^{11}B_{SW} - \alpha_{B3\text{-}B4} \cdot \delta^{11}B_{carb} - 1000 \cdot (\alpha_{B3\text{-}B4} - 1)} \right] \quad [2]$$

To determine the ocean pH, knowledge of the seawater ($\delta^{11}B_{sw}$) and carbonate ($\delta^{11}B_{carb}$) boron isotopic composition, the dissociation constant of boric acid (pK_B) and the isotopic fractionation factor of boron ($\alpha_{B3\text{-}B4}$) is required.

The $\delta^{11}B_{sw}$ value during the terminal Ediacaran is supposed to be ~24‰ resting on the hypothesis of an continuous increase in $\delta^{11}B_{sw}$ from 20-23‰ (Kasemann et al., 2010) or 20.5‰ (Ohnemueller et al., in review) at 635 Ma, to 25‰ in the middle Devonian (halite value, that is suggested to display the seawater composition, Paris et al., 2010b). Joachimski et al. (2005) suggest a significant ^{11}B-depletion of up to 10‰ for Paleozoic seawater compared with the modern ocean composition. Assuming a boron fractionation factor of $\alpha_{B3\text{-}B4}$= 1.0272 between seawater and precipitated carbonates (Klochko et al., 2006), a seawater temperature of 25°C and an equilibrium constant pK_B of 8.579 (Dickson, 1990), the Gaojiashan carbonates likely record ocean pH conditions from 7.2 to 8.7 (for alternative assumptions see supplement). These remarkable fluctuations originate not only from global changes in the carbon cycle, e.g. atmospheric pCO_2 variations and related carbon/CO_2 influx into the ocean but also, and in this particular case very likely, from variations in bioproductivity, redox states, riverine alkalinity influx and changes in the environmental setting. The residence time of boron

in the ocean is ~14-20 Ma (Lemarchand et al., 2000; Spivack, 1986) and should be similar during the terminal Ediacaran. Since this duration is far bigger than the <10 Ma deposition time of the investigated strata, we postulate that ocean pH changes instead of variations in seawater $\delta^{11}B$ composition are recorded.

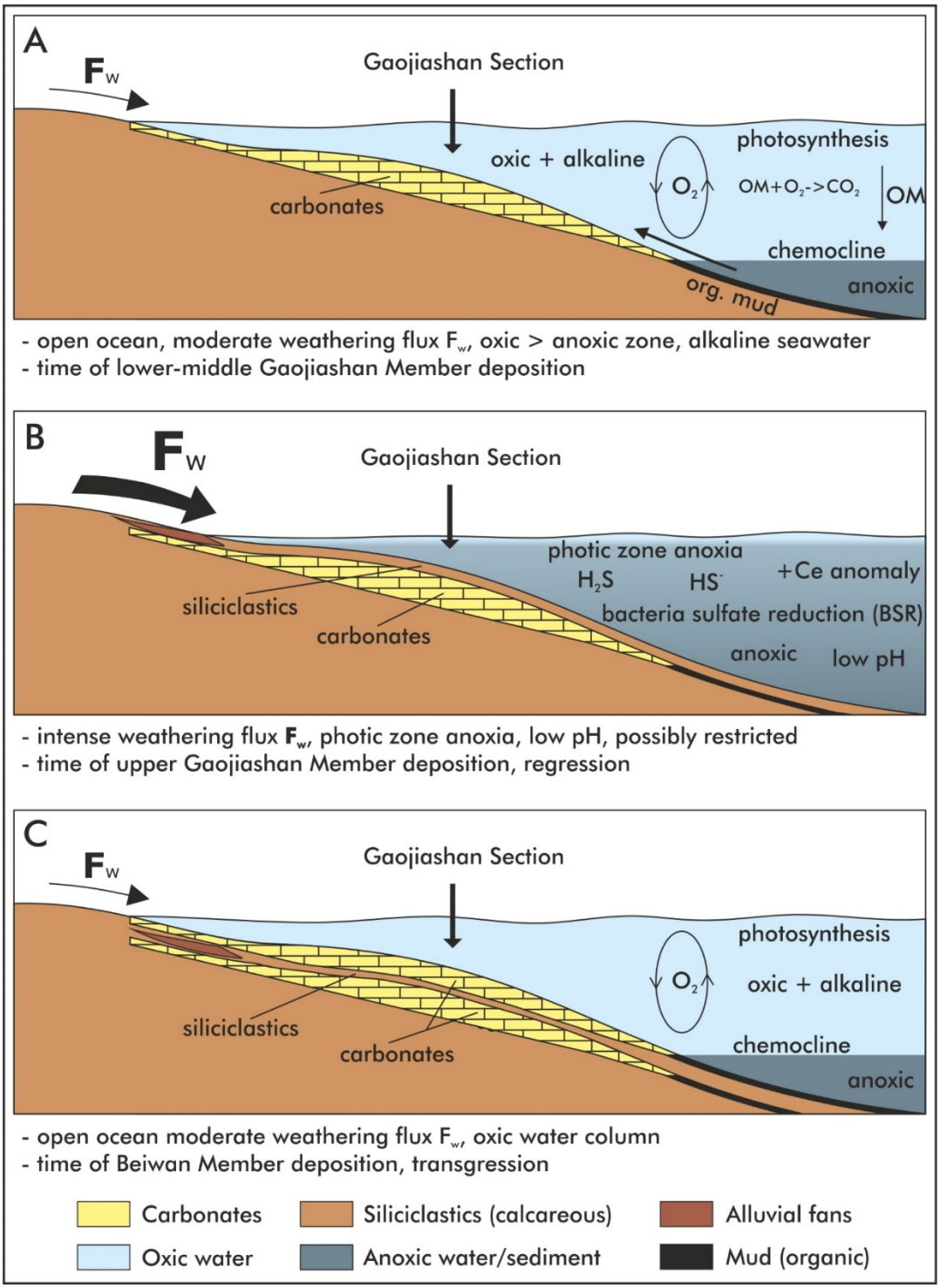

Figure 11: *Schematic palaeo environmental reconstructions through time at the Gaojiashan Section. Black arrows indicate the weathering intensity (F_w). A: Time of lower-middle Gaojiashan Member deposition; incipient shoaling of the chemocline. B: Time of upper Gaojiashan Member deposition, anoxic > oxic zone; BSR; low pH; H_2S and HS^- in the water column; regression. C: Time of Beiwan Member deposition; transgression*

In detail, the lower part of the Gaojiashan Section reveals slightly alkaline, open ocean conditions with an average ocean pH of ~8.6. Sedimentary data suggest a deltaic environment that is characterized by high riverine input fluxes to the ocean (Fig. 11A) leading to relatively high seawater pH conditions. Up to the middle part of the section, the pH sinks insignificantly to values of ~8.4. Afterwards a bloom of biological activity and propagation of organisms indicated e.g. by the *Gaojiashania* and *Cloudina* fossil record (Cai et al., 2013; Cai et al., 2010; Hong et al., 2007; Meyer et al., 2012; Weber et al., 2007) led to $\delta^{13}C_{carb}$ values of up to 5‰ because of preferential ^{12}C uptake by these organisms. This bio-radiation with its associated positive carbonate carbon excursion and enhanced organic carbon burial is also described by (Guo et al., 2012). Cai and Hua (2007) and Cai et al. (2012) define the investigated fossil assemblages as pyritized which is further indirect evidence for an alkaline water column and an anoxic sediment-water surface. Pyrite formation removes hydrosulfide ions (HS^-) out of the water column by its reaction with Fe^{2+} shifting the seawater to alkaline conditions. The enhanced organic matter export to the sea floor consequently enlarges the organic matter pool in the deepest water masses.

Generally, the enhanced biological activity leads to a shoaling chemocline, which continuously shrinks the oxic zone due to remineralization processes reducing the seawater O_2 content. Thus, anoxic conditions continuously rise from the sediment-water interface first to the deep water and subsequently into shallower water since this mechanism is self-reinforcing. Quinby-Hunt and Wilde (1994) stated that the seawater pH decreases as far as the pH of seafloor sediments is below 7 and therefore dominates the ocean pH buffers. Nitrogen and carbonate carbon data reported by Gamper et al. (2012) confirm the observation of an algal bloom and photic zone anoxia (Fig. 11B), respectively. That progression is also visible in the $\delta^{13}C_{carb}$ and $\delta^{11}B$ curve transitioning from positive values into the prominent negative peak in the upper Gaojiashan Member, representing a decrease in pH of 1.5 units to a minimal pH of 7.2 at 57 m. Two aspects induce this remarkable change in geochemical ocean conditions. On the one hand the open ocean environment most likely modifies to a restricted setting, as also suggested for this section by Zhang et al. (2014a). This modification happens due to relative sea level fall as indicated by lithological (from carbonates to sandstones) and facies (from shoreface to foreshore/tidal/coastal plain) changes. On the other hand, sulfate-reducing bacteria release large amounts of H_2S or HS^- into the water column resulting

in anoxic, acidic conditions (Mazumdar et al., 1999). The respiratory pathway of now dominating sulfate reduction operates as additional O_2 sink (Visscher and Stolz, 2005). Furthermore, several chemical reactions taking place in both, the uppermost, minimized oxic zone and directly in the anoxic layer are leading to a decrease in seawater pH values. Hydrogen sulfide produced by sulfate reducing bacteria reacts either (depending on pH) with the surrounding water to form hydrogen sulfide ions and hydronium ions [3] in the anoxic water body or with oxygen to form sulfate and hydrogen ions [4] in the oxygenated upper ocean (Tziperman et al., 2011):

$$H_2S + H_2O \rightarrow H_3O^+ + HS^- \quad [3]$$

$$HS^- + 2O_2 \rightarrow SO_4^{2-} + H^+ \quad [4]$$

Both reactions can lower the seawater pH. A modern analogue to the geochemical ocean conditions prevailing in times of most pronounced ocean acidification and anoxia is given by the Black Sea. It comprises an oxic surface layer overlying a minimized suboxic transition zone and a deeper euxinic to anoxic layer. The anoxic zone is composed of large amounts of organic matter and dominated by bacterial sulfate reduction resulting in release of abundant hydrogen sulfide to the seawater (e.g. Grégoire and Soetaert, 2010; Murray et al., 2007). Hence, the water column of the Black Sea displays increasing acidity with depth and generally low pH conditions combined with an anoxic environment (Polonsky, 2012).

These postulated euxinic or anoxic conditions are verified by associated REE data (Fig. 10). The observed positive Ce anomaly is of particular importance because it develops only under suboxic to euxinic conditions for the reason that Ce^{3+} is not oxidized to Ce^{4+}, possibly even reductively dissolved from Ce^{4+} to Ce^{3+} (German et al., 1991; Mazumdar et al., 1999). Thus, the REE record supports the $\delta^{11}B$ data and the implied low ocean pH (7.2) and anoxic conditions at the uppermost Gaojiashan Member. Furthermore, the postulated transition to a (partly) restricted environment enables such a tremendous change in ocean geochemistry due to the missing open ocean connection and mixing. Wille et al. (2008), Zhou et al. (2012) and Ishikawa et al. (2008) suggest even major global changes in ocean geochemistry and circulation patterns with shallow water anoxia and excessive H_2S concentrations occurring just before the Precambrian Cambrian boundary transition.

The overlying strata show a gradual lithological change from predominantly siliciclastic to carbonate rocks of the Beiwan Member. Consequently, a return to open

ocean conditions by relative sea level rise (Fig. 11C) is suggested. Isotope data confirm these observations. $\delta^{11}B$ imply a turn back to more alkaline seawater with a pH of ~8.6. Trace element data show a severe decrease in S (1589 µg g^{-1} to 87 µg g^{-1}) and Fe (1218 µg g^{-1} to 532 µg g^{-1}) due to FeS_2 formation in times of the most pronounced anoxic conditions within the potentially separated basin. Abundant Fe required for pyritization can be provided by basalt weathering of the hinterland (Huang et al., 2011). Pyrite formation leads to more alkaline seawater conditions (Tziperman et al., 2011), especially as soon as there is a reconnection to the open ocean. Additionally, sulfate reducing bacteria have the ability to use CO_2 instead of SO_4^{2-} for decomposition of organic matter under anoxic conditions if the sulfate is exhausted (Brown et al., 2007). Hence, the associated hydrocarbon formation leads to a rise in seawater pH.

3.6.2 Weathering conditions

Due to the 3-5 Ma-long residence time of strontium (Le Guerroué, 2010) the isotope ratio is suggested to be very homogeneous for the global seawater and therefore well suited for weathering rate estimates. The lower part of the investigated Gaojiashan Section hosts slightly enhanced but still typical open ocean $^{87}Sr/^{86}Sr$ ratios of ~0.7089 for the terminal Neoproterozoic (Halverson et al., 2007; Halverson et al., 2010; Kennedy et al., 2006). The minor elevation in comparison to literature values can be attributed to the environmental setting and its associated increased Sr input flux from the continent. Prior to the bloom of *Gaojiashania* and *Cloudina,* the $^{87}Sr/^{86}Sr$ ratio rises up to 0.7095. This indicates an additionally increased nutrient supply from the continent leading to enhanced biological activity and primary production. After a short interval of lower $^{87}Sr/^{86}Sr$ ratios (~0.7085) displaying either reduced continental input or enhanced mid-ocean ridge (MOR) activity, a conspicuous weathering pulse in terms of a pronounced positive anomaly is visible. Seawater $^{87}Sr/^{86}Sr$ ratios reach up to 0.7110 during this time of relative sea level fall noticeable by a transition from predominantly carbonate rocks to primarily siliciclastics. Besides, this regression leads to a greater land surface exposure being susceptible to continental weathering (Fig. 11B). A co-occurring relative -11‰ negative excursion in δ^7Li_{carb} confirms the interpretation of high weathering rates. Moreover, it implies silicate instead of carbonate weathering. In general, lithium is almost exclusively situated in silicate minerals and independent of host rock lithology (Kisakurek et al., 2005; Millot et al., 2010; Tomascak, 2004). Its

cycle is based on fluxes to and out of the ocean via rivers and hydrothermal activity or reverse-weathering, respectively (Huh et al., 1998; Misra and Froelich, 2012; Pogge von Strandmann et al., 2013; Vigier et al., 2008). Due to the preferential uptake of ^{6}Li into clays (Kisakurek et al., 2005; Pistiner and Henderson, 2003) and the associated fractionation it is possible to distinguish between weathering regimes by differences in $\delta^{7}Li_{riv}$ and hence different $\delta^{7}Li_{sw}$ recorded in carbonates (Misra and Froelich, 2012; Pogge von Strandmann et al., 2013). Isotopically light riverine lithium flux to the ocean causes a negative $\delta^{7}Li_{sw}$ excursion as observed in the uppermost Gaojiashan Member. These lighter lithium isotope signatures are indicative for primary silicate mineral dissolution in a transport-limited regime with enhanced chemical weathering intensities (e.g. Misra and Froelich, 2012; Pogge von Strandmann et al., 2013). Almost entirely congruent weathering produces such light $\delta^{7}Li_{riv}$ values, which in turn are similar to the host rock/upper continental crust lithium isotopic composition. Detrital Li ($\delta^{7}Li_{det}$) isotopic composition (see supplement, chapter 3.10) confirms this interpretation, since solely a short time of congruent weathering is able to produce the observed, almost unfractionated, low $\delta^{7}Li_{carb}$ values down to 1.1‰.

As the change in ocean geochemistry takes place very rapidly, we assume a modification towards either a restricted or a partly restricted environment. Hence, the restriction enables or intensifies the fast change in ocean geochemistry resulting from high weathering rates. An increase in precipitation and deposition rates could equally explain a record of local isotopic signals not in equilibrium with the open ocean, as suggested for the Shuram-Wonoka time-interval in South China (Wang et al., 2014). Jacobsen and Kaufman (1999) and Sawaki et al. (2010) explain the generally enhanced weathering between 590-550 Ma by mountain chain formation and tectonic uplift, once East Africa, India and Madagascar converging into another. A continuous increase in weathering rates is also supported by the phosphor supply to the ocean. Phosphate concentrations are rising from 404 µg g^{-1} to 3340 µg g^{-1} (see table 3 of the supplement, chapter 3.10) in times of the highest weathering rates and decrease in the uppermost part of the section concomitant with decreasing weathering intensity. Nevertheless, the positive Sr excursion is also explainable by a decrease in mantle-derived strontium as a consequence of inactive volcanism and hydrothermal activity (Shields, 2007). However, there is no evidence for a remarkable fluctuation in MOR strontium input fluxes and CO_2 levels during the terminal Ediacaran in literature.

The recurrence to open ocean conditions in the uppermost part of the section by relative sea level rise (Fig. 11C) results in minor continental weathering and lower $^{87}Sr/^{86}Sr$ ratios similar to the pre-excursion ones. The return to lower seawater Sr values of ~0.7086 is intensified via mixing of restricted basin water masses with open ocean seawater. δ^7Li_{carb} and δ^7Li_{det} values of the uppermost Gaojiashan Section are both enhanced in comparison to pre-excursion values. This can either be achieved by changing rock lithology exposed to weathering or by a modification towards a more weathering-limited regime. A variation in the detrital composition and amount is indicated by XRD data and therefore considered as main reason for a heavier lithium isotopic composition.

3.6.3 Terminal Ediacaran glaciation

Increasing evidence for local, terminal Ediacaran glacial events postdating the ~580 Ma old Gaskiers glaciation arises from geological records worldwide. Latest Precambrian glacial deposits associated with negative $\delta^{13}C_{carb}$ anomalies are known from e.g. Kazakhstan and Kyrgyzstan (Baykonur Fm; Chumakov, 2009a), Namibia (Vingerbreek Member; Germs, 1995; Hebert et al., 2010; Kaufman et al., 1991), and northern China (Hankalchough Fm; Chumakov, 2011; Xiao et al., 2004). Strata of the upper Gaojiashan Section not only reveal a change in lithology due to relative sea-level fall but also a negative carbon anomaly similar to these glacial records. However, it is highly unlikely that the studied section records a late Ediacaran local glaciation since the $\delta^{13}C_{carb}$ and $\delta^{11}B$ negative excursion amplitudes are far too big and thus unexplainable by a glaciation of only local extend. A Snowball-like ice cover accompanied by highly elevated atmospheric pCO_2 over a period of several Ma equal to the Marinoan glaciation would be required for such tremendous variations in ocean geochemistry.

3.6.4 Record of Precambrian-Cambrian boundary?

Although the isotopic systems of B, Sr and Li provide evidence for dramatic changes in ocean geochemistry resulting from local changes in bioproductivity and the environmental configuration, a global scale modification in ocean geochemistry as known from the Precambrian-Cambrian transition must be suspected likewise. If literature age constraints (551-542 Ma, Cai et al., 2013; Guo et al., 2012; Meyer et al., 2012; Zhang et al., 2014a) of the upper Gaojiashan Section are correct, the PCC-boundary transition including its prominent negative $\delta^{13}C_{carb}$ excursion must be expected

in the overlying and not exposed strata on top of the Beiwan Member dolostones. This would imply the existence of two batched and large magnitude $\delta^{13}C_{carb}$ negative anomalies. One of them in the terminal Ediacaran (this study) and the other one known as the PCC boundary peak (BACE, e.g. Shields-Zhou and Zhu, 2013) immediately on top but not exposed. However, no other section at the Yangtze Platform or even worldwide shows a second negative $\delta^{13}C_{carb}$ excursions of >10‰ magnitude during that time interval and existing correlations of the northern Yangtze Platform are solely based on litho- and biostratigraphy. Great spatial varieties and differences in strata thicknesses (Cai et al., 2010; Gamper et al., in prep.; Steiner et al., 2004) right up to the total absence of strata lead to an uncertain stratigraphic framework in the northern Yangtze Platform. Therefore, the arrangement of the entire Gaojiashan Section to the Ediacaran Dengying Formation as done by literature must not necessarily be correct and an at least platform-wide correlation with other sections recording the PCC boundary interval seems feasible. Besides, the prolonged positive $\delta^{13}C_{carb}$ trend leading into the distinct negative $\delta^{13}C_{carb}$ anomaly as observed at the Gaojiashan Section is known worldwide from the PCC boundary (Fig. 12).

Biostratigraphic evidence for a record of the PCC boundary interval is given by the extinction of *Cloudina* at the terminal Ediacaran (Amthor et al., 2003). At the Gaojiashan Section, we could not find any *Cloudina* fossils above the negative excursion. In recent publications (Cai et al., 2013; Cai et al., 2011; Guo et al., 2012; Meyer et al., 2012) there is also no evidence for *Cloudina* in the uppermost strata, so far described as Beiwan Member. Aside from the fossil record, changes in ocean geochemistry and circulation patterns with global euxinic to anoxic shallow water conditions shortly before the Precambrian-Cambrian boundary are described in literature (Ishikawa et al., 2008; Kimura and Watanabe, 2001; Mazumdar et al., 1999; Wille et al., 2008). Evidence for relative sea-level fall at the terminal Ediacaran, as visible at the Gaojiashan Section, can also be found in e.g. the Three Gorges area (South China, Ishikawa et al., 2008), in Kazakhstan (Heubeck et al., 2013) and in Siberia (Pelechaty et al., 1996). An early Cambrian transgression event, serving as indirect proof for relatively low sea-levels at the latest Ediacaran is described by several authors (Dong et al., 2009; Goldberg et al., 2007; Guo et al., 2007; Guo et al., 2013; Mazumdar et al., 1999; Och et al., 2013).

Consequently, a great variety of arguments go beyond the explanation of a solely local phenomenon and suggest a gapless record of the Precambrian-Cambrian boundary at the Gaojiashan Section, as also recently suggested by Gamper et al. (in prep.).

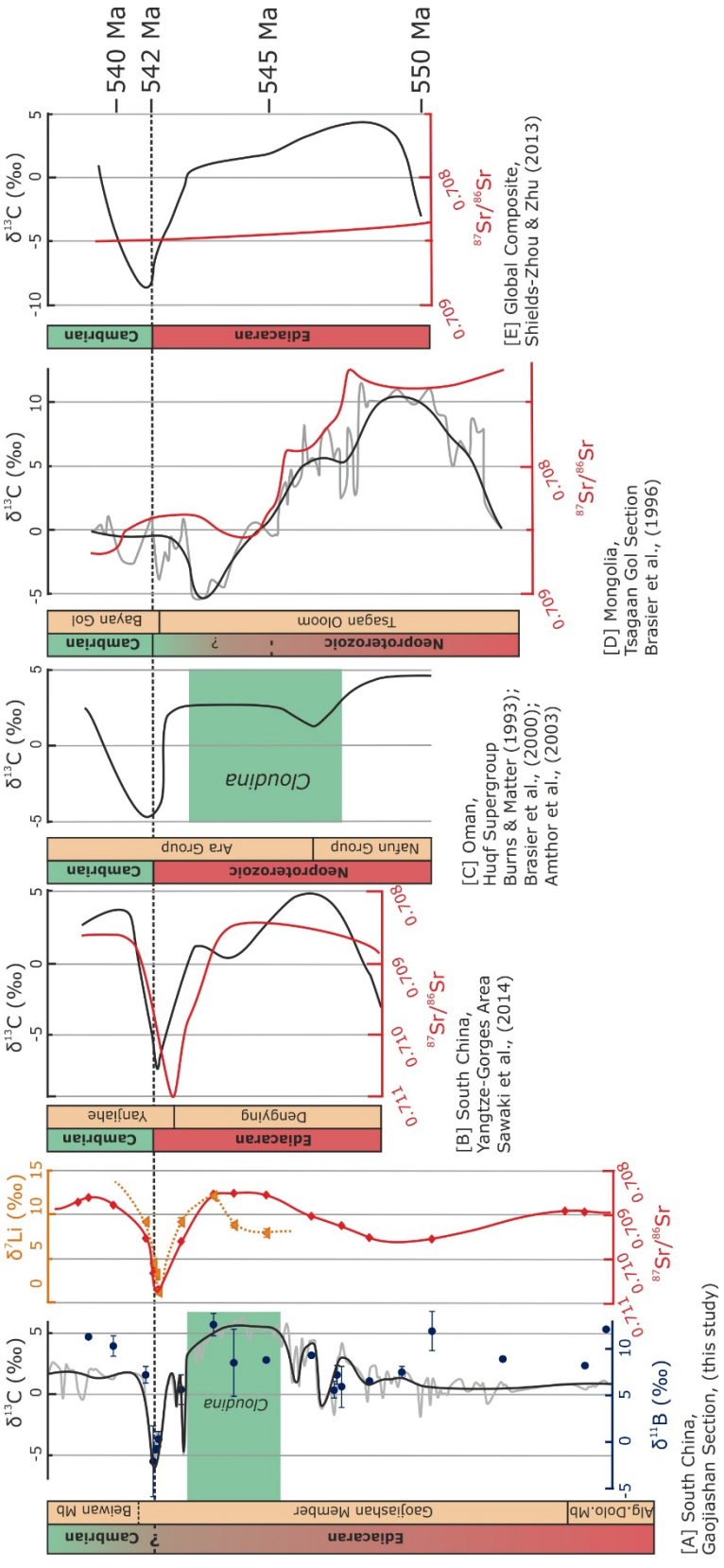

Figure 12: *Global correlation of $\delta^{13}C$ (black) and $^{87}Sr/^{86}Sr$ (red) patterns of terminal Neoproterozoic to Cambrian sections. Green bars indicate Cloudina fossil occurrences. Dotted black line represents the PCC boundary. [A] South China, Gaojiashan Section (this study), $\delta^{11}B$ (blue) $\delta^{7}Li_{carb}$ (yellow) data included. Grey line: measured $\delta^{13}C$ data, black line: trend line. [B] South China, Yangtze Gorges area (Sawaki et al., 2014). [C] Oman, Huqf Supergroup by Amthor et al. (2003), Brasier et al. (2000) and Burns and Matter (1993). [D] Mongolia, Tsagaan Gol Section by (Brasier et al., 1996). Grey line: measured $\delta^{13}C$ data, black line: trend line. [E] Global composite by (Shields-Zhou and Zhu, 2013). Time scale only applicable for column [E].*

3.7 Conclusion

The Gaojiashan Section records dramatic changes in ocean geochemistry during the terminal Ediacaran. We propose an interpretation that is more likely based on variations in the local environmental setting and biological productivity than on global effects as severe fluctuations in atmospheric CO_2 levels with associated ocean pH shifts. Continuous weathering input led to a phase of high bioproductivity ($\delta^{13}C_{carb}$ +5‰), slightly alkaline seawater conditions (pH ~8.5) and a continuously rising chemocline. Due to relative sea-level fall a restricted environment with euxinic to anoxic, acidic shallow water evolves. The increase in land surface exposed to weathering led to a strong positive excursion in $^{87}Sr/^{86}Sr$ and a co-occurring negative anomaly in $\delta^{7}Li_{carb}$. Associated strata of the uppermost Gaojiashan Member also host prominent $\delta^{11}B$ and $\delta^{13}C_{carb}$ negative excursions of -14‰ and -12‰, respectively. The prevailing euxinic to anoxic, acidic (pH 7.2) shallow-water conditions at that time might have poisoned the Ediacaran Fauna and led to mass extinction.

If these changing ocean conditions are of local scale, represent a global event or even the evolution at the Precambrian-Cambrian boundary transition is hard to prove. Main aspects for a local phenomenon are: (1) The lithological change that is associated with the prominent $\delta^{7}Li$, $\delta^{11}B$, $\delta^{13}C_{carb}$ and $^{87}Sr/^{86}Sr$ excursions, (2) the rapidity of changes to ocean geochemistry and (3) the overlying Beiwan Member, which is described as Ediacaran unit in literature.

However, strong evidence for a global event and thus a complete record of the PCC transition is given by: (1) The magnitude and shape of the negative $\delta^{13}C_{carb}$ excursion that is similar to other negative $\delta^{13}C_{carb}$ peaks at the PCC boundary worldwide, (2) the extinction of *Cloudina* beneath the excursion, (3) the regression-transgression cycle that is recorded at the Gaojiashan Section and suggested for the PCC transition worldwide, (4) the occurrence of at least temporary anoxic shallow-water conditions poisoning the Ediacaran fauna and (5) the distinct positive $^{87}Sr/^{86}Sr$ excursion that correlates precisely with previously published $^{87}Sr/^{86}Sr$ curves of the PCC boundary in South China (Sawaki et al., 2008; Sawaki et al., 2014).

To verify one of the explanations, further studies of changing ocean pH conditions at the Precambrian-Cambrian transition are needed, as there is no geochronological

data (e.g. dating of tuff layers) of upper Dengying strata in the north-western Yangtze Platform available.

3.8 Acknowledgements

The authors are grateful to Silvana Pape for ICP-OES trace element measurements, Simon Hohl for REE analyses, Christoph Vogt for XRD analyses, and Kirsten Born for help with cathodoluminescence imaging. Friedrich Lucassen is thanked for useful remarks and his help with TIMS analyses as well as Michael Steiner, Christoph Heubeck, Bernd Weber, Roman Koch and Quentin Scouflaire for detailed discussions and sample collection (QS and BW). The project is funded from the German Research Foundation (DFG FOR 736 „The Precambrian-Cambrian Ecosphere (R)evolution: Insights from Chinese microcontinents"). Fieldwork was supported by the Natural Science Foundation of China (NSFC).

3.9 References

Amthor, J. E., Grotzinger, J. P., Schröder, S., Bowring, S. A., Ramezani, J., Martin, M. W., and Matter, A., 2003, Extinction of Cloudina and Namacalathus at the Precambrian-Cambrian boundary in Oman: Geology, v. 31, no. 5, p. 431-434.

Bartley, J. K., Pope, M., Knoll, A. H., Semikhatov, M. A., and Petrov, P. Y., 1998, A Vendian–Cambrian boundary succession from the northwestern margin of the Siberian Platform: stratigraphy, palaeontology, chemostratigraphy and correlation: Geological Magazine, v. 135, no. 04, p. 473-494.

Bau, M., and Dulski, P., 1996, Distribution of yttrium and rare-earth elements in the Penge and Kuruman iron-formations, Transvaal Supergroup, South Africa: Precambrian Research, v. 79, no. 1–2, p. 37-55.

Birck, J. L., 1986, Precision K-Rb-Sr isotopic analysis: Application to Rb-Sr chronology: Chemical Geology, v. 56, no. 1–2, p. 73-83.

Bjerrum, C. J., and Canfield, D. E., 2011, Towards a quantitative understanding of the late Neoproterozoic carbon cycle: Proceedings of the National Academy of Sciences of the United States of America, v. 108, no. 14, p. 5542-5547.

Brasier, M., McCarron, G., Tucker, R., Leather, J., Allen, P., and Shields, G., 2000, New U-Pb zircon dates for the Neoproterozoic Ghubrah glaciation and for the top of the Huqf Supergroup, Oman: Geology, v. 28, no. 2, p. 175-178.

Brasier, M. D., Shields, G., Kuleshov, V. N., and Zhegallo, E. A., 1996, Integrated chemo- and biostratigraphic calibration of early animal evolution: Neoproterozoic–early Cambrian of southwest Mongolia: Geological Magazine, v. 133, no. 04, p. 445-485.

Brown, E., Colling, A., Park, D., Phillips, J., Rothery, D., and Wright, J., 2007, Chapter 6 - The seawater solution, *in* Wright, J., and Colling, A., eds., Seawater: Its composition, properties and behaviour: Oxford, Butterworth-Heinemann, p. 85-127.

Burns, S. J., and Matter, A., 1993, Carbon isotopic record of the latest Proterozoic from Oman: Eclogae Geologicae Helvetiae, v. 86, no. 2, p. 595-607.

Burton, K. W., and Vigier, N., 2012, Lithium Isotopes as Tracers in Marine and Terrestrial Environments, *in* Baskaran, M., ed., Handbook of Environmental Isotope Geochemistry, Springer Berlin Heidelberg, p. 41-59.

Cai, Y., and Hua, H., 2007, Pyritization in the Gaojiashan Biota: Chinese Science Bulletin, v. 52, no. 5, p. 645-650.

Cai, Y., Hua, H., and Zhang, X., 2013, Tube construction and life mode of the late Ediacaran tubular fossil Gaojiashania cyclus from the Gaojiashan Lagerstätte: Precambrian Research, v. 224, no. 0, p. 255-267.

Cai, Y., Hua, H., Zhuravlev, A. Y., Vintaned, J. A. G., and Ivantsov, A. Y., 2011, Discussion of 'First finds of problematic Ediacaran fossil Gaojiashania in Siberia and its origin': Geological Magazine, v. 148, no. 2, p. 329-333.

Cai, Y., Schiffbauer, J. D., Hua, H., and Xiao, S., 2012, Preservational modes in the Ediacaran Gaojiashan Lagerstätte: Pyritization, aluminosilicification, and carbonaceous compression: Palaeogeography, Palaeoclimatology, Palaeoecology, v. 326–328, no. 0, p. 109-117.

Cai, Y. P., Hua, H., Xiao, S. H., Schiffbauer, J. D., and Li, P., 2010, Biostratinomy of the late Ediacaran pyritized Gaojiashan lagerstätte from southern Shaanxi, South China: Importance of event deposits: PALAIOS, v. 25, no. 7-8, p. 487-506.

Canfield, D. E., Poulton, S. W., and Narbonne, G. M., 2007, Late-Neoproterozoic Deep-Ocean Oxygenation and the Rise of Animal Life: Science, v. 315, no. 5808, p. 92-95.

Chumakov, N., 2011, Late Proterozoic African glacial era: Stratigraphy and Geological Correlation, v. 19, no. 1, p. 1-20.

Chumakov, N. M., 2009a, The Baykonurian glaciohorizon of the Late Vendian: Stratigraphy and Geological Correlation, v. 17, no. 4, p. 373-381.

Cremonese, L., Shields-Zhou, G., Struck, U., Ling, H.-F., Och, L., Chen, X., and Li, D., 2013, Marine biogeochemical cycling during the early Cambrian constrained by a nitrogen and organic carbon isotope study of the Xiaotan section, South China: Precambrian Research, v. 225, p. 148-165.

Deniel, C., and Pin, C., 2001, Single-stage method for the simultaneous isolation of lead and strontium from silicate samples for isotopic measurements: Analytica Chimica Acta, v. 426, no. 1, p. 95-103.

Derry, L. A., 2010, A burial diagenesis origin for the Ediacaran Shuram–Wonoka carbon isotope anomaly: Earth and Planetary Science Letters, v. 294, no. 1-2, p. 152-162.

Derry, L. A., Kaufman, A. J., and Jacobsen, S. B., 1992, Sedimentary cycling and environmental change in the Late Proterozoic: Evidence from stable and radiogenic isotopes: Geochimica et Cosmochimica Acta, v. 56, no. 3, p. 1317-1329.

Dickson, A. G., 1990, Thermodynamics of the dissociation of boric acid in synthetic seawater from 273.15 to 318.15 K: Deep Sea Research Part A. Oceanographic Research Papers, v. 37, no. 5, p. 755-766.

Dong, L., Xiao, S., Shen, B., Zhou, C., Li, G., and Yao, J., 2009, Basal Cambrian Microfossils from the Yangtze Gorges Area (South China) and the Aksu Area (Tarim Block, Northwestern China): Journal of Paleontology, v. 83, no. 1, p. 30-44.

Gamper, A., Struck, U., Ohnemueller, F., and Heubeck, C., in prep., Chemo- and Biostratigraphy of the Gaojiashan section (northern Yangtze platform, South China): A new Pc-C boundary section.

Gamper, A., Struck, U., Scouflaire, Q., and Weber, B., 2012, Carbon and Nitrogen isotope study of the upper Ediacaran Gaojiashan Member in South China: Insights in causes of the Cambrian Explosion: Terra Nostra, v. Schriften der GeoUnion Alfred-Wegener-Stiftung – 2012/3, Centenary Meeting of the Paläontologische Gesellschaft, p. 61.

German, C. R., Holliday, B. P., and Elderfield, H., 1991, Redox cycling of rare earth elements in the suboxic zone of the Black Sea: Geochimica et Cosmochimica Acta, v. 55, no. 12, p. 3553-3558.

Germs, G. J. B., 1995, The Neoproterozoic of southwestern Africa, with emphasis on platform stratigraphy and paleontology: Precambrian Research, v. 73, no. 1–4, p. 137-151.

Goldberg, T., Poulton, S. W., and Strauss, H., 2005, Sulphur and oxygen isotope signatures of late Neoproterozoic to early Cambrian sulphate, Yangtze Platform, China: Diagenetic constraints and seawater evolution: Precambrian Research, v. 137, no. 3–4, p. 223-241.

Goldberg, T., Strauss, H., Guo, Q., and Liu, C., 2007, Reconstructing marine redox conditions for the Early Cambrian Yangtze Platform: Evidence from biogenic sulphur and organic carbon

isotopes: Palaeogeography, Palaeoclimatology, Palaeoecology, v. 254, no. 1–2, p. 175-193.

Grégoire, M., and Soetaert, K., 2010, Carbon, nitrogen, oxygen and sulfide budgets in the Black Sea: A biogeochemical model of the whole water column coupling the oxic and anoxic parts: Ecological Modelling, v. 221, no. 19, p. 2287-2301.

Guo, Q., Deng, Y., and Yang, X., 2012, Carbon Isotopic Evolution of the Late Ediacaran Gaojiashan Biota on the Northern Yangtze Platform, South China: Acta Geologica Sinica - English Edition, v. 86, no. 6, p. 1447-1454.

Guo, Q., Strauss, H., Liu, C., Goldberg, T., Zhu, M., Pi, D., Heubeck, C., Vernhet, E., Yang, X., and Fu, P., 2007, Carbon isotopic evolution of the terminal Neoproterozoic and early Cambrian: Evidence from the Yangtze Platform, South China: Palaeogeography, Palaeoclimatology, Palaeoecology, v. 254, no. 1-2, p. 140-157.

Guo, Q., Strauss, H., Zhu, M., Zhang, J., Yang, X., Lu, M., and Zhao, F., 2013, High resolution organic carbon isotope stratigraphy from a slope to basinal setting on the Yangtze Platform, South China: Implications for the Ediacaran–Cambrian transition: Precambrian Research, v. 225, no. 0, p. 209-217.

Halverson, G. P., Dudas, F. O., Maloof, A. C., and Bowring, S. A., 2007, Evolution of the Sr-87/Sr-86 composition of Neoproterozoic seawater: Palaeogeography Palaeoclimatology Palaeoecology, v. 256, no. 3-4, p. 103-129.

Halverson, G. P., and Hurtgen, M. T., 2007, Ediacaran growth of the marine sulfate reservoir: Earth and Planetary Science Letters, v. 263, no. 1-2, p. 32-44.

Halverson, G. P., Wade, B. P., Hurtgen, M. T., and Barovich, K. M., 2010, Neoproterozoic chemostratigraphy: Precambrian Research, v. 182, no. 4, p. 337-350.

Hebert, C. L., Kaufman, A. J., Penniston-Dorland, S. C., and Martin, A. J., 2010, Radiometric and stratigraphic constraints on terminal Ediacaran (post-Gaskiers) glaciation and metazoan evolution: Precambrian Research, v. 182, no. 4, p. 402-412.

Hemming, N. G., and Hanson, G. N., 1992, Boron isotopic composition and concentration in modern marine carbonates: Geochimica et Cosmochimica Acta, v. 56, no. 1, p. 537-543.

Heubeck, C., Ergaliev, G., and Evseev, S., 2013, Large-Scale Seismogenic Deformation of A Carbonate Platform Straddling the Precambrian–Cambrian Boundary, Karatau Range, Kazakhstan: Journal of Sedimentary Research, v. 83, no. 11, p. 1004-1024.

Hong, H., Zhe, C., and Xunlai, Y., 2007, The advent of mineralized skeletons in Neoproterozoic Metazoa—new fossil evidence from the Gaojiashan Fauna: Geological Journal, v. 42, no. 3-4, p. 263-279.

Hönisch, B., Bickert, T., and Hemming, N. G., 2008, Modern and Pleistocene boron isotope composition of the benthic foraminifer Cibicidoides wuellerstorfi: Earth and Planetary Science Letters, v. 272, no. 1-2, p. 309-318.

Huang, J., Chu, X., Jiang, G., Feng, L., and Chang, H., 2011, Hydrothermal origin of elevated iron, manganese and redox-sensitive trace elements in the c. 635 Ma Doushantuo cap carbonate: Journal of the Geological Society, v. 168, no. 3, p. 805-816.

Huh, Y., Chan, L.-H., Zhang, L., and Edmond, J. M., 1998, Lithium and its isotopes in major world rivers: implications for weathering and the oceanic budget: Geochimica et Cosmochimica Acta, v. 62, no. 12, p. 2039-2051.

Ishikawa, T., Ueno, Y., Komiya, T., Sawaki, Y., Han, J., Shu, D., Li, Y., Maruyama, S., and Yoshida, N., 2008, Carbon isotope chemostratigraphy of a Precambrian/Cambrian boundary section in the Three Gorge area, South China: Prominent global-scale isotope excursions just before the Cambrian Explosion: Gondwana Research, v. 14, no. 1-2, p. 193-208.

Jacobsen, S. B., and Kaufman, A. J., 1999, The Sr, C and O isotopic evolution of Neoproterozoic seawater: Chemical Geology, v. 161, no. 1–3, p. 37-57.

James, R. H., and Palmer, M. R., 2000, The lithium isotope composition of international rock standards: Chemical Geology, v. 166, no. 3–4, p. 319-326.

Jeffcoate, A. B., Elliott, T., Thomas, A., and Bouman, C., 2004, Precise/ Small Sample Size Determinations of Lithium Isotopic Compositions of Geological Reference Materials and Modern Seawater by MC-ICP-MS: Geostandards and Geoanalytical Research, v. 28, no. 1, p. 161-172.

Joachimski, M. M., Simon, L., van Geldern, R., and Lécuyer, C., 2005, Boron isotope geochemistry of Paleozoic brachiopod calcite: Implications for a secular change in the boron isotope geochemistry of seawater over the Phanerozoic: Geochimica et Cosmochimica Acta, v. 69, no. 16, p. 4035-4044.

Johnston, D. T., Poulton, S. W., Goldberg, T., Sergeev, V. N., Podkovyrov, V., Vorob'eva, N. G., Bekker, A., and Knoll, A. H., 2012, Late Ediacaran redox stability and metazoan evolution: Earth and Planetary Science Letters, v. 335–336, no. 0, p. 25-35.

Kakihana, H., Kotaka, M., Satoh, S., Nomura, M., and Okamoto, M., 1977, Fundamental Studies on the Ion-Exchange Separation of Boron Isotopes: Bulletin of the Chemical Society of Japan, v. 50, no. 1, p. pp.158-163.

Kasemann, S. A., Hawkesworth, C. J., Prave, A. R., Fallick, A. E., and Pearson, P. N., 2005, Boron and calcium isotope composition in Neoproterozoic carbonate rocks from Namibia: evidence for extreme environmental change: Earth and Planetary Science Letters, v. 231, no. 1-2, p. 73-86.

Kasemann, S. A., Meixner, A., Rocholl, A., Vennemann, T., Rosner, M., Schmitt, A. K., and Wiedenbeck, M., 2001, Boron and Oxygen Isotope Composition of Certified Reference Materials NIST SRM 610/612 and Reference Materials JB-2 and JR-2: Geostandards Newsletter, v. 25, no. 2-3, p. 405-416.

Kasemann, S. A., Prave, A. R., Fallick, A. E., Hawkesworth, C. J., and Hoffmann, K.-H., 2010, Neoproterozoic ice ages, boron isotopes, and ocean acidification: Implications for a snowball Earth: Geology, v. 38, no. 9, p. 775-778.

Kasemann, S. A., Schmidt, D. N., Bijma, J., and Foster, G. L., 2009, In situ boron isotope analysis in marine carbonates and its application for foraminifera and palaeo-pH: Chemical Geology, v. 260, no. 1-2, p. 138-147.

Kaufman, A. J., Hayes, J. M., Knoll, A. H., and Germs, G. J. B., 1991, Isotopic composition of carbonates and organic-carbon from upper Proterozoic successions in Namibia - Stratigraphic variation and the effects of diagenesis and metamorphism: Precambrian Research, v. 49, no. 3-4, p. 301-327.

Kaufman, A. J., Jacobsen, S. B., and Knoll, A. H., 1993, The Vendian record of Sr and C isotopic variations in seawater: Implications for tectonics and paleoclimate: Earth and Planetary Science Letters, v. 120, no. 3–4, p. 409-430.

Kennedy, M., Droser, M., Mayer, L. M., Pevear, D., and Mrofka, D., 2006, Late Precambrian Oxygenation; Inception of the Clay Mineral Factory: Science, v. 311, no. 5766, p. 1446-1449.

Kimura, H., and Watanabe, Y., 2001, Oceanic anoxia at the Precambrian-Cambrian boundary: Geology, v. 29, no. 11, p. 995-998.

Kisakurek, B., James, R. H., and Harris, N. B. W., 2005, Li and [delta]7Li in Himalayan rivers: Proxies for silicate weathering?: Earth and Planetary Science Letters, v. 237, no. 3-4, p. 387-401.

Klochko, K., Kaufman, A. J., Yao, W., Byrne, R. H., and Tossell, J. A., 2006, Experimental measurement of boron isotope fractionation in seawater: Earth and Planetary Science Letters, v. 248, no. 1-2, p. 276-285.

Kouchinsky, A., Bengtson, S., Runnegar, B., Skovsted, C., Steiner, M., and Vendrasco, M., 2012, Chronology of early Cambrian biomineralization: Geological Magazine, v. 149, no. 02, p. 221-251.

Krienitz, M.-S., Garbe-Schönberg, C.-D., Romer, R. L., Meixner, A., Haase, K. M., and Stroncik, N. A., 2012, Lithium Isotope Variations in Ocean Island Basalts—Implications for the Development of Mantle Heterogeneity: Journal of Petrology, v. 53, no. 11, p. 2333-2347.

Le Guerroué, E., 2010, Duration and synchroneity of the largest negative carbon isotope excursion on Earth: The Shuram/Wonoka anomaly: Comptes Rendus Geoscience, v. 342, no. 3, p. 204-214.

Lemarchand, D., Gaillardet, J., Lewin, E., and Allegre, C. J., 2000, The influence of rivers on marine boron isotopes and implications for reconstructing past ocean pH: Nature, v. 408, no. 6815, p. 951-954.

Li, D., Ling, H.-F., Shields-Zhou, G. A., Chen, X., Cremonese, L., Och, L., Thirlwall, M., and Manning, C. J., 2013, Carbon and strontium isotope evolution of seawater across the

Ediacaran–Cambrian transition: Evidence from the Xiaotan section, NE Yunnan, South China: Precambrian Research, v. 225, no. 0, p. 128-147.
Li, P., 2008, The sedimentary characters and carbon isotope chemostratigraphy of the Gaojiashan Biota in Southern Shaanxi, China [MSc: Northwest University, 104 p.
Lin, S., Zhang, Y., and Zhang, L., 1986, Body and trace fossils of metazoa and algal macrofossils from the upper Sinian Gaojiashan Formation in southern Shaanxi: Geology of Shaanxi, v. 4, no. 6, p. 9-17.
Ling, H.-F., Feng, H.-Z., Pan, J.-Y., Jiang, S.-Y., Chen, Y.-Q., and Chen, X., 2007, Carbon isotope variation through the Neoproterozoic Doushantuo and Dengying Formations, South China: Implications for chemostratigraphy and paleoenvironmental change: Palaeogeography, Palaeoclimatology, Palaeoecology, v. 254, no. 1-2, p. 158-174.
Mazumdar, A., Banerjee, D. M., Schidlowski, M., and Balaram, V., 1999, Rare-earth elements and Stable Isotope Geochemistry of early Cambrian chert-phosphorite assemblages from the Lower Tal Formation of the Krol Belt (Lesser Himalaya, India): Chemical Geology, v. 156, no. 1–4, p. 275-297.
Meyer, M., Schiffbauer, J. D., Xiao, S., Cai, Y., and Hua, H., 2012, Taphonomy of the upper Ediacaran enigmatic ribbonlike fossil Shaanxilithes: PALAIOS, v. 27, no. 5, p. 354-372.
Miller, N. R., Stern, R. J., Avigad, D., Beyth, M., and Schilman, B., 2009, Cryogenian slate-carbonate sequences of the Tambien Group, Northern Ethiopia (I): Pre-"Sturtian" chemostratigraphy and regional correlations: Precambrian Research, v. 170, no. 3–4, p. 129-156.
Millot, R., Vigier, N., and Gaillardet, J., 2010, Behaviour of lithium and its isotopes during weathering in the Mackenzie Basin, Canada: Geochimica et Cosmochimica Acta, v. 74, no. 14, p. 3897-3912.
Misra, S., and Froelich, P. N., 2012, Lithium Isotope History of Cenozoic Seawater: Changes in Silicate Weathering and Reverse Weathering: Science, v. 335, no. 6070, p. 818-823.
Moriguti, T., and Nakamura, E., 1998, High-yield lithium separation and the precise isotopic analysis for natural rock and aqueous samples: Chemical Geology, v. 145, no. 1-2, p. 91-104.
Murray, J., Stewart, K., Kassakian, S., Krynytzky, M., and DiJulio, D., 2007, Oxic, suboxic, and anoxic conditions in the Black Sea, *in* Yanko-Hombach, V., Gilbert, A., Panin, N., and Dolukhanov, P., eds., The Black Sea Flood Question: Changes in Coastline, Climate, and Human Settlement, Springer Netherlands, p. 1-21.
Nance, W. B., and Taylor, S. R., 1976, Rare earth element patterns and crustal evolution—I. Australian post-Archean sedimentary rocks: Geochimica et Cosmochimica Acta, v. 40, no. 12, p. 1539-1551.
Nishio, Y., and Nakai, S. i., 2002, Accurate and precise lithium isotopic determinations of igneous rock samples using multi-collector inductively coupled plasma mass spectrometry: Analytica Chimica Acta, v. 456, no. 2, p. 271-281.
Och, L. M., Shields-Zhou, G. A., Poulton, S. W., Manning, C., Thirlwall, M. F., Li, D., Chen, X., Ling, H., Osborn, T., and Cremonese, L., 2013, Redox changes in Early Cambrian black shales at Xiaotan section, Yunnan Province, South China: Precambrian Research, v. 225, no. 0, p. 166-189.
Ohnemueller, F., Prave, A. R., Fallick, A. E., and Kasemann, S., in review, Ocean acidification in the aftermath of the Marinoan glaciation: Geology, v. G35937.
Paris, G., Bartolini, A., Donnadieu, Y., Beaumont, V., and Gaillardet, J., 2010a, Investigating boron isotopes in a middle Jurassic micritic sequence: Primary vs. diagenetic signal: Chemical Geology, v. 275, no. 3-4, p. 117-126.
Paris, G., Gaillardet, J., and Louvat, P., 2010b, Geological evolution of seawater boron isotopic composition recorded in evaporites: Geology, v. 38, no. 11, p. 1035-1038.
Pearson, P. N., and Palmer, M. R., 1999, Middle eocene seawater pH and atmospheric carbon dioxide concentrations: Science, v. 284, no. 5421, p. 1824-1826.
Pelechaty, S. M., Grotzinger, J. P., Kashirtsev, V. A., and Zhernovsky, V. P., 1996, Chemostratigraphic and Sequence Stratigraphic Constraints on Vendian-Cambrian Basin Dynamics, Northeast Siberian Craton: The Journal of Geology, v. 104, no. 5, p. 543-563.

Peters, S. E., and Gaines, R. R., 2012, Formation of the `Great Unconformity' as a trigger for the Cambrian explosion: Nature, v. 484, no. 7394, p. 363-366.

Pin, C., and Bassin, C., 1992, Evaluation of a strontium-specific extraction chromatographic method for isotopic analysis in geological materials: Analytica Chimica Acta, v. 269, no. 2, p. 249-255.

Pistiner, J. S., and Henderson, G. M., 2003, Lithium-isotope fractionation during continental weathering processes: Earth and Planetary Science Letters, v. 214, no. 1–2, p. 327-339.

Pogge von Strandmann, P. A. E., Burton, K. W., James, R. H., van Calsteren, P., and Gislason, S. R., 2010, Assessing the role of climate on uranium and lithium isotope behaviour in rivers draining a basaltic terrain: Chemical Geology, v. 270, no. 1–4, p. 227-239.

Pogge von Strandmann, P. A. E., Jenkyns, H. C., and Woodfine, R. G., 2013, Lithium isotope evidence for enhanced weathering during Oceanic Anoxic Event 2: Nature Geosci, v. 6, no. 8, p. 668-672.

Polonsky, A., 2012, Had Been Observing the Acidification of the Black Sea Upper Layer in XX Century?: Turkish Journal of Fisheries and Aquatic Sciences, v. 12, p. 391-396.

Quinby-Hunt, M. S., and Wilde, P., 1994, Thermodynamic zonation in the black shale facies based on iron-manganese-vanadium content: Chemical Geology, v. 113, no. 3–4, p. 297-317.

Raub, T. D., Evans, D. A. D., and Smirnov, A. V., 2007, Siliciclastic prelude to Elatina–Nuccaleena deglaciation: lithostratigraphy and rock magnetism of the base of the Ediacaran system: Geological Society, London, Special Publications, v. 286, no. 1, p. 53-76.

Raven, J., Caldeira, K., Elderfield, H., Hoegh-Guldberg, O., Liss, P., Riebesell, U., Shepherd, J., Turley, C., and Watson, A. J., 2005, Ocean acidification due to increasing atmospheric carbon dioxide: The Royal Society 2005, v. Policy document '05, no. 12, p. 1-68.

Sanyal, A., Nugent, M., Reeder, R. J., and Bijma, J., 2000, Seawater pH control on the boron isotopic composition of calcite: evidence from inorganic calcite precipitation experiments: Geochimica et Cosmochimica Acta, v. 64, no. 9, p. 1551-1555.

Sawaki, Y., Ohno, T., Fukushi, Y., Komiya, T., Ishikawa, T., Hirata, T., and Maruyama, S., 2008, Sr isotope excursion across the Precambrian–Cambrian boundary in the Three Gorges area, South China: Gondwana Research, v. 14, no. 1–2, p. 134-147.

Sawaki, Y., Ohno, T., Tahata, M., Komiya, T., Hirata, T., Maruyama, S., Windley, B. F., Han, J., Shu, D. G., and Li, Y., 2010, The Ediacaran radiogenic Sr isotope excursion in the Doushantuo Formation in the Three Gorges area, South China: Precambrian Research, v. 176, no. 1-4, p. 46-64.

Sawaki, Y., Tahata, M., Ohno, T., Komiya, T., Hirata, T., Maruyama, S., Han, J., and Shu, D., 2014, The anomalous Ca cycle in the Ediacaran ocean: Evidence from Ca isotopes preserved in carbonates in the Three Gorges area, South China: Gondwana Research, v. 25, no. 3, p. 1070-1089.

Scouflaire, Q., Heubeck, C., Weber, B., and Zhu, M., 2010, Transgressive-regressive sedimentation in the late Ediacaran of South China and its impact on metazoan communities: 2010 GSA Denver Annual Meeting.

Shields-Zhou, G., and Zhu, M., 2013, Biogeochemical changes across the Ediacaran–Cambrian transition in South China: Precambrian Research, v. 225, no. 0, p. 1-6.

Shields, G., 2007, A normalised seawater strontium isotope curve: possible implications for Neoproterozoic-Cambrian weathering rates and the further oxygenation of the Earth: eEarth Discussion, v. 2, p. 35-42.

Smith, M. P., and Harper, D. A. T., 2013, Causes of the Cambrian Explosion: Science, v. 341, no. 6152, p. 1355-1356.

Spivack, A. J., 1986, Boron isotope geochemistry [Ph.D.: Massachusetts Institute of Technology], 184 p.

Steiner, M., Li, G., Qian, Y., and Zhu, M., 2004, Lower Cambrian Small Shelly Fossils of northern Sichuan and southern Shaanxi (China), and their biostratigraphic importance: Geobios, v. 37, no. 2, p. 259-275.

Tomascak, P. B., 2004, Developments in the Understanding and Application of Lithium Isotopes in the Earth and Planetary Sciences: Reviews in Mineralogy and Geochemistry, v. 55, no. 1, p. 153-195.

Tomascak, P. B., Carlson, R. W., and Shirey, S. B., 1999, Accurate and precise determination of Li isotopic compositions by multi-collector sector ICP-MS: Chemical Geology, v. 158, no. 1–2, p. 145-154.

Tziperman, E., Halevy, I., Johnston, D. T., Knoll, A. H., and Schrag, D. P., 2011, Biologically induced initiation of Neoproterozoic snowball-Earth events: Proceedings of the National Academy of Sciences, v. 108, no. 37, p. 15091-15096.

Veizer, J., Ala, D., Azmy, K., Bruckschen, P., Buhl, D., Bruhn, F., Carden, G. A. F., Diener, A., Ebneth, S., Godderis, Y., Jasper, T., Korte, C., Pawellek, F., Podlaha, O. G., and Strauss, H., 1999, 87Sr/86Sr, δ13C and δ18O evolution of Phanerozoic seawater: Chemical Geology, v. 161, no. 1–3, p. 59-88.

Vigier, N., Decarreau, A., Millot, R., Carignan, J., Petit, S., and France-Lanord, C., 2008, Quantifying Li isotope fractionation during smectite formation and implications for the Li cycle: Geochimica et Cosmochimica Acta, v. 72, no. 3, p. 780-792.

Visscher, P. T., and Stolz, J. F., 2005, Microbial mats as bioreactors: populations, processes, and products: Palaeogeography, Palaeoclimatology, Palaeoecology, v. 219, no. 1–2, p. 87-100.

Wang, J., Chen, D., Wang, D. A. N., Yan, D., Zhou, X., and Wang, Q., 2012, Petrology and geochemistry of chert on the marginal zone of Yangtze Platform, western Hunan, South China, during the Ediacaran–Cambrian transition: Sedimentology, v. 59, no. 3, p. 809-829.

Wang, W., Zhou, C., Guan, C., Yuan, X., Chen, Z., and Wan, B., 2014, An integrated carbon, oxygen, and strontium isotopic studies of the Lantian Formation in South China with implications for the Shuram anomaly: Chemical Geology, v. 373, no. 0, p. 10-26.

Weber, B., Steiner, M., and Zhu, M. Y., 2007, Precambrian-Cambrian trace fossils from the Yangtze Platform (South China) and the early evolution of bilaterian lifestyles: Palaeogeography, Palaeoclimatology, Palaeoecology, v. 254, no. 1-2, p. 328-349.

Wille, M., Nagler, T. F., Lehmann, B., Schroder, S., and Kramers, J. D., 2008, Hydrogen sulphide release to surface waters at the Precambrian/Cambrian boundary: Nature, v. 453, no. 7196, p. 767-769.

Wootton, J. T., Pfister, C. A., and Forester, J. D., 2008, Dynamic Patterns and Ecological Impacts of Declining Ocean pH in a High-Resolution Multi-Year Dataset: Proceedings of the National Academy of Sciences of the United States of America, v. 105, no. 48, p. 18848-18853.

Xiao, S., Bao, H., Wang, H., Kaufman, A. J., Zhou, C., Li, G., Yuan, X., and Ling, H., 2004, The Neoproterozoic Quruqtagh Group in eastern Chinese Tianshan: evidence for a post-Marinoan glaciation: Precambrian Research, v. 130, no. 1-4, p. 1-26.

Yeghicheyan, D., Carignan, J., Valladon, M., Bouhnik Le Coz, M., Samuel, J., BenBakkar, M., Bruguier, O., Keller, F., Pin, C., Pourtales, L., Henin, O., Mace, J., Morin, N., Guilmette, C., and Marin, L., 2003, The new carbonate reference material Cal–S: preliminary results: Abs. Geoanal., v. 146.

Zhang, P., Hua, H., and Liu, W., 2014a, Isotopic and REE Evidence for the Paleoenvironmental Evolution of the Late Ediacaran Dengying Section, Ningqiang of Shaanxi Province, China: Precambrian Research, v. 242, no. 0, p. 96-111.

Zhang, X., Shu, D., Han, J., Zhang, Z., Liu, J., and Fu, D., 2014b, Triggers for the Cambrian explosion: Hypotheses and problems: Gondwana Research, v. 25, no. 3, p. 896-909.

Zhou, C. M., Jiang, S. Y., Xiao, S. H., Chen, Z., and Yuan, X. L., 2012, Rare earth elements and carbon isotope geochemistry of the Doushantuo Formation in South China: Implication for middle Ediacaran shallow marine redox conditions: Chinese Science Bulletin, v. 57, no. 16, p. 1998-2006.

Zhu, M., Zhang, J., and Yang, A., 2007, Integrated Ediacaran (Sinian) chronostratigraphy of South China: Palaeogeography, Palaeoclimatology, Palaeoecology, v. 254, no. 1-2, p. 7-61.

Zhu, M. Y., Zhang, J., Steiner, M., Yang, A., Li, G., and Erdtmann, B.-D., 2003, Sinian-Cambrian stratigraphic framework for shallow-to-deep-water environments of the Yangtze Platform: an integrated approach: Progress in Natural Science, v. 13, no. 12, p. 951-960.

3.10 Supplemental material

Additional Results

In table 3 additional trace element and δ^7Li_{det} isotope data are listed.

Sample (m)	Member	δ^7Li_{det} (‰) (2sd)	Al (ppm)	Ba (ppm)	S (ppm)	P (ppm)	Mn (ppm)	Sr (ppm)	B (ppm)	Mn/Sr
-3.30	Algal Dol. Mb	n.a.	2345	23	306	6720	232	68	6	3.39
-0.30	Algal Dol. Mb	n.a.	174	2	26	46	620	48	2	12.95
20.00	Gaojiashan Mb	n.a.	761	23	169	433	1102	348	2	3.16
28.30	Gaojiashan Mb	n.a.	789	14	168	690	985	362	2	2.72
32.00	Gaojiashan Mb	n.a.	1134	56	303	1517	401	404	2	0.99
32.60	Gaojiashan Mb	n.a.	1517	24	134	929	922	427	3	2.16
33.00	Gaojiashan Mb	n.a.	6631	68	63	1475	193	52	6	3.70
36.00	Gaojiashan Mb	n.a.	1045	17	123	639	447	506	2	0.88
42.00	Gaojiashan Mb	0.7 ±0.2	447	15	171	404	248	1292	3	0.19
46.30	Gaojiashan Mb	1.2 ±0.3	371	109	189	545	151	1081	2	0.14
49.00	Gaojiashan Mb	-0.2 ±0.7	294	8	266	578	207	1170	3	0.18
53.30	Gaojiashan Mb	4.0 ±0.5	163	4	375	1332	184	130	1	1.41
56.30	Gaojiashan Mb	7.9 ±0.4	1039	21	1589	3340	277	138	2	2.01
56.60	Gaojiashan Mb	8.6 ±0.3	822	20	87	3106	261	81	3	3.21
57.00	Gaojiashan Mb	12.8 ±0.3	892	20	83	2141	662	48	3	13.82
58.00	Gaojiashan Mb	10.6 ±0.0	77	3	137	205	24	110	6	0.22
62.60	Beiwan Mb	5.7 ±0.2	148	4	151	418	123	92	4	1.33
65.60	Beiwan Mb	17.2 ±0.1	55	4	136	219	95	105	5	0.90

Table 3: *δ^7Li_{det} [‰, vs. NIST 8545] and trace element concentrations of Al, Ba, S, P, Mn, Sr and B [ppm].*

Carbon and oxygen isotopes:

Carbon and oxygen isotopic analyses were performed on a Thermo Finnigan GASBENCH II linked online to a Thermo Finnigan DELTA V isotope ratio mass spectrometer at the Museum fuer Naturkunde Berlin (Berlin, Germany). Isotope ratios are reported in δ-notation in [‰] relative to the Vienna Peedee Belemnite (VPDB). The analytical reproducibility of $\delta^{13}C_{carb}$ and $\delta^{18}O$ values is generally better than ±0.2‰ (2sd) for both isotopic systems. A complete list of all 150 measured samples (Gamper et al., 2012) can be found in table 4. All carbonate carbon and oxygen values (Table 4, Fig. 13) are in very good agreement with values reported from literature (e.g. Halverson et al., 2005; Li et al., 2013).

Sample	Height [m]	Member	$\delta^{13}C_{carb}$ [‰,VPDB]	$\delta^{18}O$ [‰,VPDB]
GJ -3,6	-3.60	Algal Dolomite Mb	0.86	-2.58
GJ -3,3	-3.30	Algal Dolomite Mb	0.79	-0.14
GJ -3	-3.00	Algal Dolomite Mb	0.98	-0.82
GJ -2,6	-2.60	Algal Dolomite Mb	1.05	-1.88
GJ -2	-2.00	Algal Dolomite Mb	0.81	-2.73
GJ -1,6	-1.60	Algal Dolomite Mb	0.57	-3.58
GJ -1,3	-1.30	Algal Dolomite Mb	0.63	-1.43
GJ -1	-1.00	Algal Dolomite Mb	0.56	-3.14
GJ -0,6	-0.60	Algal Dolomite Mb	0.52	-1.63
GJ -0,3	-0.30	Algal Dolomite Mb	0.33	-3.06
GJ 2,3	2.30	Gaojiashan Member	0.80	-2.01
GJ 8,6	8.60	Gaojiashan Member	0.26	-0.20
GJ 9,5	9.50	Gaojiashan Member	0.14	-0.44
GJ 10,3	10.30	Gaojiashan Member	0.71	-0.73
GJ 10,6	10.60	Gaojiashan Member	0.67	-0.91
GJ 11	11.00	Gaojiashan Member	0.92	0.01
GJ 12,6	12.60	Gaojiashan Member	-0.81	-3.73
GJ 13	13.00	Gaojiashan Member	-0.05	-5.35
GJ 13,3	13.30	Gaojiashan Member	0.85	-4.54
GJ 13,6	13.60	Gaojiashan Member	0.61	-4.04
GJ 14,3	14.30	Gaojiashan Member	0.90	
GJ 14,8	14.80	Gaojiashan Member	0.32	
GJ 15,6	15.60	Gaojiashan Member	0.26	
GJ 16,3	16.30	Gaojiashan Member	1.19	-4.83
GJ 17,6	17.60	Gaojiashan Member	0.65	
GJ 18	18.00	Gaojiashan Member	-0.09	
GJ 18,3	18.30	Gaojiashan Member	0.02	
GJ 18,6	18.60	Gaojiashan Member	-0.06	-8.60
GJ 19	19.00	Gaojiashan Member	0.23	-6.27
GJ 19,3	19.30	Gaojiashan Member	-0.33	
GJ 19,6	19.60	Gaojiashan Member	0.56	
GJ 20	20.00	Gaojiashan Member	1.18	-6.67
GJ 20,3	20.30	Gaojiashan Member	-0.94	
GJ 20,6	20.60	Gaojiashan Member	1.22	
GJ 21	21.00	Gaojiashan Member	0.85	
GJ 21,3	21.30	Gaojiashan Member	0.42	
GJ 21,6	21.60	Gaojiashan Member	-1.90	-7.57
GJ 22	22.00	Gaojiashan Member	0.72	-6.05
GJ 22,3	22.30	Gaojiashan Member	0.82	
GJ 22,6	22.60	Gaojiashan Member	0.96	
GJ 23,3	23.30	Gaojiashan Member	1.68	
GJ 24	24.00	Gaojiashan Member	1.54	
GJ 24,3	24.30	Gaojiashan Member	1.27	
GJ 24,6	24.60	Gaojiashan Member	0.55	
GJ 25	25.00	Gaojiashan Member	1.33	
GJ 25,3	25.30	Gaojiashan Member	1.04	-6.64
GJ 25,5	25.50	Gaojiashan Member	0.85	-7.12
GJ 26	26.00	Gaojiashan Member	1.81	
GJ 26,3	26.30	Gaojiashan Member	0.99	
GJ 26,6	26.60	Gaojiashan Member	-0.35	-7.59
GJ 27	27.00	Gaojiashan Member	1.32	-6.51
GJ 27,3	27.30	Gaojiashan Member	1.33	
GJ 27,6	27.60	Gaojiashan Member	2.29	
GJ 28,3	28.30	Gaojiashan Member	2.00	
GJ 28,6	28.60	Gaojiashan Member	-0.65	
GJ 29	29.00	Gaojiashan Member	0.95	-6.63

Sample	Height [m]	Member	$\delta^{13}C_{carb}$ [‰,VPDB]	$\delta^{18}O$ [‰,VPDB]
GJ 30	30.00	Gaojiashan Member	2.04	
GJ 31,3	31.30	Gaojiashan Member	2.58	-5.52
GJ 31,6	31.60	Gaojiashan Member	3.04	-5.70
GJ 32	32.00	Gaojiashan Member	4.13	
GJ 32,3	32.30	Gaojiashan Member	3.16	
GJ 32,6	32.60	Gaojiashan Member	2.75	-6.07
GJ 33	33.00	Gaojiashan Member	-1.69	
GJ 33,6	33.60	Gaojiashan Member	0.22	-7.31
GJ 34,6	34.60	Gaojiashan Member	-1.20	
GJ 35	35.00	Gaojiashan Member	-0.82	-7.84
GJ 35,3	35.30	Gaojiashan Member	0.30	
GJ 35,6	35.60	Gaojiashan Member	4.21	-4.99
GJ 36	36.00	Gaojiashan Member	4.33	-5.88
GJ 36,3	36.30	Gaojiashan Member	4.27	
GJ 37	37.00	Gaojiashan Member	2.26	
GJ 37,3	37.30	Gaojiashan Member	4.56	-5.65
GJ 37,6	37.60	Gaojiashan Member	1.60	-7.37
GJ 37,7	37.70	Gaojiashan Member	0.65	-5.22
GJ 38	38.00	Gaojiashan Member	6.30	-3.42
GJ 38,3	38.30	Gaojiashan Member	2.96	-7.61
GJ 38,6	38.60	Gaojiashan Member	0.92	-7.85
GJ 39	39.00	Gaojiashan Member	4.62	-5.55
GJ 39,3	39.30	Gaojiashan Member	5.71	-5.62
GJ 39,6	39.60	Gaojiashan Member	5.16	-5.02
GJ 40	40.00	Gaojiashan Member	3.84	-8.88
GJ 40,3	40.30	Gaojiashan Member	5.12	-5.29
GJ 40,6	40.60	Gaojiashan Member	5.66	-6.56
GJ 41	41.00	Gaojiashan Member	4.56	-5.49
GJ 41,3	41.30	Gaojiashan Member	5.31	-5.66
GJ 42	42.00	Gaojiashan Member	5.45	-5.38
GJ 42,3	42.30	Gaojiashan Member	5.07	
GJ 42,6	42.60	Gaojiashan Member	5.57	-5.69
GJ 43	43.00	Gaojiashan Member	5.47	-6.36
GJ 43,3	43.30	Gaojiashan Member	5.33	-7.05
GJ 43,6	43.60	Gaojiashan Member	5.55	-6.00
GJ 44	44.00	Gaojiashan Member	5.27	
GJ 44,3	44.30	Gaojiashan Member	4.38	-6.12
GJ 45	45.00	Gaojiashan Member	6.17	
GJ 45,3	45.30	Gaojiashan Member	6.18	-6.14
GJ 45,5	45.50	Gaojiashan Member	5.64	-6.01
GJ 46	46.00	Gaojiashan Member	5.98	-5.77
GJ 46,3	46.30	Gaojiashan Member	5.86	-6.24
GJ 46,6	46.60	Gaojiashan Member	5.33	-5.43
GJ 47,3	47.30	Gaojiashan Member	5.77	-5.32
GJ 47,6	47.60	Gaojiashan Member	5.11	-5.81
GJ 48	48.00	Gaojiashan Member	4.47	-6.01
GJ 48,3	48.30	Gaojiashan Member	5.37	-5.59
GJ 48,6	48.60	Gaojiashan Member	4.90	-5.42
GJ 49	49.00	Gaojiashan Member	5.28	-5.68
GJ 49,3	49.30	Gaojiashan Member	5.34	-5.54
GJ 49,6	49.60	Gaojiashan Member	4.56	-5.32
GJ 50	50.00	Gaojiashan Member	4.06	
GJ 50,3	50.30	Gaojiashan Member	4.25	-4.72
GJ 50,6	50.60	Gaojiashan Member	2.85	-6.98
GJ 51	51.00	Gaojiashan Member	4.02	-5.90
GJ 51,3	51.30	Gaojiashan Member	2.35	-6.36

Sample	Height [m]	Member	$\delta^{13}C_{carb}$ [‰,VPDB]	$\delta^{18}O$ [‰,VPDB]
GJ 51,6	51.60	Gaojiashan Member	3.88	-3.36
GJ 52	52.00	Gaojiashan Member	3.56	-4.03
GJ 52,3	52.30	Gaojiashan Member	3.50	-2.59
GJ 52,6	52.60	Gaojiashan Member	2.96	-5.17
GJ 53	53.00	Gaojiashan Member	-4.92	-6.63
GJ 53,3	53.30	Gaojiashan Member	0.42	-7.69
GJ 53,6	53.60	Gaojiashan Member	1.44	-3.49
GJ 54	54.00	Gaojiashan Member	-0.84	-6.17
GJ 54,6	54.60	Gaojiashan Member	1.59	-7.75
GJ 55	55.00	Gaojiashan Member	0.78	-6.94
GJ 55,3	55.30	Gaojiashan Member	0.35	-6.95
GJ 56	56.00	Gaojiashan Member	-3.86	-7.45
GJ 56,3	56.30	Gaojiashan Member	-3.75	-9.73
GJ 56,6	56.60	Gaojiashan Member	-3.29	-8.99
GJ 57	57.00	Gaojiashan Member	-6.00	-8.05
GJ 58	58.00	Gaojiashan Member	-0.80	-7.21
GJ 58,6	58.60	Gaojiashan Member	2.06	-5.15
GJ 58,7	58.70	Gaojiashan Member	1.04	
GJ 59,6	59.60	Gaojiashan Member	1.09	-6.85
GJ 61,6	61.60	Beiwan Member	1.65	
GJ 62,3	62.30	Beiwan Member	1.20	
GJ 62,6	62.60	Beiwan Member	1.28	
GJ 63,3	63.30	Beiwan Member	1.35	-2.40
GJ 64	64.00	Beiwan Member	1.63	
GJ 64,6	64.60	Beiwan Member	1.99	-2.09
GJ 65	65.00	Beiwan Member	1.94	-2.86
GJ 65,3	65.30	Beiwan Member	2.04	-2.67
GJ 65,6	65.60	Beiwan Member	1.80	-2.55
GJ 66,3	66.30	Beiwan Member	-0.44	-2.65
GJ 67	67.00	Beiwan Member	0.27	-2.32
GJ 67,3	67.30	Beiwan Member	1.57	-2.30
GJ 67,6	67.60	Beiwan Member	1.91	-2.58
GJ 68	68.00	Beiwan Member	1.91	-2.44
GJ 68,3	68.30	Beiwan Member	2.05	-2.16
GJ 68,6	68.60	Beiwan Member	2.37	-1.60
GJ 69	69.00	Beiwan Member	-0.39	-4.66
GJ 69,3	69.30	Beiwan Member	1.85	-2.15
GJ 69,6	69.60	Beiwan Member	2.17	-2.51

Table 4: *List of all samples analyzed for $\delta^{18}O$ [‰, VPDB] and $\delta^{13}C_{carb}$ [‰, VPDB].*

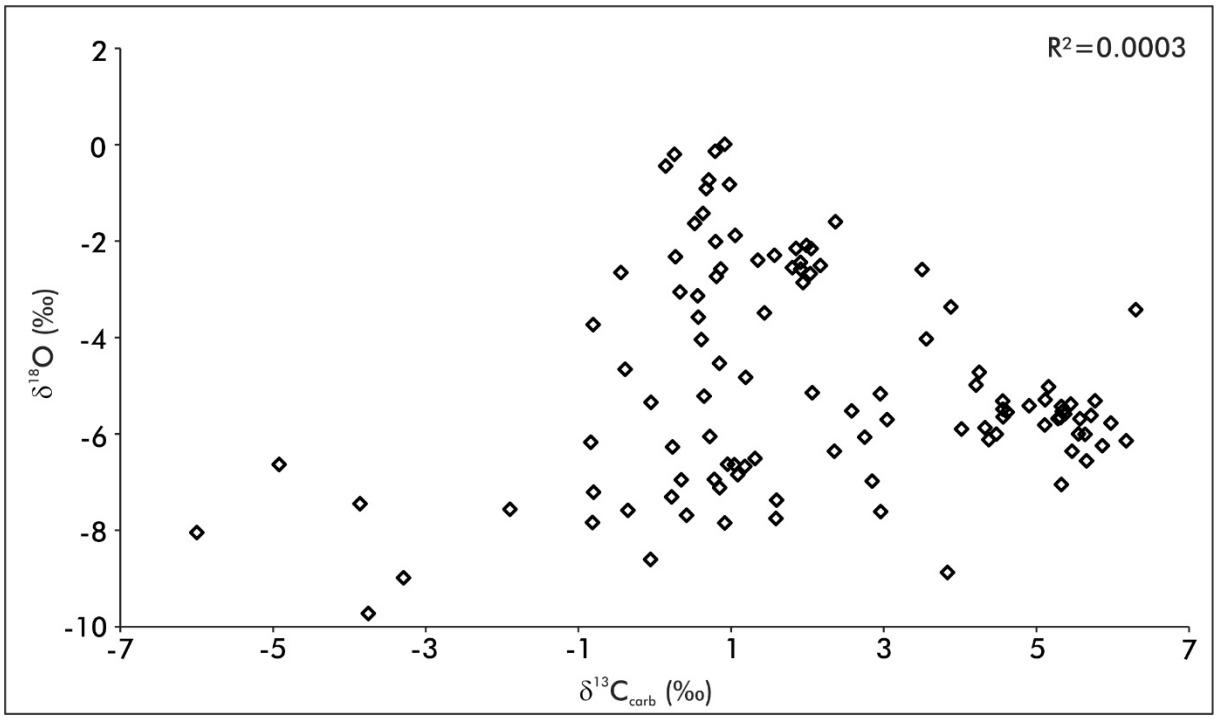

Figure 13: *Cross plot of $\delta^{13}C_{carb}$ [‰, VPDB] vs. $\delta^{18}O$ [‰, VPDB] of all analyzed samples. R^2=0.0003. None of the samples show $\delta^{18}O$ values below -10‰.*

Boron isotopes

A secondary alteration by depletion or enrichment of boron (e.g. by fluid migration or palaeo karst) could change the primary boron isotopic composition (Spivack and You, 1997). Therefore, samples were checked for a potential correlation of $\delta^{11}B$ values and boron concentration resulting from secondary alteration. However, $\delta^{11}B$ values and the boron concentration of the Gaojiashan Section show no significant correlation at the 5% significance level (R^2=0.04, Fig. 14).

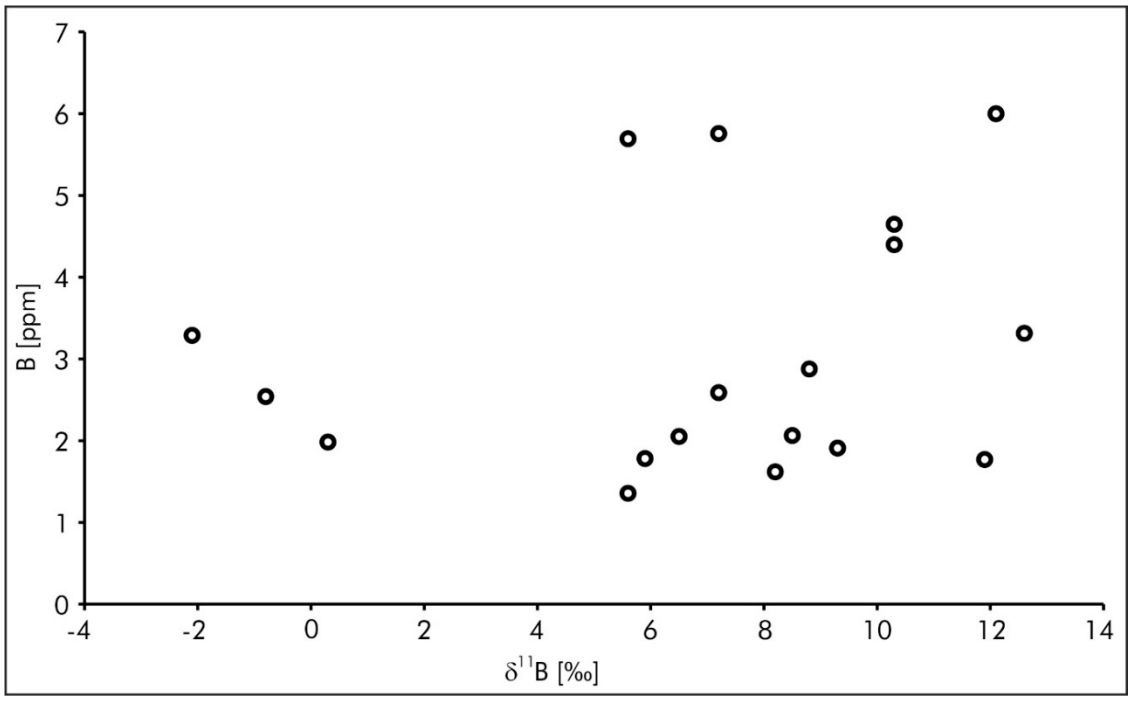

Figure 14: Cross plot of $\delta^{11}B$ [‰] vs. boron concentration [ppm]. No correlation is obvious, $R^2=0.04$.

Palaeo pH reconstruction

To infer ocean pH values we performed our calculations with a $\delta^{11}B_{sw}$ value of 24‰ (see 3.6.1 for reasons). Changes to this assumption (e.g. 23.5-24.5‰) lead to minor deviations in supposed seawater pH (<0.2), nevertheless the overall pattern including the strong ocean acidification >1 pH units visible at the uppermost section part stays the same.

Due to the fact that the boron isotopic composition and the abundance of the two dominant boron species are also temperature and salinity dependent (Dickson, 1990; Klochko et al., 2006), we checked for variations induced by these factors. A deviation of ±10°C to the assumed seawater temperature of 25°C would result in a maximum difference of 0.2 pH, whereby colder temperatures lead to slightly higher pH conditions and vice versa. We used a salinity S=35 ppt for our seawater pH calculations. Variations by ±10 ppt modify the calculated pH only negligible.

Lithium isotopes:

For the reason that no Proterozoic or even Paleozoic lithium isotope data is available in literature it is difficult to precisely constrain fluxes from and to the ocean like it is possible for recent data. Moreover, the lithium isotopic composition of the Ediacaran seawater

(δ^7Li_{sw}) and its exact residence time is unknown. Misra and Froelich (2012) suggested a δ^7Li_{sw} composition of approximately 22‰ for the time 60 Ma ago together with a similar residence time to nowadays. Whether and in which order of magnitude the δ^7Li_{sw} composition has changed since the Ediacaran can only be estimated. Hence, we only interpret the overall isotopic pattern with its relative shifts and no absolute values. Nevertheless, valuable insights into changing weathering regimes and conditions are given due to significant variations in our δ^7Li_{carb} and δ^7Li_{det} data (Fig. 15). Since neither a significant positive nor a significant anti correlation at 5% significance level is obvious for the whole dataset (R^2= 0.002) a dissolution of ^{6}Li-enriched clays as source of the negative excursion in δ^7Li_{carb} from 12 to 1‰ can be ruled out. The interpretation (see chapter 3.6.2) of a congruent weathering regime with complete rock dissolution as predominant factor for the negative excursion seems valid for the reason that δ^7Li_{det} shows similar values of ~1‰ shortly prior to the negative δ^7Li_{carb} anomaly.

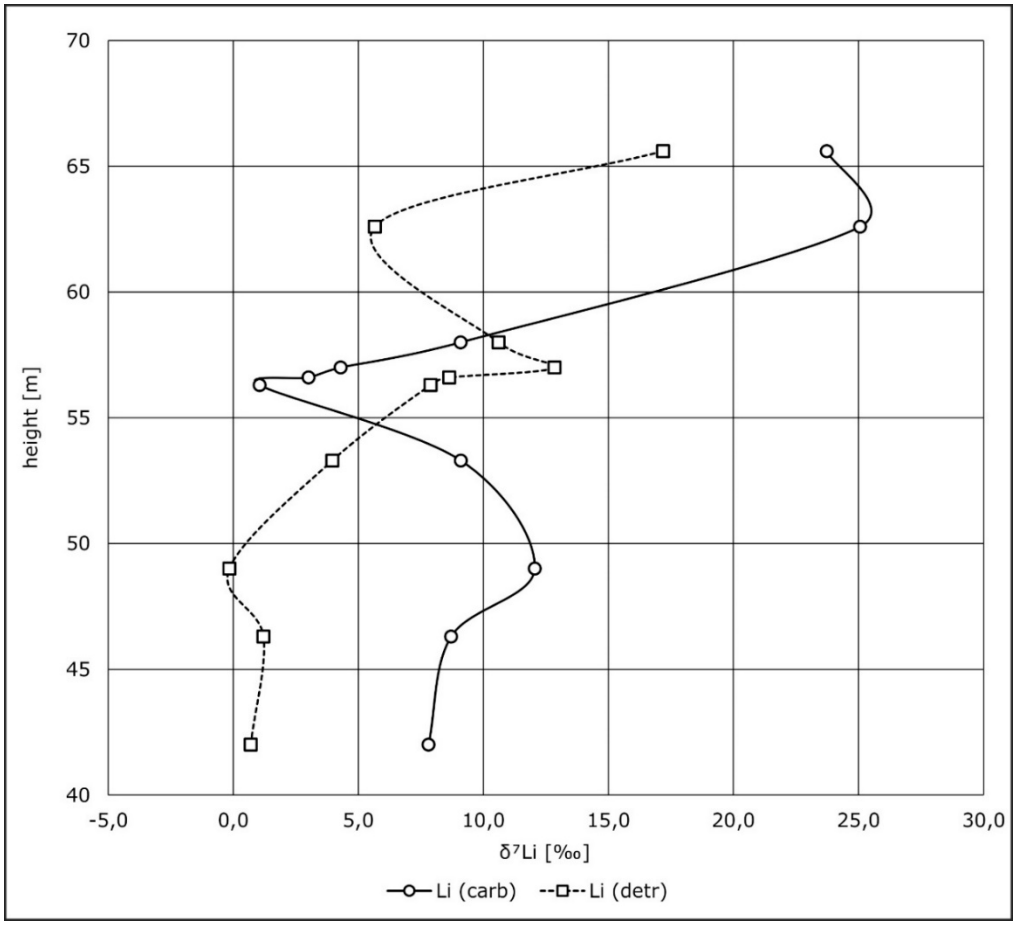

Figure 15: δ^7Li_{carb} (black line with circles) and δ^7Li_{det} (dashed line with squares) isotopic composition of the upper Gaojiashan Member at the Gaojiashan Section. Neither a positive nor a negative correlation is obvious at the 5% significance level.

References

Dickson, A. G., 1990, Thermodynamics of the dissociation of boric acid in synthetic seawater from 273.15 to 318.15 K: Deep Sea Research Part A. Oceanographic Research Papers, v. 37, no. 5, p. 755-766.

Gamper, A., Struck, U., Scouflaire, Q., and Weber, B., 2012, Carbon and Nitrogen isotope study of the upper Ediacaran Gaojiashan Member in South China: Insights in causes of the Cambrian Explosion: Terra Nostra, v. Schriften der GeoUnion Alfred-Wegener-Stiftung – 2012/3, Centenary Meeting of the Paläontologische Gesellschaft, p. 61.

Halverson, G. P., Hoffman, P. F., Schrag, D. P., Maloof, A. C., and Rice, A. H. N., 2005, Toward a Neoproterozoic composite carbon-isotope record: Geological Society of America Bulletin, v. 117, no. 9-10, p. 1181-1207.

Klochko, K., Kaufman, A. J., Yao, W., Byrne, R. H., and Tossell, J. A., 2006, Experimental measurement of boron isotope fractionation in seawater: Earth and Planetary Science Letters, v. 248, no. 1-2, p. 276-285.

Li, D., Ling, H.-F., Shields-Zhou, G. A., Chen, X., Cremonese, L., Och, L., Thirlwall, M., and Manning, C. J., 2013, Carbon and strontium isotope evolution of seawater across the Ediacaran–Cambrian transition: Evidence from the Xiaotan section, NE Yunnan, South China: Precambrian Research, v. 225, no. 0, p. 128-147.

Misra, S., and Froelich, P. N., 2012, Lithium Isotope History of Cenozoic Seawater: Changes in Silicate Weathering and Reverse Weathering: Science, v. 335, no. 6070, p. 818-823.

Spivack, A. J., and You, C.-F., 1997, Boron isotopic geochemistry of carbonates and pore waters, Ocean Drilling Program Site 851: Earth and Planetary Science Letters, v. 152, no. 1–4, p. 113-122.

CHAPTER 4:

EDIACARAN TO CAMBRIAN OCEAN PH AND CONTINENTAL WEATHERING CONDITIONS: IMPLICATIONS FROM SOUTHERN KAZAKHSTAN

Manuscript in preparation for submission to *Precambrian Research*.

Simone Kasemann helped during data interpretation and with comments on the late-stage manuscript versions.

Ediacaran to Cambrian ocean pH and continental weathering conditions: Implications from Southern Kazakhstan

Frank Ohnemueller[1], Gappar Ergaliev[2], Simone A. Kasemann[1]

[1]*Department of Geosciences and MARUM - Center for Marine Environmental Sciences, University of Bremen, Leobener Str., D-28359 Bremen*
[2]*Kazakh Academy of Sciences, KZ-050010 Almaty*

4.1 Abstract

From the aftermath of the late Cryogenian Marinoan glaciation (~635 Ma) to the Early Cambrian the Earth underwent major changes in (bio-)geochemical processes, climate and ocean-atmosphere interactions. This time period was intensely investigated within the last decades, yet the Karatau microcontinent (Kazakhstan, Central Asia) received little attention. The studied Kyrshabakty Section is located at the Malyi Karatau Range and hosts a >500 m succession of volcanic, siliciclastic and predominantly carbonate rocks of Early Cryogenian to Ordovician age.

Here we present the first boron ($\delta^{11}B$) and strontium ($^{87}Sr/^{86}Sr$) isotope dataset for the Karatau microcontinent to elucidate long-term modifications to ocean pH and weathering fluxes from the Ediacaran until the Early Cambrian (Stage 3, ~515 Ma). Within the Marinoan-age cap dolomites an ocean acidification event is indicated by a transient negative $\delta^{11}B$ excursion of 7‰. Corresponding $^{87}Sr/^{86}Sr$ as low as 0.7083 are close to published primary post-glacial seawater values of ~0.707. The middle part of the section records the tremendous negative $\delta^{13}C_{carb}$ Shuram-Wonoka anomaly with values down to -9.7‰ and radiogenic $^{87}Sr/^{86}Sr$ ratios scattering around 0.713. $\delta^{11}B$ data of this time period show a constant decline of ~9‰, probably representing a continuous decrease in ocean pH; however a primary origin must be questioned. At the Precambrian-Cambrian transition boron isotopes indicate a steady decrease in ocean pH by >0.7. Coeval $^{87}Sr/^{86}Sr$ ratios show an increasing trend during the latest Ediacaran from 0.7086 to 0.7094 and decrease to 0.7092 within the Cambrian.

Overall, the Kyrshabakty Section provides valuable insights into changing ocean pH and weathering conditions over a time span of ~120 Ma, namely the general rise of seawater $^{87}Sr/^{86}Sr$ during the Ediacaran and several fluctuations in ocean pH until the Cambrian.

Keywords: Ediacaran, boron, strontium, ocean pH, weathering, Kazakhstan

4.2 Introduction

The Kazakh Karatau microcontinent provides access to various well exposed carbonate and siliciclastic successions giving us the opportunity to study the palaeo ocean geochemical evolution from the Neoproterozoic to Early Paleozoic Era. Precambrian to Cambrian rocks worldwide record and proof the existence of global-scale glaciations, atmospheric and marine oxygenation events, major modifications in (bio-) geochemical cycles together with the development of novel organisms and body plans finally resulting in the diversification and rise of metazoa (Bjerrum and Canfield, 2011; Canfield et al., 2007; Halverson et al., 2010; Hoffman et al., 1998; Johnston et al., 2012; Macdonald et al., 2010; Sahoo et al., 2012). Due to the rare combination of an extensive fossil record, especially for the Cambrian, and abundant sections suitable for chemostratigraphy it is remarkable how little attraction the Karatau microcontinent has gotten thus far. Almost all literature dealing with the Karatau microcontinent has a strong focus on the phosphorite deposits that are intensely mined at the working area (see Eganov et al., 1984 and references therein) and on Cambrian fossil assemblages. Meert et al. (2011) provided one of the first Ediacaran chemostratigraphic investigations ($\delta^{13}C_{carb}$) of Southern Kazakhstan and tried to constrain the occurrence of *Nimbia occlusa* and *Aspidella terranovica* to >766 Ma.

We studied the same section to get insights into the ocean pH and weathering evolution over a timespan of ~120 Ma. We provide the first available boron ($\delta^{11}B$) and strontium ($^{87}Sr/^{86}Sr$) isotope dataset of Southern Kazakhstan beginning from the aftermath of the late Cryogenian Marinoan glaciation (~635 Ma, Hoffmann et al., 2004) to the lower Cambrian (Stage 3, ~515 Ma, Weber et al., 2013). This multi-proxy geochemical approach based on carbonate strata of the Kyrshabakty Section (Fig. 16) will contribute to a better understanding of crucial stages in Earth's history like the

deglacial phase of the Marinoan ice age, the time slice hosting the Shuram-Wonoka $\delta^{13}C$ negative anomaly and the Precambrian-Cambrian transition.

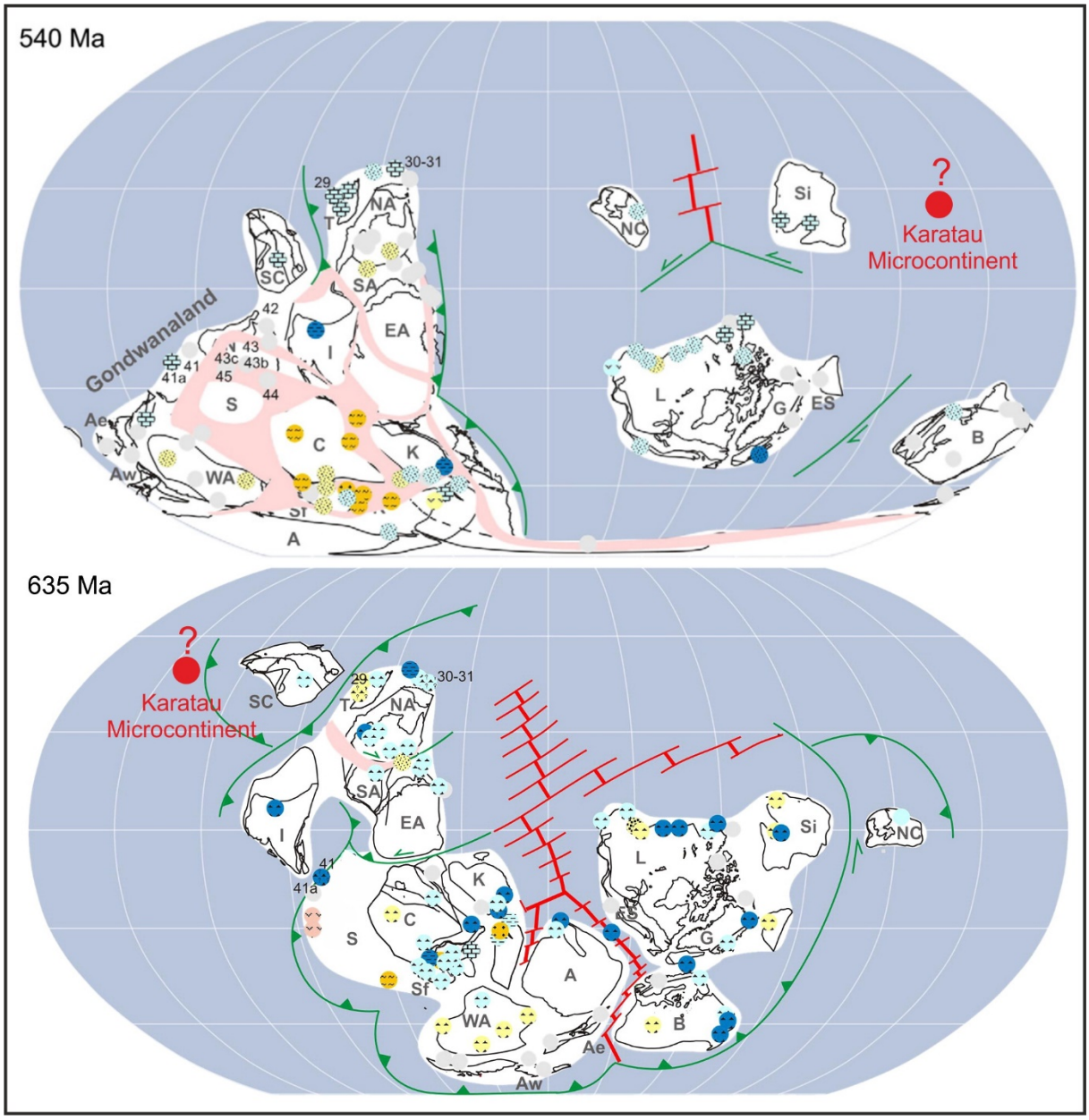

Figure 16: *Slightly modified palaeogeographic reconstruction for 635 Ma and 540 Ma by Li et al. (2013b) The investigated Karatau microcontinent (red solid circle) is suggested to be near Siberia at least during the Early Cambrian (Weber et al., 2013).*

4.3 Geological setting

In southern Kazakhstan, near the border to Kyrgyzstan, the Karatau Mountains comprise abundant Neoproterozoic to Cambrian rocks. Fossil data, as well as palaeomagnetic and palaeogeographic reconstructions suggest the Karatau microcontinent to be near South China, Mongolia and the Tarim Block (Fig. 16) during Neoproterozoic times (Li et al., 2013b; Weber et al., 2013).

The Bolshoi (NW) and Malyi (SE) Karatau Range form the foothills of the central Asian Tian Shan orogen, in turn being part of the Himalayan orogenic belt. Both are divided by the Main Karatau Fault (Alexeiev et al., 2009 and references therein) and surrounded by the Syr Dar'ya Basin to the SW and the Chu Sarysu Basin to the NE (Allen et al., 2001). Our study area (Fig. 17) is part of the Malyi Karatau which is characterized by a far lesser thermal and tectonic history in comparison to the Bolshoi Karatau (Weber et al., 2013) which has obvious indices of metamorphic overprint. The investigated Kyrshabakty Section (Fig. 17, 43°32'2.1''N, 69°57'7.7''E) is located approximately 18 km E of Zhanatas, Zhambyl Province, and provides access to a >500 m thick succession of volcanics, siliciclastics and carbonates. From the base to the top the section consists of the Kurgan Formation corresponding to the Malokaroy Series and the Aktas, Kyrshabakty, Chuluktau and Shabakty Formations corresponding to the Tamdy Series (Eganov et al., 1984; Levashova et al., 2011). The Neoproterozoic Kurgan Formation comprises mainly red and green volcanoclastic rocks, tuffaceous siltstones and sandstones without any carbonate admixtures (Eganov et al., 1984). On top of the Kurgan Formation a roughly 45 m thick diamictite is deposited. The so called Aktas tillite is part of the lowermost Kyrshabakty Formation and, for that matter, of the Tamdy Series. The predominantly reddish rocks with cm- to dm-scale green clasts and dropstones are overlain by ~3.5-4 m thick pinkish to ivory-colored cap dolomites without any noticeable sedimentary features besides a fine lamination. Up-section the Kyrshabakty Formation continues with an alternation of dolomitic sandstones and sandy dolostones with an increasing trend in dolomite content towards the top. This lower part of the section is defined by a transgressive system tract and the palaeoenvironment is suggested to represent a very shallow water platform setting which is also confirmed by Eganov et al. (1986). The middle part of the Kyrshabakty Formation (samples KY 20-KY 37) consists of red and beige, sandy limestones that are partly phosphate-bearing. After ~12 m of unexposed strata the uppermost Kyrshabakty Formation is represented by the Berkuty Dolomite that usually overlies Kyrshabakty red beds (Eganov et al., 1984). The ~6 m of greyish, ivory- to buff-colored dolomites can be subdivided into 3 units (Heubeck et al., 2013). Unit 1 displays large scale folded, medium bedded dolograinstones. Subunit 2 is described by a thin-bedded, partly arenaceous dolostone with minor quartz lenses and phosphatic interlayers (Eganov et al., 1984). Heubeck et al. (2013) suggest the middle unit 2 to represent a megaconglomerate developed as

consequence of large-scale seismogenic deformation at nearby sections. However, at the sampled transect no disruptions induced by seismic activity are obvious. The uppermost Berkuty Dolomite (unit 3) consists of grey thick- and thin-bedded dolostones and dolomitic limestones that contain few chert and phosphate lenses and nodules. Of major importance are also findings of the first lowermost Cambrian small shelly fossils (SSFs, *Protohertzina anabarica,* Missarzhevsky and Mambetov, 1981) within the uppermost 70 cm of the Berkuty Dolomite (Eganov et al., 1984 and Seidig, pers. comm.).

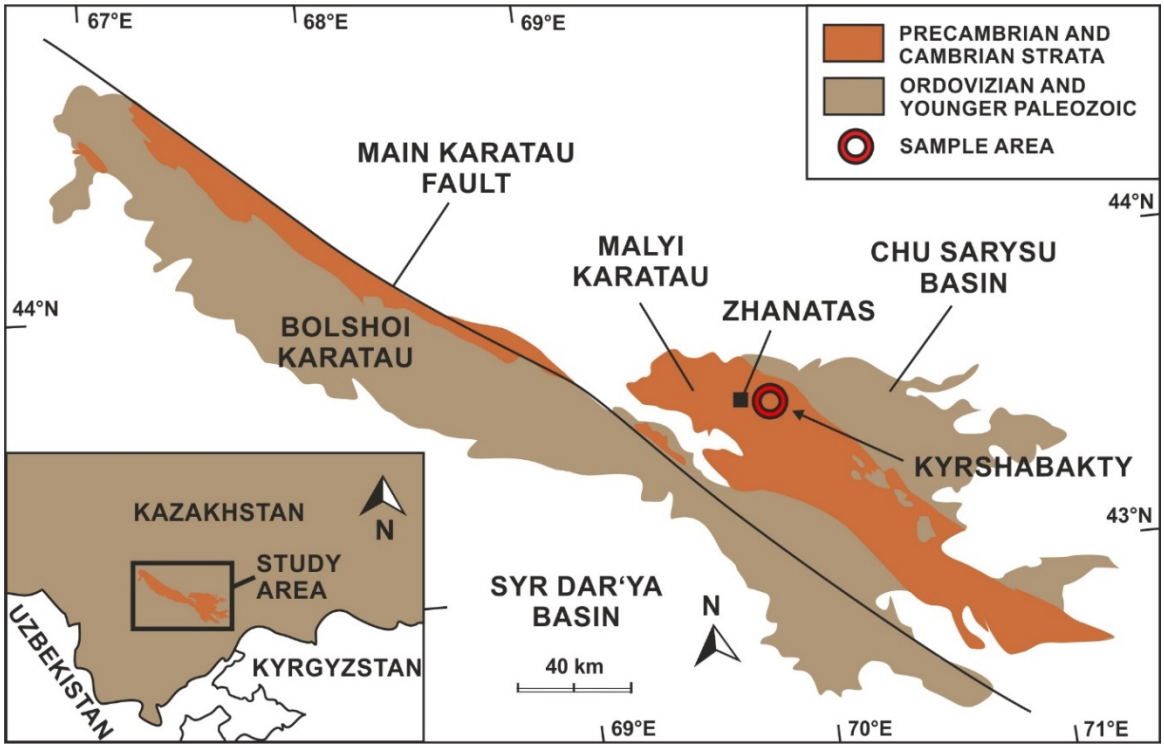

Figure 17: *Geological sketch map of the Malyi and Bolshoi Karatau Range displaying the study area E of Zhanatas (modified after Alexeiev et al., 2009; Chakabaev, 1979). Inset map shows the supra-regional position in southern Kazakhstan, next to the borders of Kyrgyzstan and Uzbekistan.*

The lower Cambrian of the Kyrshabakty Section is generally very condensed and not continuously exposed. It consists of the Chuluktau and Shabakty Formation, being equivalents to the Fortunian, Cambrian Stage 2 and Stage 3 (Weber et al., 2013). The Aksai Member (lowermost Chuluktau Formation) overlies the Berkuty Dolomite and consists of a thin black chert layer as well as cherty and intensely weathered shales. On top of the ~1.5 m thick Aksai Member, 6 m of phosphorites corresponding to the Karatau Member are exposed. These show a change from predominantly argillo-calcareous-phosphatic shales to beds of granular cherty phosphorites. The overlying Fe-Mn horizon and conglomerate unit of the Ushbass Member seem to be missing at the

Kyrshabakty Section and thus the succession is capped by massive, thick-bedded, light grey dolostones of the Shabakty Formation. Near the base of the Shabakty Formation numerous cm-scale phosphorite and chert layers as well as nodules are present. Due to a couple of disconformities and hiatuses and the general condensed character of the Cambrian members, precise geochronological constraints are hard to determine. Nevertheless, the Kyrshabakty Section is one of the most suitable sections to study changes in Neoproterozoic-Cambrian ocean geochemistry for the reason that predominantly marine carbonate rocks from the Marinoan time (~635 Ma) to the lower Cambrian stage 3 (~515 Ma) are exposed within a single transect.

4.4 Methods

4.4.1 Sample selection and quality control

In total more than 60 fresh carbonate rock hand samples were taken in decimeter-meter intervals along a ~200 m transect at the Kyrshabakty Section. We stuck to strict selection criteria beginning in the field. Samples with visible alteration rims or obvious veining were directly excluded. Afterwards, individual selected samples were checked by thin section analyses and almost every sample for their oxygen isotopic composition (Table 5). Rock powders used for further isotope measurements were prepared from cleaned, fresh surface rock chips with an agate vibratory disc mill at the Museum fuer Naturkunde Berlin, Germany.

Ohnemueller et al. (in review) already stated that clay contamination is a minor issue for Kyrshabakty Section carbonates and can be excluded for two reasons: (i) analyzed carbonates only possess clay contents <2% as determined by XRD analyses (semi quantitative evaluation after Cook et al. (1975)) performed at the TU Berlin, Germany and (ii) for the reason that the sample preparation procedure does not dissolve clays. Besides clay contamination also secondary alteration by late diagenesis can affect the primary isotopic signal. Oxygen isotopes are thought to be a powerful tool as an evaluation criteria for late diagenetic effects and hydrothermal overprint. For Neoproterozoic rocks primary isotopic signatures can be expected for samples with $\delta^{18}O$ >-10‰ (Bartley et al., 1998; Li et al., 2013a; Ling et al., 2007). Only three samples (KY 19, KY 22 and KY 23) of our dataset show more negative $\delta^{18}O$ values. In addition, a correlation between $\delta^{18}O$ and $\delta^{13}C$ can be indicative of secondary processes

like diagenesis (Fig. 18). Nevertheless, also correlated primary datasets exist (e.g. Halverson et al., 2007), which is why this evaluation criteria is doubted by several authors. For the lower part of the Kyrshabakty Section (KY 3 to KY 13) no significant correlation between carbon and oxygen isotopes is obvious ($R^2=0.01$). On the contrary, the complete dataset shows a distinct correlation within the 5% significance level between $\delta^{18}O$ and $\delta^{13}C$ ($R^2=0.76$), however, their average $\delta^{18}O$ values only scatter around -5‰ far-off the suggested diagenesis criteria of -10‰. For the middle part of the section (recording the Shuram-Wonoka interval, KY 20-KY 37, solid circles in Fig. 18) an anti-correlation between $\delta^{11}B$ and $\delta^{13}C$ as well as $\delta^{18}O$ is obvious, which is unusual for late open-system diagenesis. Usually, $\delta^{11}B$, $\delta^{13}C$ and $\delta^{18}O$ values decrease with advanced diagenesis (Paris et al., 2010a; Spivack and You, 1997; Veizer et al., 1999), albeit the exact opposite is shown in our data. The most negative $\delta^{18}O$ and $\delta^{13}C$ values possess the highest $\delta^{11}B$ values. It appears likely that only very early, closed system diagenesis, not effecting the primary signal, occurred. Therefore, we have no good reason to distrust our isotopic data and thus claim for a primary origin, at least for all data points aside from the Shuram-Wonoka time slice, which could be secondary altered.

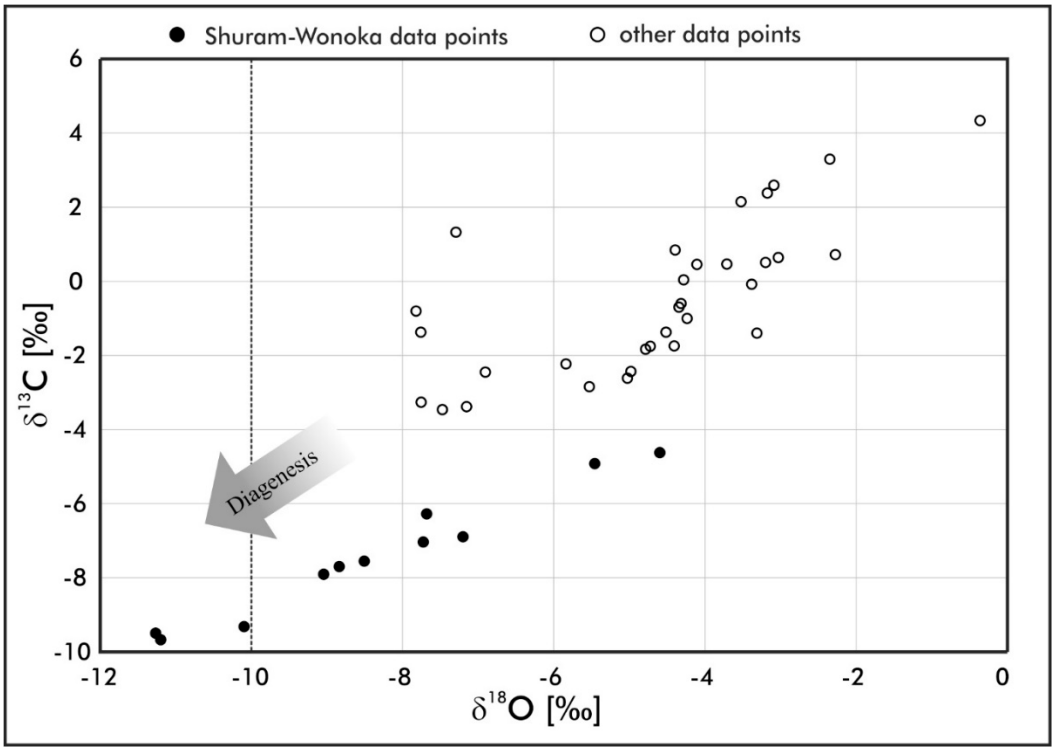

Figure 18: *Cross-plot of $\delta^{18}O$ [‰] vs. $\delta^{13}C_{carb}$ [‰]. Solid circles represent samples corresponding to the Shuram-Wonoka time interval. Open circles show all remaining data points. Only three data points are fulfilling the $\delta^{18}O$ < -10‰ diagenesis criteria (to the left of the dotted line).*

4.4.2 Analytical techniques

Boron ($\delta^{11}B$) isotope analyses were performed following the method described in Kasemann et al. (2001). For analyses 10 mg of the sample powder was dissolved in 100 µl 1 N HCl for 24 h at 20°C and centrifuged afterwards. This procedure allows complete carbonate and dolomite dissolution and avoids detrital mineral contamination. The $n(^{11}B)/n(^{10}B)$ measurements were performed on a Thermo Fisher Scientific TRITON *Plus* mass spectrometer, using negative thermal ionization mass spectrometry (N-TIMS). 1 µl boron-free seawater emitter was placed on a degassed Re single filament and dried at 0.7 A. Subsequently, 1 µl of the sample solution containing ~1 ng B was added, evaporated to complete dryness at 0.7 A and afterwards heated at 1.2 A for 30 s. Boron isotopes were registered as BO_2^- complexes on masses 42 and 43, and measurements were carried out at 970°-1050°C with an ion beam intensity of 3-30 pA on mass 43. Each measuring process consisted of up to 200 blocks with 10 cycles, taking about 3 hours of data acquisition. To correct for a CNO^- interference on mass 42 occurring at the beginning of some measurements and for isotopic fractionation during analysis, the extrapolation technique described by Kasemann et al. (2001) was used during data evaluation.

Boron isotope ratios are given in $\delta^{11}B$-notation relative to the certified reference material NIST SRM 951 that showed a $^{11}B/^{10}B$ ratio of 4.0068±0.0016 (2sd=0.4‰, n=40 over a period of 12 month). In addition to the NIST material, the standard material M93-TB-FC-1, a *Porites* coral with a published value of 24.8±0.4‰ ($2\sigma_{mean}$), as determined by different multicollector techniques (Kasemann et al., 2009), was also regularly analyzed. The coral was reproduced with a $\delta^{11}B$ value of 24.1±0.7‰ (2sd, n=16).

Sr separation methods of Pin and Bassin (1992) and Deniel and Pin (2001) were slightly modified and adapted for differing resin-volumes and rock-types used in this study. Prior to the column separation the carbonates were dissolved in cold 2 N HNO_3. Isotope measurements were performed on a Thermo Fisher Scientific TRITON *Plus* mass spectrometer on Re single filaments with a Ta emitter (Birck, 1986). The total strontium blank of this procedure is <40 pg. Strontium isotopic ratios are given in $^{87}Sr/^{86}Sr$ notation and were normalized to $^{86}Sr/^{88}Sr$ of 0.1194. The external reproducibility

according to the NIST SRM 987 reference material is $^{87}Sr/^{86}Sr$ 0.710250±16 (2sd, n=113; period: December 2011 to April 2014).

Carbon ($\delta^{13}C_{carb}$) and oxygen ($\delta^{18}O$) isotopic analyses were performed on a Thermo Finnigan GASBENCH II linked online to a Thermo Finnigan DELTA V isotope ratio mass spectrometer at the Museum fuer Naturkunde Berlin, Germany. Isotope ratios are reported in δ-notation in [‰] relative to the Vienna Peedee Belemnite (VPDB). The analytical reproducibility of $\delta^{13}C_{carb}$ and $\delta^{18}O$ values is generally better than ±0.2‰ (2sd) for both isotopic systems. A complete list of all analyzed samples can be found in table 5.

4.5 Results

All isotope data is summarized in table 5 and graphically illustrated in figure 19.

Sample	Height	$\delta^{13}C_{carb}$	$\delta^{18}O$	$\delta^{11}B$	2σ	pH	$^{87}Sr/^{86}Sr$	2SE
KY 3	58.40	-0.1	-3.4	8.7	±0.4	8.7	0.709461	±8
KY 4	58.60	-0.7	-4.3	6.5	±1.2	8.6	0.709084	±52
KY 5a	58.80	-1.4	-4.5	6.5	±1.6	8.6		
KY 5b	58.85	-1.8	-4.8	8.2	±0.4	8.7		
KY 6a	59.20			6.1	±1.0	8.6		
KY 6b	59.25	-1.7	-4.4	2.9	±0.4	8.3		
KY 7a	59.65	-2.4	-5.0	1.7	±0.8	8.2	0.709300	±23
KY 7b	59.70	-2.8	-5.5	5.6	±0.4	8.5		
KY 8	60.50	-1.3		6.2	±1.0	8.6		
KY 9	61.55	-2.6	-5.0	7.3	±0.4	8.6	0.708292	±172
KY 10	61.85	-1.0	-4.2	8.1	±0.4	8.7		
KY 10a	67.00	-1.4	-7.8	13.8	±0.8	9.1		
KY 11	77.65	0.0	-4.3	14.2	±0.4	9.1		
KY 12	87.50	-2.6						
KY 13	87.90	1.3	-7.3	7.8	±0.7	8.7		
KY 14	88.50	0.4						
KY 15	89.10	-0.6						
KY 16	89.20	-0.8	-7.8					
KY 17	92.50	0.0		5.8	±0.5	8.5		
KY 18	107.20	-7.9	-9.0	6.0	±1.0	8.5	0.713452	±19
KY 19	107.70	-9.3	-10.1					
KY 20	114.20	-8.4					0.712040	±34
KY 21	115.30	-7.6	-8.5			8.8		
KY 22	117.70	-9.5	-11.3	14.3	±1.6	8.9	0.712370	±9
KY 23	118.90	-9.7	-11.2					
KY 24	120.40	-8.2						
KY 25	122.60	-7.7	-8.8	13.3		8.7	0.711805	±36
KY 26	123.90	-7.7						

Sample	Height	$\delta^{13}C_{carb}$	$\delta^{18}O$	$\delta^{11}B$	2σ	pH	$^{87}Sr/^{86}Sr$	2SE
KY 27	125.50	-6.3						
KY 28	126.90	-6.3	-7.7	9.7	±1.3	8.6	0.711983	±10
KY 29	127.70	-7.7						
KY 30	128.70	-7.1						
KY 31	129.50	-5.8		10.3	±0.8	8.7		
KY 33	135.60	-7.0	-7.7	5.8	±0.9	8.4	0.713641	±9
KY 34	136.10	-6.9						
KY 35	138.70	-6.9	-7.2					
KY 36	139.00	-4.6	-4.6	4.7	±0.4	8.3	0.713710	±26
KY 37	140.50	-4.9	-5.5					
KY 38	166.30	2.7		12.5	±1.7	8.7	0.708611	±158
KY 39	166.90	4.3	-0.4	11.8	±0.4	8.7		
KY 41	168.20	3.3	-2.3	13.2	±0.4	8.8	0.709058	±24
KY 42	168.30	2.4	-3.2	15.9	±0.4	9.0		
KY 43	168.50	2.1	-3.5	6.8	±0.4	8.4	0.709152	±11
KY 44	169.10	2.6	-3.1	9.1	±0.9	8.5		
KY 45	169.25	0.5	-4.1	11.3	±0.6	8.7	0.709316	±8
KY 46	169.80	0.6	-3.0	11.3	±0.6	8.7		
KY 47	169.90	-1.8	-4.7	10.5	±0.6	8.6		
KY 48	170.90	1.5		8.1	±0.6	8.5	0.709172	±8
KY 49	172.20	-2.2	-5.8	7.5	±0.4	8.4	0.709413	±10
KY 53	179.80	-1.4	-3.3	5.3	±1.7	8.3		
KY 54	183.00	-4.2						
KY 55	184.30	-2.4	-6.9					
KY 56	184.90	-1.1						
KY 57	185.40	0.7	-2.3	3.2	±1.2	8.1		
KY 58	188.30	-3.5	-7.5					
KY 59	189.00	-0.9		11.6	±0.8	8.7	0.709160	±26
KY 60	191.80	0.5	-3.2					
KY 61	192.75	-3.4	-7.2					
KY 62a	193.85	-3.3	-7.8					
KY 62c	193.90	0.8	-4.4					
KY 63a	194.60	-0.6	-4.3					
KY 63c	194.65	0.5	-3.7	12.0	±1.1	8.7	0.709205	±8
KY 64	198.20	-0.9						

Table 5: *List of samples and their corresponding $\delta^{11}B$ [‰], $\delta^{13}C_{carb}$ [‰], $\delta^{18}O$ [‰] isotopic compositions and $^{87}Sr/^{86}Sr$ ratios.*

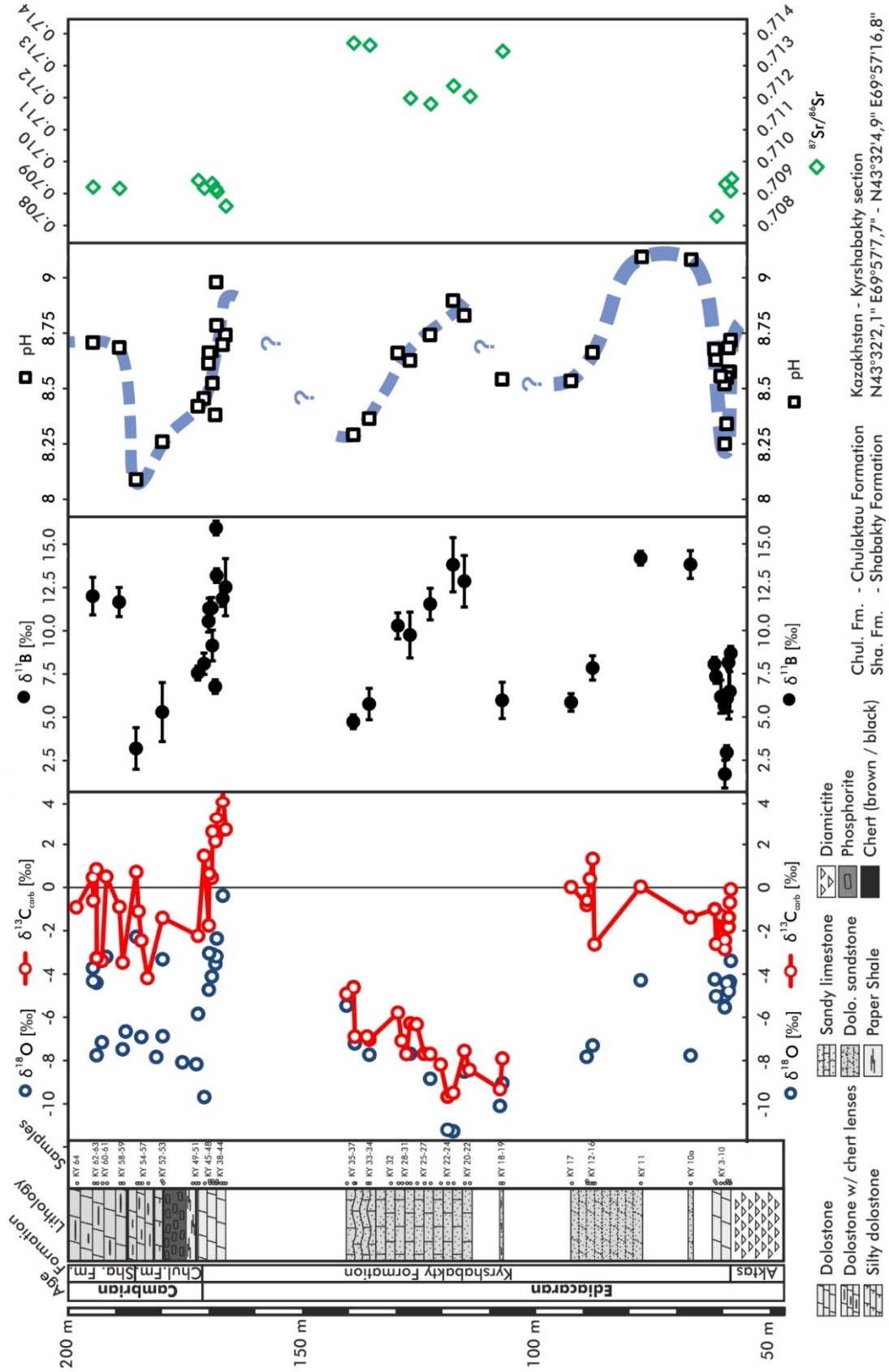

Figure 19: *Stratigraphic column of the investigated Kyrshabakty Section with corresponding isotope data of $\delta^{11}B$ [‰] in black circles, $\delta^{13}C_{carb}$ [‰] in red circles, $\delta^{18}O_{carb}$ [‰] in blue circles and $^{87}Sr/^{86}Sr$ in green diamonds. Ocean pH estimates (black squares, dotted blue line) are based on boron isotope data*

4.5.1 Carbon and oxygen isotopes

The Kyrshabakty Section $\delta^{13}C_{carb}$ and $\delta^{18}O$ data include the most important negative anomalies of the Ediacaran to Cambrian. Beginning with the negative excursion recorded within the Marinoan cap dolomites (Halverson et al., 2005) via the tremendous Shuram-Wonoka negative $\delta^{13}C$ excursion to the global PCC Boundary Peak (BACE, e.g. Shields-Zhou and Zhu, 2013).

In detail, the cap dolomites and directly overlying sandy dolostones display $\delta^{18}O$ values scattering within a range from -3.4 to -7.8‰ (avg.: -5.3‰). Corresponding $\delta^{13}C_{carb}$ data show a negative anomaly down to -2.8‰ (KY 7b) and no significant correlation with oxygen isotopes in this part of the section ($R^2=0.01$). The middle section part records the Shuram-Wonoka anomaly with $\delta^{13}C_{carb}$ values down to -9.7‰ (KY 23) at its base and -4.6‰ (KY 36) at the top. $\delta^{18}O$ values range from -11.3 to -5.8‰, likewise with a continuous increase throughout the excursion. The section top records the worldwide appearing $\delta^{13}C_{carb}$ negative excursion. $\delta^{13}C$ values decrease from 4.3 to -2.2‰ within the Berkuty Dolomite and scatter around -1‰ during the Early Cambrian. Oxygen isotopes range from -0.4 to -7.8‰ (avg.: -4.2‰).

4.5.2 Boron isotopes

$\delta^{11}B$ data display a sinusoidal profile for the lower part of the section. First a negative shift of >7‰ down to 1.7‰ and afterwards a return to values as high as 14‰ is recorded within and slightly above the cap dolomites. Subsequently, $\delta^{11}B$ values stay stable and range from 5.8 to 7.8‰ (KY 13 to KY 19) for the next 20 m. A steady decrease by >9‰ from 14.3 to 4.7‰ is obvious for the middle part hosting the Shuram-Wonoka excursion. Following a major hiatus, boron isotopes constantly drop from ~13.5 to 7.5‰ at the Precambrian-Cambrian transition recorded within the Berkuty Dolomite, and even to 3.2‰ (KY 57) during the Early Cambrian. The uppermost samples (KY 59 to KY 63c) corresponding to Cambrian Stage 3 show a heavier boron isotopic composition of ~11.6-12.0‰.

4.5.3 Strontium isotopes

$^{87}Sr/^{86}Sr$ ratios recorded within the cap dolomites range from 0.7083 (close to the expected earliest Ediacaran Sr seawater curve, Narbonne et al., 2012 and references therein) to more radiogenic ratios of 0.7094. Up section highly radiogenic $^{87}Sr/^{86}Sr$ ratios scattering from 0.7118 to 0.7137 are recorded during the entire Shuram-Wonoka

time. The Berkuty Dolomite displays constantly increasing strontium ratios from 0.7086 to a peak of 0.7094 at the Precambrian Cambrian boundary and a slightly decrease to 0.7092 at the uppermost Cambrian Stage 3. In comparison to the global open ocean $^{87}Sr/^{86}Sr$ seawater curve the values at the PCC boundary are equally to the lower section part slightly enhanced.

4.6 Discussion

4.6.1 Ocean pH evolution

Ocean pH reconstructions rely on the pH-dependent abundance, the isotope exchange and the isotopic composition of the two dominant boron species in seawater: boric acid ($B(OH)_3$) and borate in solution ($B(OH)_4^-$), of which the latter is preferentially incorporated into marine carbonates (Hemming and Hanson, 1992; Kakihana et al., 1977; Spivack, 1986). The unknown boron isotopic composition of ancient seawater ($\delta^{11}B_{sw}$), the boron fractionation factor (α_{B3-B4}) between boron in solution and the precipitated carbonates and the dissociation constant of boric acid (pK_B) must be determined as precisely as possible to make accurate pH calculations. We used a fractionation factor α_{B3-B4} of 1.0272 (Klochko et al., 2006) and a dissociation constant pK_B of 8.579 (Dickson, 1990) both valid for a seawater temperature of 25°C and a salinity S of 35 ppt (uncertainties related to variations in e.g. ocean temperature and salinity can be found in the supplement, chapter 4.10).

For the Early Ediacaran Kasemann et al. (2010) and Ohnemueller et al. (in review) suggested $\delta^{11}B_{sw}$ values between 20 and 23‰ or 20.5‰, respectively. These estimates are far lower than the modern ocean boron isotopic composition of ~39.61‰ (Foster et al., 2010). A significant ^{11}B depletion for Phanerozoic seawater attributed to changes in the global boron budget is also modelled by Joachimski et al. (2005). Additionally, Paris et al. (2010b) reported halite values of ~25‰ for the Devonian (380 Ma) which they suggest to be roughly equal to the B composition of seawater. Based on these information we postulate an increase in $\delta^{11}B_{SW}$ through the investigated ~120 Ma by 3.5‰. Consequently, our pH reconstructions were done with different $\delta^{11}B_{sw}$ assumptions. We used 20.5‰ for the direct aftermath of the late Cryogenian Marinoan glaciation (sample KY 3 to KY 17), 23‰ for the Shuram-Wonoka interval (KY 18 to KY36) and finally 24‰ for the Precambrian-Cambrian transition and the Early

Cambrian (KY 37 to KY 63c). If we take these prerequisites, the onset of cap dolomite deposition implies an ocean pH of ~8.7. Afterwards, most probably enhanced atmospheric pCO_2 led to an ocean acidification event that is globally recognizable (Kasemann et al., 2010; Ohnemueller et al., in review). Due to the re-enabled atmosphere-ocean interaction beginning with the deglacial and the oceanic uptake of CO_2, an ocean acidification event occurs and the seawater pH sinks to 8.2. Subsequently, the ocean pH recovers to more alkaline conditions at the end and shortly after cap dolomite deposition. This recovery phase is characterized by a period of ultra-greenhouse conditions, including high weathering intensities, temperatures and CO_2 drawdown. Enhanced weathering delivers alkalinity to the ocean resulting in an ocean pH overshoot up to 9.1 for a short period of time. Kasemann et al. (2014) and Ohnemueller et al. (in review) further stated that the seawater pH is also strongly dependent on the environmental setting. The Kyrshabakty Section is thought to represent a very proximal, shallow marine environment that generally appears to be affected by continuous high weathering and alkalinity influx, driving the "normal" seawater pH to more alkaline conditions.

This earliest Ediacaran ocean acidification is followed by a phase of most likely stable climatic conditions with an associated stable ocean pH of ~8.5. Unfortunately, no age constraints are present for this part of the succession and it is challenging to provide precise ages prior to the middle part of the Kyrshabakty Section hosting the Shuram-Wonoka anomaly. If this middle section part is of primary origin, first a shift to more alkaline ocean pH conditions of 8.8-8.9 and subsequently a steady decrease and thus acidification event down to an ocean pH of 8.3 is indicated. The origin of the Shuram-Wonoka neg. $\delta^{13}C$ anomaly is still under debate but frequently proposed models involve a continuous or spontaneous release of methane. Our data support this idea, since a release of methane to the ocean and its further oxidation to CO_2 within the water column induces a constant decrease in seawater pH. Biastoch et al. (2011) postulate that continuous destabilization of methane hydrates due to global warming is leading to deeper water column acidification in modern times. This phenomenon appears be an important factor and its contribution to general ocean acidification should not to be underestimated. Similar models also exist for the Palaeocene-Eocene Thermal Maximum (PETM, ~55.8 Ma ago) and seep-related water-column methane oxidation resulting in ocean acidification is assumed e.g. by Pohlman et al. (2011). For

the Neoproterozoic era, Bjerrum and Canfield (2011) use the hypothesis of a slow release of clathrate hydrates during the Shuram-Wonoka interval to explain the tremendous negative $\delta^{13}C$ anomaly. Cui et al. (2013) even suggest the presence of the first cold seeps during that time. Although an explanation involving methane release seems feasible, the isotopic pattern of the Shuram-Wonoka interval remains obscure. Recently, Wang et al. (2014) postulated the existence of a local-scale glaciation at the southern Chinese Yangtze Platform being responsible for the characteristic $\delta^{13}C$ and $\delta^{18}O$ excursions recognizable during the Shuram-Wonoka interval. A glacial event could be the cause of the observed ocean acidification. Nevertheless, no glacial deposits are present at the corresponding part of the Kyrshabakty Section and a severe Snowball-like glaciation, similar to the post-Marinoan ice age, would be necessary to produce an ocean acidification of the recognized extend.

Within the Berkuty Dolomite the Precambrian-Cambrian transition is directly exposed at the Kyrshabakty Section. Proof is given by the globally occurring $\delta^{13}C$ negative anomaly that is visible by a relative 6.5‰ shift from 4.3 to -2.2‰ and the first appearance of the Cambrian small shelly index fossil *Protohertzina anabarica* (Missarzhevsky and Mambetov, 1981), ~70 cm below the top of the Berkuty Dolomite (Seidig, personal communication). Corresponding boron isotopes show a decrease from pH 8.8 to 8.3, similar to a PCC boundary $\delta^{11}B$ record from the southern Chinese Yangtze Platform (see chapter 3, Ohnemueller et al., in prep.). Hence, even a global ocean acidification event appears to exist at the PCC boundary, however, likewise to the ocean acidification in the aftermath of the Marinoan glaciation its magnitude and primarily its duration seem to vary between different palaeo continents. Due to the condensed Cambrian strata the resolution of the uppermost part of the Kyrshabakty Section decreases. Still an ongoing acidification down to pH ~8.1 until the transition from Cambrian Stage 2 to Stage 3 (~520 Ma) is obvious and comparable to the ocean acidification event of the Gaojiashan Section at the Yangtze Platform (Ohnemueller et al., in prep.). It is striking that even photic zone anoxic conditions were prevailing for both palaeo continents, as indicated by $\delta^{13}C$ and $\delta^{15}N$ data (Gamper et al., in prep.). This combination of acidic and anoxic conditions could have led to a poisoning of the Ediacaran biota and possibly enabled the evolvement of metazoa.

The uppermost part of the section (middle Cambrian Stage 3, ~515 Ma and younger) reveals stable, slightly alkaline, ocean pH-states (~8.6-8.7) indicating a time of climate normalcy.

4.6.2 Continental weathering and seawater $^{87}Sr/^{86}Sr$ evolution

A continuous rise in seawater $^{87}Sr/^{86}Sr$ from ~0.7071 to ~0.7087 with only minor perturbations is recorded during the Ediacaran period (Halverson et al., 2007; Kennedy et al., 2006; Narbonne et al., 2012). Main drivers for this trend are amongst others increasing weathering rates resulting from the Pan-African orogeny (Jacobsen and Kaufman, 1999; Kaufman et al., 1993; Shields, 2007). Overall, seawater $^{87}Sr/^{86}Sr$ ratios of Kyrshabakty Section carbonates are slightly enhanced in comparison to the global seawater strontium curve for the Early Ediacaran and the Precambrian-Cambrian transition and show strongly radiogenic $^{87}Sr/^{86}Sr$ values for the Shuram-Wonoka period. These minor to major discrepancies could be attributed to the palaeo environmental setting of the section that seems to be noticeably influenced by weathering and alkalinity influx to the ocean.

Although cap carbonates often display radiogenic strontium isotope compositions (Yoshioka et al., 2003) and do not seem suitable for strontium analyses, primary seawater values (~0.7070-0.7075) are for example known from Namibia (Halverson et al., 2007) and Brazil (Sandoval Romero et al., 2013). Our cap dolomite dataset shows $^{87}Sr/^{86}Sr$ values as low as 0.7083. In combination with the boron data indicating high alkalinity supply and high buffer capacities we interpret these values as a pristine seawater signal.

Limestones of the middle section part, recording the negative $\delta^{13}C$ Shuram-Wonoka anomaly, are highly radiogenic and scatter around ~0.7127. This could be a result of diagenesis tending to increase carbonate $^{87}Sr/^{86}Sr$ values by the release of radiogenic ^{87}Sr from silicate minerals (Li et al., 2013a) or a secondary overprint by a radiogenic fluid. Derry (2010) tried to estimate the influence of radiogenic Sr bearing fluids to the host rock isotopic composition and came up with a burial diagenesis origin for the Shuram-Wonoka anomaly. Yet, especially our boron data speak against a diagenetic origin. Thus a primary seawater signal shifted to higher $^{87}Sr/^{86}Sr$ values by a strong continental weathering pulse must also be taken into account. The highly alkaline seawater at the Shuram-Wonoka onset supports this idea, however, there is a huge

difference from globally reported open ocean $^{87}Sr/^{86}Sr$ ratios of ~0.7080 to 0.7085 (Melezhik et al., 2009) to our highly radiogenic values of up to 0.7137. If the carbonate precipitation rate was high enough to record a local Sr signal influenced by weathering influx before it was in perfect equilibrium with the open ocean $^{87}Sr/^{86}Sr$ composition the observed shift to more radiogenic values must be expected. Similar seawater $^{87}Sr/^{86}Sr$ values for the Shuram-Wonoka interval are known from South China (0.7147, Wang et al., 2014) and interpreted as result of enhanced radiogenic runoff after a local glaciation. For several reasons (see chapter 4.6.1) we do not agree with this scenario, yet we cannot certainly preclude it.

At the Precambrian-Cambrian boundary (Berkuty Dolomite) the $^{87}Sr/^{86}Sr$ ratios are again close to literature data. In particular the basal Berkuty Dolomite records an $^{87}Sr/^{86}Sr$ seawater composition of 0.7086, which is in perfect agreement with terminal Ediacaran data from Mongolia, Namibia, South China and Siberia (Brasier et al., 1996; Halverson et al., 2007; Kaufman et al., 1996; Li et al., 2013a). The lower Cambrian Stage 3 (~515 Ma) seawater $^{87}Sr/^{86}Sr$ values are ~0.7090 and also close to published data (Shields-Zhou and Zhu, 2013).

4.7 Conclusion

(1) An ocean acidification event in the direct aftermath of the late Cryogenian (Marinoan) glaciation recorded within the cap dolomites is indicated by a negative excursion in $\delta^{11}B$. The duration and magnitude are similar to the ocean acidification events observed in Namibia and South China and therefore the acidification event is thought to be of global extend.

(2) Assuming a primary isotope signal, boron isotopes suggest a continuous decrease in ocean pH by >0.6 for the time span of the Shuram-Wonoka anomaly, starting at very alkaline pH conditions. This trend could probably be associated with methane release to the ocean.

(3) An ongoing acidification from pH 8.8 to pH 8.1 is recorded for the Precambrian-Cambrian transition, with a return to more alkaline seawater conditions at ~520 Ma. This acidification event combined with photic zone anoxia is similar to the observations from South China although the acidification duration is far longer in Kazakhstan.

(4) In-between major ocean pH perturbations, the Ediacaran and Early Cambrian ocean pH stays steadily at ~8.5-8.6 for the onset and termination of cap dolomite deposition, the time pre- and post-dating the Shuram-Wonoka anomaly and the Early Cambrian.

(5) $^{87}Sr/^{86}Sr$ ratios are close to the expected seawater curve. An overall increasing trend during the Ediacaran is obvious by a rise from ~0.7083 recorded within the cap dolomites to 0.7094 at the PCC boundary. Subsequently, the values decrease to ~0.709 during the Early Cambrian at ~520 Ma. More radiogenic $^{87}Sr/^{86}Sr$ ratios, scattering around 0.713, are recorded for the Shuram-Wonoka anomaly. These seem to result from high continental runoff possibly related to a local glaciation or alternatively from a secondary overprint.

(6) Minor elevations of the $^{87}Sr/^{86}Sr$ signal in comparison to the global seawater curve of the Ediacaran to Cambrian could be a result of the very proximal section environment. High local weathering flux to the ocean is also implied by $\delta^{11}B$ data showing generally slightly alkaline pH-states in times of climate normalcy at the Kyrshabakty Section.

4.8 Acknowledgements

The project is part of the DFG FOR 736 „The Precambrian-Cambrian Ecosphere (R)evolution: Insights from Chinese microcontinents“. We thank Antonia Gamper and Ulrich Struck (Museum fuer Naturkunde Berlin) for providing $\delta^{13}C$ and $\delta^{18}O$ data as well as Caroline Seidig and Michael Steiner (Freie Universitaet Berlin) for providing fossil data of the Berkuty Dolomite. The authors are grateful to Silvana Pape (University of Bremen) for ICP-OES trace element measurements, to Ralf Oeser and Dorothee Hippler (Technische Universitaet Berlin) for XRD analyses, and to Friedrich Lucassen and Anette Meixner (University of Bremen) for useful remarks and discussions. Fieldwork was guided S. Zhemzhushnikov (Kazakh Academy of Sciences, Almaty).

4.9 References

Alexeiev, D. V., Cook, H. E., Buvtyshkin, V. M., and Golub, L. Y., 2009, Structural evolution of the Ural-Tian Shan junction: A view from Karatau ridge, South Kazakhstan: Comptes Rendus Geosciences, v. 341, no. 2-3, p. 287-297.

Allen, M. B., Alsop, G. I., and Zhemchuzhnikov, V. G., 2001, Dome and basin refolding and transpressive inversion along the Karatau Fault System, southern Kazakstan: Journal of the Geological Society, v. 158, no. 1, p. 83-95.

Bartley, J. K., Pope, M., Knoll, A. H., Semikhatov, M. A., and Petrov, P. Y., 1998, A Vendian–Cambrian boundary succession from the northwestern margin of the Siberian Platform: stratigraphy, palaeontology, chemostratigraphy and correlation: Geological Magazine, v. 135, no. 04, p. 473-494.

Biastoch, A., Treude, T., Rüpke, L. H., Riebesell, U., Roth, C., Burwicz, E. B., Park, W., Latif, M., Böning, C. W., Madec, G., and Wallmann, K., 2011, Rising Arctic Ocean temperatures cause gas hydrate destabilization and ocean acidification: Geophysical Research Letters, v. 38, no. 8, p. L08602.

Birck, J. L., 1986, Precision K-Rb-Sr isotopic analysis: Application to Rb-Sr chronology: Chemical Geology, v. 56, no. 1–2, p. 73-83.

Bjerrum, C. J., and Canfield, D. E., 2011, Towards a quantitative understanding of the late Neoproterozoic carbon cycle: Proceedings of the National Academy of Sciences of the United States of America, v. 108, no. 14, p. 5542-5547.

Brasier, M. D., Shields, G., Kuleshov, V. N., and Zhegallo, E. A., 1996, Integrated chemo- and biostratigraphic calibration of early animal evolution: Neoproterozoic–early Cambrian of southwest Mongolia: Geological Magazine, v. 133, no. 04, p. 445-485.

Canfield, D. E., Poulton, S. W., and Narbonne, G. M., 2007, Late-Neoproterozoic Deep-Ocean Oxygenation and the Rise of Animal Life: Science, v. 315, no. 5808, p. 92-95.

Chakabaev, S. E., 1979, Geological Map of Kazakh SSR, Scale 1:500,000, South Kazakhstan series: Aerogeologiya Map Enterprise, Leningrad, USSR.

Cook, H. E., Johnson, P. D., Matti, J. C., and Zemmels, I., 1975, Methods of sample preparation and X-ray diffraction data analysis, X-ray Mineralogy Laboratory, Deep Sea Drilling Project, University of California, Riverside: In: Hayes, D.E., Frakes, L.A., et al., Init. Repts.

Cui, H., Kaufman, A. J., Xiao, S., Zhou, C., and Zhu, M., 2013, Was The Shuram Carbon isotope anomaly driven by an oxidative pulse of alkalinity and sulfate to the Ediacaran ocean?: Geological Society of America Abstracts with Programs; Paper No. 303-1, v. 45, no. 7, p. 700.

Deniel, C., and Pin, C., 2001, Single-stage method for the simultaneous isolation of lead and strontium from silicate samples for isotopic measurements: Analytica Chimica Acta, v. 426, no. 1, p. 95-103.

Derry, L. A., 2010, A burial diagenesis origin for the Ediacaran Shuram–Wonoka carbon isotope anomaly: Earth and Planetary Science Letters, v. 294, no. 1-2, p. 152-162.

Dickson, A. G., 1990, Thermodynamics of the dissociation of boric acid in synthetic seawater from 273.15 to 318.15 K: Deep Sea Research Part A. Oceanographic Research Papers, v. 37, no. 5, p. 755-766.

Eganov, E. A., Ergaliev, G. K., Ilyin, A. V., and Krasnov, A. A., 1984, Guidebook / International Geological Congress, XXVII Session Kazakhstan: Karatau Phosphorite Basin, Moskau, Nauka.

Eganov, E. A., Sovetov, Y. K., and Yanshin, A. L., 1986, Proterozoic and Cambrian phosphorite deposits: Karatau, southern Kazakhstan, USSR: In: Cook, P.J., Shergold, J.H. (Eds.), Phosphate Deposits of the World: Volume 1 Proterozoic and Cambrian Phosphorites. Cambridge University Press, Cambridge, UK, p. 175-189.

Foster, G. L., Pogge von Strandmann, P. A. E., and Rae, J. W. B., 2010, Boron and magnesium isotopic composition of seawater: Geochemistry, Geophysics, Geosystems, v. 11.

Gamper, A., Struck, U., and Ergaliev, G., in prep., Carbon and nitrogen isotopes of the sedimentary Ediacaran to Cambrian Kyrshabakty section of Malyi Karatau area and its implications for biogeochemical cycling on the Kazakh microcontinent.

Halverson, G. P., Dudas, F. O., Maloof, A. C., and Bowring, S. A., 2007, Evolution of the Sr-87/Sr-86 composition of Neoproterozoic seawater: Palaeogeography Palaeoclimatology Palaeoecology, v. 256, no. 3-4, p. 103-129.

Halverson, G. P., Hoffman, P. F., Schrag, D. P., Maloof, A. C., and Rice, A. H. N., 2005, Toward a Neoproterozoic composite carbon-isotope record: Geological Society of America Bulletin, v. 117, no. 9-10, p. 1181-1207.

Halverson, G. P., Wade, B. P., Hurtgen, M. T., and Barovich, K. M., 2010, Neoproterozoic chemostratigraphy: Precambrian Research, v. 182, no. 4, p. 337-350.
Hemming, N. G., and Hanson, G. N., 1992, Boron isotopic composition and concentration in modern marine carbonates: Geochimica et Cosmochimica Acta, v. 56, no. 1, p. 537-543.
Heubeck, C., Ergaliev, G., and Evseev, S., 2013, Large-Scale Seismogenic Deformation of A Carbonate Platform Straddling the Precambrian–Cambrian Boundary, Karatau Range, Kazakhstan: Journal of Sedimentary Research, v. 83, no. 11, p. 1004-1024.
Hoffman, P. F., Kaufman, A. J., Halverson, G. P., and Schrag, D. P., 1998, A Neoproterozoic Snowball Earth: Science, v. 281, no. 5381, p. 1342-1346.
Hoffmann, K.-H., Condon, D. J., Bowring, S. A., and Crowley, J. L., 2004, U-Pb zircon date from the Neoproterozoic Ghaub Formation, Namibia: Constraints on Marinoan glaciation: Geology, v. 32, no. 9, p. 817-820.
Jacobsen, S. B., and Kaufman, A. J., 1999, The Sr, C and O isotopic evolution of Neoproterozoic seawater: Chemical Geology, v. 161, no. 1–3, p. 37-57.
Joachimski, M. M., Simon, L., van Geldern, R., and Lécuyer, C., 2005, Boron isotope geochemistry of Paleozoic brachiopod calcite: Implications for a secular change in the boron isotope geochemistry of seawater over the Phanerozoic: Geochimica et Cosmochimica Acta, v. 69, no. 16, p. 4035-4044.
Johnston, D. T., Macdonald, F. A., Gill, B. C., Hoffman, P. F., and Schrag, D. P., 2012, Uncovering the Neoproterozoic carbon cycle: Nature, v. 483, no. 7389, p. 320-323.
Kakihana, H., Kotaka, M., Satoh, S., Nomura, M., and Okamoto, M., 1977, Fundamental Studies on the Ion-Exchange Separation of Boron Isotopes: Bulletin of the Chemical Society of Japan, v. 50, no. 1, p. pp.158-163.
Kasemann, S. A., Meixner, A., Rocholl, A., Vennemann, T., Rosner, M., Schmitt, A. K., and Wiedenbeck, M., 2001, Boron and Oxygen Isotope Composition of Certified Reference Materials NIST SRM 610/612 and Reference Materials JB-2 and JR-2: Geostandards Newsletter, v. 25, no. 2-3, p. 405-416.
Kasemann, S. A., Pogge von Strandmann, P. A. E., Prave, A. R., Fallick, A. E., Elliott, T., and Hoffmann, K.-H., 2014, Continental weathering following a Cryogenian glaciation: Evidence from calcium and magnesium isotopes: Earth and Planetary Science Letters, v. 396, no. 0, p. 66-77.
Kasemann, S. A., Prave, A. R., Fallick, A. E., Hawkesworth, C. J., and Hoffmann, K.-H., 2010, Neoproterozoic ice ages, boron isotopes, and ocean acidification: Implications for a snowball Earth: Geology, v. 38, no. 9, p. 775-778.
Kasemann, S. A., Schmidt, D. N., Bijma, J., and Foster, G. L., 2009, In situ boron isotope analysis in marine carbonates and its application for foraminifera and palaeo-pH: Chemical Geology, v. 260, no. 1-2, p. 138-147.
Kaufman, A. J., Jacobsen, S. B., and Knoll, A. H., 1993, The Vendian record of Sr and C isotopic variations in seawater: Implications for tectonics and paleoclimate: Earth and Planetary Science Letters, v. 120, no. 3–4, p. 409-430.
Kaufman, A. J., Knoll, A. H., Semikhatov, M. A., Grotzinger, J. P., Jacobsen, S. B., and Adams, W., 1996, Integrated chronostratigraphy of Proterozoic-Cambrian boundary beds in the western Anabar region, northern Siberia: Geological Magazine, v. 133, no. 5, p. 509-533.
Kennedy, M., Droser, M., Mayer, L. M., Pevear, D., and Mrofka, D., 2006, Late Precambrian Oxygenation; Inception of the Clay Mineral Factory: Science, v. 311, no. 5766, p. 1446-1449.
Klochko, K., Kaufman, A. J., Yao, W., Byrne, R. H., and Tossell, J. A., 2006, Experimental measurement of boron isotope fractionation in seawater: Earth and Planetary Science Letters, v. 248, no. 1-2, p. 276-285.
Levashova, N. M., Meert, J. G., Gibsher, A. S., Grice, W. C., and Bazhenov, M. L., 2011, The origin of microcontinents in the Central Asian Orogenic Belt: Constraints from paleomagnetism and geochronology: Precambrian Research, v. 185, no. 1-2, p. 37-54.
Li, D., Ling, H.-F., Shields-Zhou, G. A., Chen, X., Cremonese, L., Och, L., Thirlwall, M., and Manning, C. J., 2013a, Carbon and strontium isotope evolution of seawater across the

Ediacaran–Cambrian transition: Evidence from the Xiaotan section, NE Yunnan, South China: Precambrian Research, v. 225, no. 0, p. 128-147.

Li, Z.-X., Evans, D. A. D., and Halverson, G. P., 2013b, Neoproterozoic glaciations in a revised global palaeogeography from the breakup of Rodinia to the assembly of Gondwanaland: Sedimentary Geology, v. 294, no. 0, p. 219-232.

Ling, H.-F., Feng, H.-Z., Pan, J.-Y., Jiang, S.-Y., Chen, Y.-Q., and Chen, X., 2007, Carbon isotope variation through the Neoproterozoic Doushantuo and Dengying Formations, South China: Implications for chemostratigraphy and paleoenvironmental change: Palaeogeography, Palaeoclimatology, Palaeoecology, v. 254, no. 1-2, p. 158-174.

Macdonald, F. A., Schmitz, M. D., Crowley, J. L., Roots, C. F., Jones, D. S., Maloof, A. C., Strauss, J. V., Cohen, P. A., Johnston, D. T., and Schrag, D. P., 2010, Calibrating the Cryogenian: Science, v. 327, no. 5970, p. 1241-1243.

Meert, J. G., Gibsher, A. S., Levashova, N. M., Grice, W. C., Kamenov, G. D., and Ryabinin, A. B., 2011, Glaciation and ~ 770 Ma Ediacara (?) Fossils from the Lesser Karatau Microcontinent, Kazakhstan: Gondwana Research, v. 19, no. 4, p. 867-880.

Melezhik, V. A., Pokrovsky, B. G., Fallick, A. E., Kuznetsov, A. B., and Bujakaite, M. I., 2009, Constraints on Sr-87/Sr-86 of Late Ediacaran seawater: insight from Siberian high-Sr limestones: Journal of the Geological Society, v. 166, p. 183-191.

Missarzhevsky, V. V., and Mambetov, A. M., 1981, Stratigrafiya i fauna pogranichnykh sloyev Kembriya i Dokembriya Malogo Karatau [Stratigraphy and fauna of the Precambrian-Cambrian boundary beds of the Malyy Karatau]: Trudy Ordena Trudovogo Krasnogo Znameni Geologicheskiy Institut Akademiya NAUK SSSR, v. 326, p. 1-90.

Narbonne, G. M., Xiao, S., Shields, G. A., and Gehling, J. G., 2012, Chapter 18 - The Ediacaran Period, *in* Gradstein, F. M., Ogg, J. G., Schmitz, M. D., and Ogg, G. M., eds., The Geologic Time Scale: Boston, Elsevier, p. 413-435.

Ohnemueller, F., Gamper, A., Meixner, A., Jiang, S.-Y., and Kasemann, S. A., in prep., Ocean pH and weathering conditionsduring the upper Ediacaran: Insights from the Chinese Gaojiashan Section.

Ohnemueller, F., Prave, A. R., Fallick, A. E., and Kasemann, S., in review, Ocean acidification in the aftermath of the Marinoan glaciation: Geology, v. G35937.

Paris, G., Bartolini, A., Donnadieu, Y., Beaumont, V., and Gaillardet, J., 2010a, Investigating boron isotopes in a middle Jurassic micritic sequence: Primary vs. diagenetic signal: Chemical Geology, v. 275, no. 3-4, p. 117-126.

Paris, G., Gaillardet, J., and Louvat, P., 2010b, Geological evolution of seawater boron isotopic composition recorded in evaporites: Geology, v. 38, no. 11, p. 1035-1038.

Pin, C., and Bassin, C., 1992, Evaluation of a strontium-specific extraction chromatographic method for isotopic analysis in geological materials: Analytica Chimica Acta, v. 269, no. 2, p. 249-255.

Pohlman, J. W., Bauer, J. E., Waite, W. F., Osburn, C. L., and Chapman, N. R., 2011, Methane hydrate-bearing seeps as a source of aged dissolved organic carbon to the oceans: Nature Geoscience, v. 4, no. 1, p. 37-41.

Sahoo, S. K., Planavsky, N. J., Kendall, B., Wang, X., Shi, X., Scott, C., Anbar, A. D., Lyons, T. W., and Jiang, G., 2012, Ocean oxygenation in the wake of the Marinoan glaciation: Nature, v. 489, no. 7417, p. 546-549.

Sandoval Romero, J. A., Lafon, J. M., Rodrigues Nogueira, A. C., and Soares, J. L., 2013, Sr isotope geochemistry and Pb-Pb geochronology of the Neoproterozoic cap carbonates, Tangara da Serra, Brazil: International Geology Review, v. 55, no. 2, p. 185-203.

Shields-Zhou, G., and Zhu, M., 2013, Biogeochemical changes across the Ediacaran–Cambrian transition in South China: Precambrian Research, v. 225, no. 0, p. 1-6.

Shields, G., 2007, A normalised seawater strontium isotope curve: possible implications for Neoproterozoic-Cambrian weathering rates and the further oxygenation of the Earth: eEarth Discussion, v. 2, p. 35-42.

Spivack, A. J., 1986, Boron isotope geochemistry [Ph.D.: Massachusetts Institute of Technology, 184 p.

Spivack, A. J., and You, C.-F., 1997, Boron isotopic geochemistry of carbonates and pore waters, Ocean Drilling Program Site 851: Earth and Planetary Science Letters, v. 152, no. 1–4, p. 113-122.

Veizer, J., Ala, D., Azmy, K., Bruckschen, P., Buhl, D., Bruhn, F., Carden, G. A. F., Diener, A., Ebneth, S., Godderis, Y., Jasper, T., Korte, C., Pawellek, F., Podlaha, O. G., and Strauss, H., 1999, 87Sr/86Sr, δ13C and δ18O evolution of Phanerozoic seawater: Chemical Geology, v. 161, no. 1–3, p. 59-88.

Wang, W., Zhou, C., Guan, C., Yuan, X., Chen, Z., and Wan, B., 2014, An integrated carbon, oxygen, and strontium isotopic studies of the Lantian Formation in South China with implications for the Shuram anomaly: Chemical Geology, v. 373, no. 0, p. 10-26.

Weber, B., Steiner, M., Evseev, S., and Yergaliev, G., 2013, First report of a Meishucun-type early Cambrian (Stage 2) ichnofauna from the Malyi Karatau area (SE Kazakhstan): Palaeoichnological, palaeoecological and palaeogeographical implications: Palaeogeography, Palaeoclimatology, Palaeoecology, v. 392, no. 0, p. 209-231.

Yoshioka, H., Asahara, Y., Tojo, B., and Kawakami, S.-i., 2003, Systematic variations in C, O, and Sr isotopes and elemental concentrations in Neoproterozoic carbonates in Namibia: implications for a glacial to interglacial transition: Precambrian Research, v. 124, no. 1, p. 69-85.

4.10 Supplemental material

Assumptions and uncertainties on the ocean pH reconstruction

In the modern ocean boron has a long residence time of ~14-20 Ma (Lemarchand et al., 2000; Spivack, 1986) and a similar residence time can be expected during the Precambrian-Cambrian. Owing to the long time period of ~120 Ma that is recorded at the Kyrshabakty Section it must be expected that the seawater boron isotopic composition has increased through time (see chapter 4.6.1). We postulate an increase in $\delta^{11}B_{sw}$ by 3.5‰, from 20.5‰ in times of cap dolomite deposition (~635 Ma) to 24‰ for the Early Cambrian (~520 Ma). Nevertheless, it must be supposed that during crucial time periods like the Marinoan aftermath, the deposition time of the Shuram-Wonoka event and the Precambrian-Cambrian transition ocean pH changes instead of $\delta^{11}B_{sw}$ fluctuations are recorded by the marine carbonates. This is due to the fact that the boron residence time in seawater exceeds the deposition time of the above mentioned individual investigated time slices.

Since the boron fractionation factor $\alpha_{B3\text{-}B4}$, and the dissociation constant pK_B are both temperature dependent (Dickson, 1990; Klochko et al., 2006) an assumption to the unknown seawater temperature of the Precambrian and Cambrian time must be made. We performed our calculations with an assumed seawater temperature of 25°C as an average of modelled Precambrian seawater temperatures by Higgins and Schrag (2003) and Jaffrés et al. (2007). If this precondition is changed by ±10°C the ocean pH calculations are only differing by <0.2 pH. In general, colder temperatures lead to slightly higher pH conditions and vice versa. However, our isotopic trends and interpretations stay valid independent from reasonable changes to the seawater temperature assumptions even if the seawater temperature changed through time as it must be expected.

The dissociation constant (pK_B) is also salinity dependent (Dickson, 1990), for that reason we checked for modifications to the pH pattern, if our salinity estimate of S=35 ppt is changed by ±10 ppt. Only negligible changes to the ocean pH estimate are observed.

References

Dickson, A. G., 1990, Thermodynamics of the dissociation of boric acid in synthetic seawater from 273.15 to 318.15 K: Deep Sea Research Part A. Oceanographic Research Papers, v. 37, no. 5, p. 755-766.

Higgins, J. A., and Schrag, D. P., 2003, Aftermath of a snowball Earth: Geochemistry, Geophysics, Geosystems, v. 4, no. 3, p. 1028.

Jaffrés, J. B. D., Shields, G. A., and Wallmann, K., 2007, The oxygen isotope evolution of seawater: A critical review of a long-standing controversy and an improved geological water cycle model for the past 3.4 billion years: Earth-Science Reviews, v. 83, no. 1–2, p. 83-122.

Klochko, K., Kaufman, A. J., Yao, W., Byrne, R. H., and Tossell, J. A., 2006, Experimental measurement of boron isotope fractionation in seawater: Earth and Planetary Science Letters, v. 248, no. 1-2, p. 276-285.

Lemarchand, D., Gaillardet, J., Lewin, E., and Allegre, C. J., 2000, The influence of rivers on marine boron isotopes and implications for reconstructing past ocean pH: Nature, v. 408, no. 6815, p. 951-954.

Spivack, A. J., 1986, Boron isotope geochemistry [Ph.D.: Massachusetts Institute of Technology], 184 p.

CHAPTER 5:

CONCLUSION

5.1 Conclusion

The detailed study of ocean pH fluctuations and weathering conditions during the Ediacaran and Early Cambrian by boron, strontium and lithium isotope analyses reveals significant changes in ocean geochemistry. In particular, the combination of well-chosen case studies from crucial time intervals like the Early Ediacaran cap dolomite deposition (manuscript 1) or the PCC interval (manuscript 2) with long-term development investigations (manuscript 3) of the late Neoproterozoic and Early Paleozoic expand the knowledge of that period in Earth's history.

In the direct aftermath of the late Cryogenian (Marinoan) glaciation a global ocean acidification event is observed. Boron isotopes from Namibia (Kasemann et al., 2010) together with new isotope data from Kazakhstan and South China (manuscript 1, chapter 2) indicate similar alkaline ocean pH conditions (~8.7) prevailing at the onset of cap dolomite deposition. Subsequently, most probably enhanced atmospheric CO_2 levels and oceanic CO_2 uptake led to a global ocean acidification, down to pH ~7. It appears that local controls influence the general acidification pattern and cause differences in acidification magnitudes and durations. The later turnback to climate normalcy and more alkaline pH-states was enabled by enhanced continental weathering associated by CO_2 drawdown during the ensuing greenhouse period. Generally, more proximal platform environments show a faster return to normal ocean pH conditions than slope settings. Amongst others, the buffer capacity and alkalinity influx seem to be major forces in modifying the ocean pH. The overshoot to pH ~9.1 at the end of cap dolomite deposition, obvious in South China and Kazakhstan, could also be originating from the proposed increased continental weathering accompanied by alkalinity supply to the ocean. Cap dolomite $^{87}Sr/^{86}Sr$ data (0.7083-0.7094) from the Kyrshabakty Section (Karatau microcontinent) are slightly enhanced compared to the assumed global strontium seawater isotopic composition (~0.7075, Halverson et al., 2007) for the earliest Ediacaran. This could likewise be a direct consequence of an enhanced weathering influx owing to a very proximal section environment.

During the middle Ediacaran time (~580-550 Ma) one of the most pronounced negative carbon anomalies, the so-called Shuram-Wonoka anomaly (Le Guerroué et al., 2006), can be found in strata worldwide. The Kazak dataset (manuscript 3, chapter 4) provides information about its geochemical ocean conditions. Highly radiogenic strontium isotope ratios of ~0.713 are recorded in corresponding strata.

These could possibly result from enhanced radiogenic continental run-off after a local glaciation, as recently suggested for South China by Wang et al. (2014). However, such radiogenic $^{87}Sr/^{86}Sr$ ratios are only interpretable as primary seawater signals if a very high carbonate precipitation rate existed that allowed the record of a local signal not in equilibrium with the open ocean. In addition, no glacial deposits are exposed that could prove the theory of a glacial phase. Alternatively, the values could be resulting from burial diagenesis (Derry, 2010) or hydrothermal fluid overprint, which both can also explain the observed $\delta^{13}C$ and $\delta^{18}O$ values down to -9.7‰ and -11.3‰, respectively. If a primary signal is recorded by boron isotopes, it indicates a continuous decrease in ocean pH by >0.6 for the Shuram-Wonoka time interval, starting at very alkaline seawater conditions (pH 8.8). This trend could be resulting from a continuous or sudden methane release, as suggested by e.g. Bjerrum and Canfield (2011) or glacial meltwater influx (Wang et al., 2014).

During the PCC transition boron data of the Gaojiashan and Kyrshabakty Section both hint towards an ocean acidification event accompanied by a temporary photic zone anoxia as indicated by $\delta^{13}C$ and $\delta^{15}N$ data (Gamper et al., 2012 and Gamper, pers. comm.). In comparison to the global Sr seawater curve (~0.7085 Narbonne et al., 2012; Shields-Zhou and Zhu, 2013), associated $^{87}Sr/^{86}Sr$ ratios are slightly enhanced for the Kazak dataset (~0.709) and noticeably higher (0.709 - 0.711) for South China. It appears that a continuous weathering influx serves as nutrient supply, fuels bioproductivity, and in turn leads to trapping of organic matter (produced in the photic zone) within the deeper anoxic zone. This ongoing process shoals the chemocline and would finally result in shallow water anoxic and acidic conditions as we observe them in nitrogen, carbon and boron isotopes. Changes in the ocean circulation patterns, like upwelling, could also facilitate this development. Hence, the continental weathering is suggested as prerequisite and one of the main drivers towards shallow water anoxic conditions prevailing at the PCC boundary. The simultaneously observed ocean acidification is more short-lived in South China than in Kazakhstan, where it appears to continue over several Ma. This could be a result of changing environmental settings, like temporary (partly) restrictions especially for the Chinese section. Besides, strontium and lithium isotopes of the Gaojiashan Section suggest increased continental weathering rates and a high alkalinity influx buffering the seawater pH probably earlier and subsequently driving it back to more alkaline conditions. After the termination of the

PCC boundary ocean acidification event seawater pH stabilizes at ~8.6-8.7 within the Early Cambrian at both palaeo continents.

Consequently, our boron data suggest global ocean acidifications not only at the very Early Ediacaran but also at the Precambrian-Cambrian transition. Both time slices equally reveal local, distinct features that seem to be controlled by environmental factors like different facies, section settings and local weathering regimes and intensities as proven by strontium and lithium isotopes as well as differing buffer capacities of the seawater. These local controls result in varying ocean acidification durations and magnitudes as shown by boron isotopes.

Overall, this study confirms the applicability of boron isotopes for palaeo ocean pH reconstructions of the Ediacaran period, that was previously only proven by Kasemann et al. (2005) and Kasemann et al. (2010). In addition, the combination with strontium isotopes serving as a well-established weathering proxy, appears to be very suitable to improve the understanding of the complex interrelationship of ocean pH, ocean alkalinity and weathering fluxes. Hence, the study of changing ocean geochemistry by using these isotopic systems makes it possible to gain more profound knowledge even for such ancient times.

5.2 Perspectives

The interdisciplinary approach of the DFG FOR 736 to combine various geochemical, paleontological, sedimentological and stratigraphical data helped a lot to obtain detailed insights into environmental and climate change leading to the advent and radiation of metazoa. Although sections from two different continents (South China and Kazakhstan) were processed and compared to a third one (Namibia), it is still demanding to draw globally valid conclusions on ocean pH and weathering changes instead of solely local applicable implications.

During both, the very Early Ediacaran (manuscript 1) and the PCC transition (manuscript 2 and 3) global similarities are obvious, nonetheless, local differences exist and are challenging to interpret. To present more precise ocean pH calculations and weathering intensity estimations further boron and strontium datasets from additional palaeo continents and different facies environments are required and need to be extended by more proxy data, e.g. lithium, calcium or magnesium isotope studies. It could be helpful to verify the proposed changes in ocean geochemistry by different kinds

of static and dynamic models to make more precise statements to e.g. response times or durations of ocean pH variations and weathering intensity fluctuations.

If this can be achieved, there is a very good potential to improve the evaluation of ocean geochemical trigger mechanisms enabling the Precambrian-Cambrian Ecosphere (R)evolution.

5.3 References

Bjerrum, C. J., and Canfield, D. E., 2011, Towards a quantitative understanding of the late Neoproterozoic carbon cycle: Proceedings of the National Academy of Sciences of the United States of America, v. 108, no. 14, p. 5542-5547.

Derry, L. A., 2010, A burial diagenesis origin for the Ediacaran Shuram–Wonoka carbon isotope anomaly: Earth and Planetary Science Letters, v. 294, no. 1-2, p. 152-162.

Gamper, A., Struck, U., Scouflaire, Q., and Weber, B., 2012, Carbon and Nitrogen isotope study of the upper Ediacaran Gaojiashan Member in South China: Insights in causes of the Cambrian Explosion: Terra Nostra, v. Schriften der GeoUnion Alfred-Wegener-Stiftung – 2012/3, Centenary Meeting of the Paläontologische Gesellschaft, p. 61.

Halverson, G. P., Dudas, F. O., Maloof, A. C., and Bowring, S. A., 2007, Evolution of the Sr-87/Sr-86 composition of Neoproterozoic seawater: Palaeogeography Palaeoclimatology Palaeoecology, v. 256, no. 3-4, p. 103-129.

Kasemann, S. A., Hawkesworth, C. J., Prave, A. R., Fallick, A. E., and Pearson, P. N., 2005, Boron and calcium isotope composition in Neoproterozoic carbonate rocks from Namibia: evidence for extreme environmental change: Earth and Planetary Science Letters, v. 231, no. 1-2, p. 73-86.

Kasemann, S. A., Prave, A. R., Fallick, A. E., Hawkesworth, C. J., and Hoffmann, K.-H., 2010, Neoproterozoic ice ages, boron isotopes, and ocean acidification: Implications for a snowball Earth: Geology, v. 38, no. 9, p. 775-778.

Le Guerroué, E., Allen, P. A., and Cozzi, A., 2006, Chemostratigraphic and sedimentological framework of the largest negative carbon isotopic excursion in Earth history: The Neoproterozoic Shuram Formation (Nafun Group, Oman): Precambrian Research, v. 146, no. 1–2, p. 68-92.

Narbonne, G. M., Xiao, S., Shields, G. A., and Gehling, J. G., 2012, Chapter 18 - The Ediacaran Period, *in* Gradstein, F. M., Ogg, J. G., Schmitz, M. D., and Ogg, G. M., eds., The Geologic Time Scale: Boston, Elsevier, p. 413-435.

Shields-Zhou, G., and Zhu, M., 2013, Biogeochemical changes across the Ediacaran–Cambrian transition in South China: Precambrian Research, v. 225, no. 0, p. 1-6.

Wang, W., Zhou, C., Guan, C., Yuan, X., Chen, Z., and Wan, B., 2014, An integrated carbon, oxygen, and strontium isotopic studies of the Lantian Formation in South China with implications for the Shuram anomaly: Chemical Geology, v. 373, no. 0, p. 10-26.

APPENDICES

Appendix I: Measured reference materials and standards

Boron reference and standard materials:

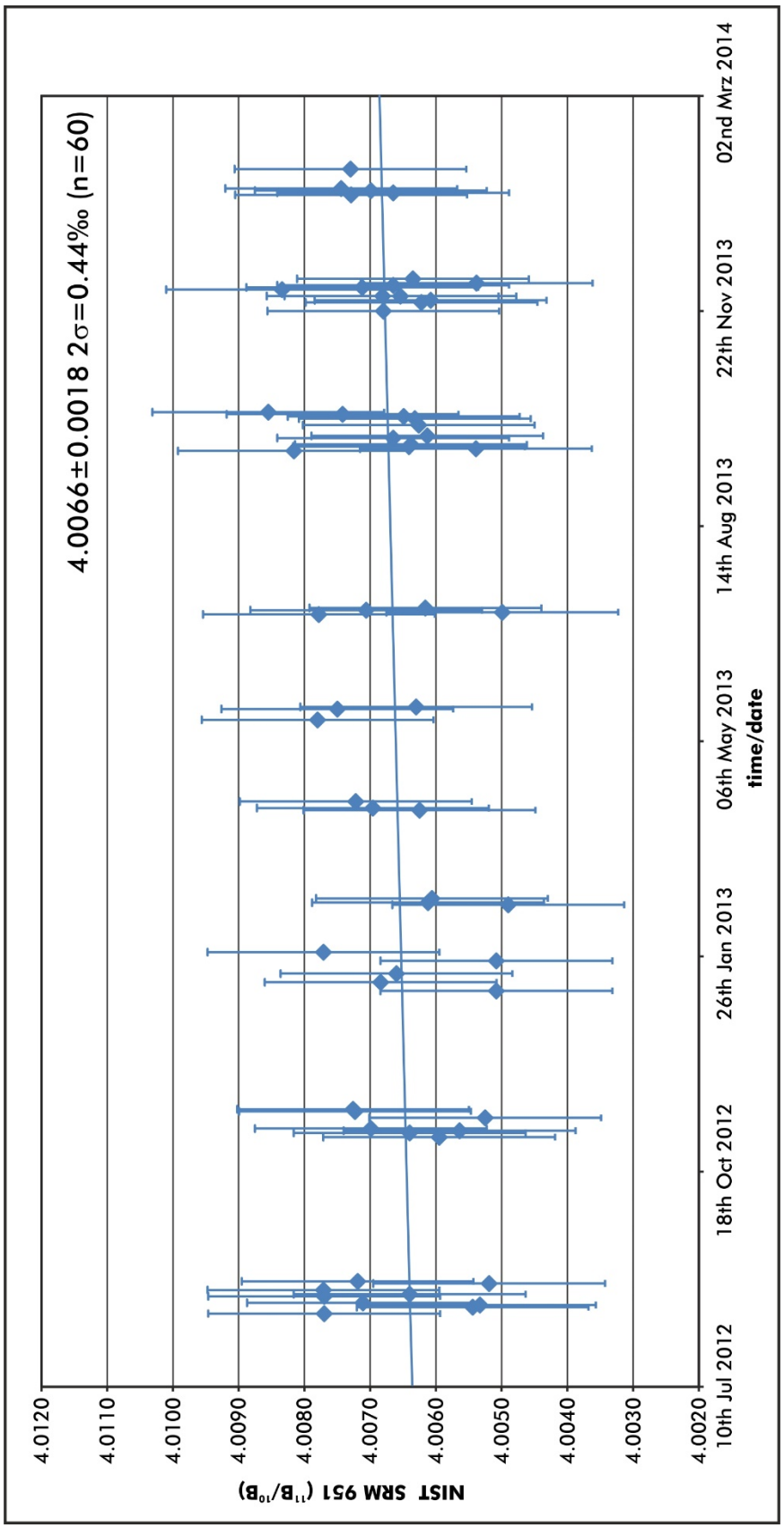

Figure 20: *Plot of all measured NIST SRM 951 reference materials within the last three years. The average $^{11}B/^{10}B$ ratio is: 40066±0.0018, 2σ=0.44‰ (n=60). Over the entire measuring period (~2.5 years) the reproducibility was very good. No seasonal fluctuations and no measurement drift was observed.*

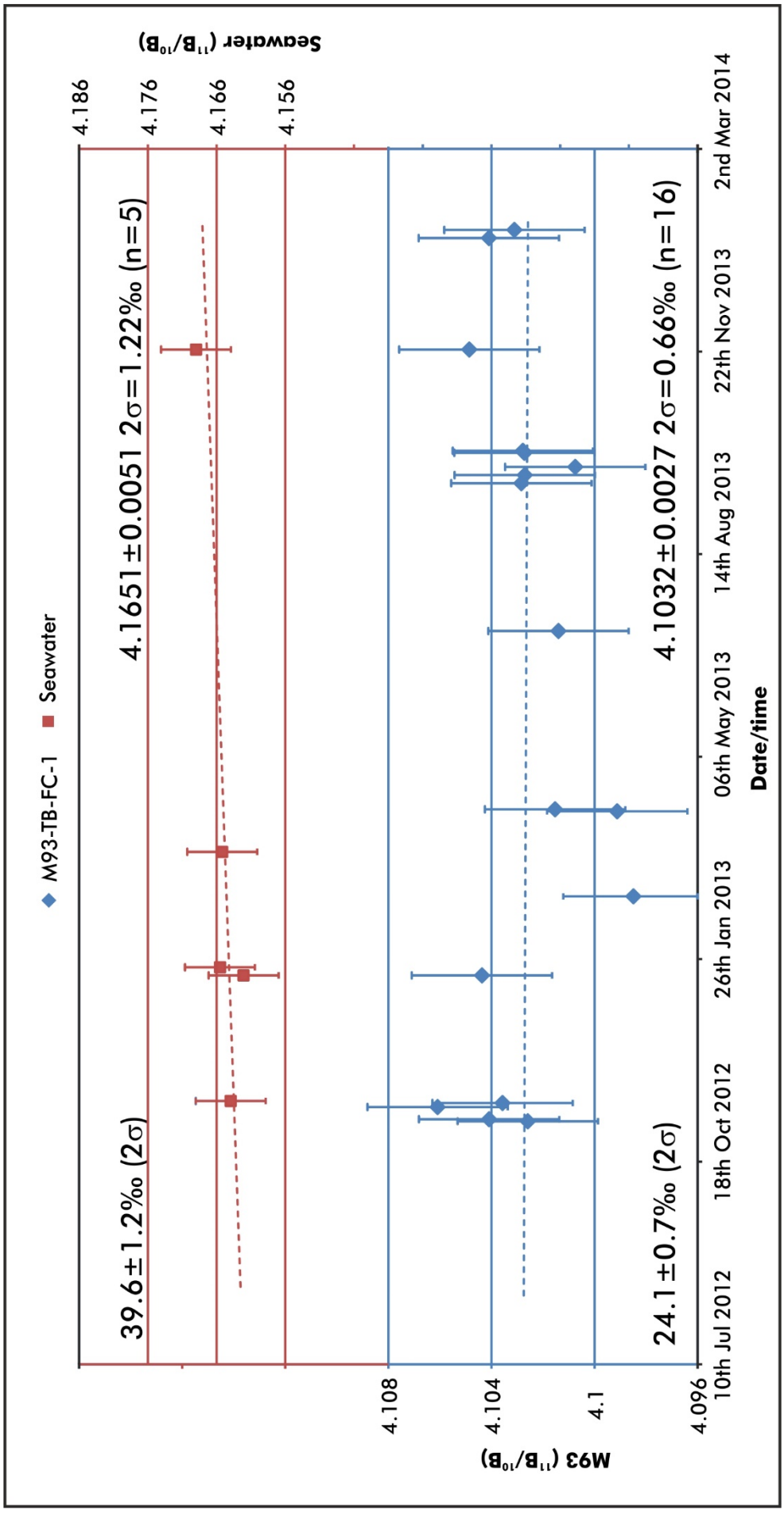

Figure 21: *Plot of measured Porites coral (M93-TB-FC-1, blue) and seawater (red) reference material within the last three years. The average $^{11}B/^{10}B$ ratio of the M93-TB-FC-1 is: 4.1032±0.0027, 2σ=0.66‰ (n=16), 24.1±0.7‰. The average $^{11}B/^{10}B$ ratio of the seawater reference material is: 4.1651±0.0051, 2σ=1.22‰ (n=5), 39.6±1.2‰.*

Date	NIST951	Date	M93	Date	Seawater	Date	CT	Date	CP
13.08.12	4.0077	07.11.12	4.1026	17.11.12	4.1639	03.12.13	4.0698	03.12.13	4.1020
16.08.12	4.0053	08.11.12	4.1041	18.01.13	4.1621	11.12.13	4.0692	11.12.13	4.1026
16.08.12	4.0056	14.11.12	4.1061	22.01.13	4.1655	06.12.13	4.0698	06.12.13	4.1044
17.08.12	4.0053	16.11.12	4.1036	20.03.13	4.1652	20.01.14	4.0682	21.01.14	4.1000
18.08.12	4.0071	18.01.13	4.1044	23.11.13	4.1690	$^{11}B/^{10}B$	**4.0693**	$^{11}B/^{10}B$	**4.1023**
21.08.12	4.0077	23.01.13	4.1038	$^{11}B/^{10}B$	**4.1651**		**±0.0016**		**±0.0036**
22.08.12	4.0064	10.04.13	4.1015		**±0.0051**	**2σ**	**0.39‰**	**2σ**	**0.89‰**
24.08.12	4.0077	07.07.13	4.1014	**2σ**	**1.22‰**				
27.08.12	4.0052	18.09.13	4.1028			**15.63**	**±0.39‰**	**23.87**	**±0.89‰**
28.08.12	4.0072	22.09.13	4.1027	**39.56**	**±1.22‰**				
03.11.12	4.0060	26.09.13	4.1008						
05.11.12	4.0064	03.10.13	4.1027						
06.11.12	4.0056	04.10.13	4.1028						
07.11.12	4.0070	23.11.13	4.1049						
12.11.12	4.0053	17.01.14	4.1041						
15.11.12	4.0072	21.01.14	4.1031						
16.11.12	4.0073	$^{11}B/^{10}B$	**4.1032**						
10.01.13	4.0051		**±0.0027**						
14.01.13	4.0068	**2σ**	**0.66‰**						
18.01.13	4.0066								
24.01.13	4.0055	**24.11**	**±0.66‰**						
28.01.13	4.0077								
19.02.13	4.0049								
20.02.13	4.0061								
22.02.13	4.0061								
04.04.13	4.0063								
05.04.13	4.0070								
08.04.13	4.0072								
16.05.13	4.0078								
21.05.13	4.0075								
22.05.13	4.0063								
04.07.13	4.0078								
05.07.13	4.0050								
06.07.13	4.0071								
07.07.13	4.0062								
18.09.13	4.0082								
19.09.13	4.0054								
20.09.13	4.0064								
21.09.13	4.0064								
24.09.13	4.0067								
25.09.13	4.0061								
30.09.13	4.0063								
03.10.13	4.0063								
04.10.13	4.0065								
05.10.13	4.0074								

Date	NIST951	Date	M93	Date	Seawater	Date	CT	Date	CP
06.10.13	4.0086								
22.11.13	4.0068								
26.11.13	4.0062								
27.11.13	4.0061								
29.11.13	4.0065								
02.12.13	4.0083								
03.12.13	4.0071								
04.12.13	4.0067								
07.12.13	4.0064								
15.01.14	4.0073								
16.01.14	4.0067								
17.01.14	4.0070								
18.01.14	4.0074								
27.01.14	4.0073								
$^{11}B/^{10}B$	**4.0066**								
	±0.0018								
2σ	**0.44 ‰**								

Table 6: *Measured reference and standard materials NIST SRM 951, Porites coral M93-TB-FC-1, seawater, coral reference material CT, coral reference material CP with 2sd uncertainties. $\delta^{11}B$ values of the Porites coral M93-TB-FC-1, seawater, reference material CT and reference material CP are given with 2σ uncertainties vs. the NIST SRM 951 in [‰].*

Strontium reference material NIST SRM 987:

During the period of my PhD Thesis the strontium reference material NIST SRM 987 was regularly analyzed. Strontium isotopic ratios are given in $^{87}Sr/^{86}Sr$ notation and were normalized to $^{86}Sr/^{88}Sr$ of 0.1194. The external reproducibility according to the NIST SRM 987 reference material over the entire period is $^{87}Sr/^{86}Sr$ 0.710250±16 (2sd, n=113; December 2011 to April 2014).

Appendix II: Additional contributions and conference abstracts

Co-author on manuscript by Gamper *et al.* (in preparation):

Chemo- and Biostratigraphy of the Gaojiashan section (northern Yangtze platform, South China): A new Pc-C boundary section

Antonia Gamper [a], Ulrich Struck [a], Frank Ohnemueller [b], Christoph Heubeck [c]

[a] *Museum für Naturkunde Berlin, Invalidenstr. 43, D-10115 Berlin*
[b] *Department of Geosciences, University of Bremen, Leobener Str., D-28359 Bremen*
[c] *Institut für Geowissenschaften, Friedrich-Schiller-Universität Jena, Burgweg 11, D-07749 Jena*

Abstract

The widespread, terminal Ediacaran Dengying Formation (~551 to ~542 Ma) of South China hosts one of the most prominent negative carbonate carbon isotope excursions in Earth's history and thus bears on the correlation of Precambrian-Cambrian boundary events worldwide. The dominantly carbonate strata of the Dengying Formation are largely studied for its unique preservation of its terminal Ediacaran fauna but their geochemical context is poorly known. This study presents the first high-resolution stable isotope record ($\delta^{13}C$, $\delta^{18}O$) of calcareous siliciclastic shallow-water deposits of the Gaojiashan section (Shaanxi Province). The section includes (in ascending order) the Algal Dolomite Member, the Gaojiashan Member and the Beiwan Member of the Dengying Formation. Our data record a major $\delta^{13}C$ (carbonate carbon) negative excursion to -6‰ in the uppermost Gaojiashan Member which is comparable in shape and magnitude to the global Precambrian-Cambrian boundary negative $\delta^{13}C$ excursion. Our dataset is consistent with a "shallow-water anoxia" scenario which is thought to contribute to events at the "Cambrian explosion". The stratigraphic occurrence of Cloudina and the negative $\delta^{13}C$ excursion suggest that the Precambrian-Cambrian boundary near the top of the Gaojiashan Member, and that consequently overlying carbonates and dolomites of the Beiwan Member are of lowermost Cambrian age. Thus the Gaojiashan section may represent a new shallow-water section spanning the Precambrian-Cambrian boundary. Although bio- and chemostratigraphic data support

this novel interpretation we cannot exclude the possibility that the key excursions may represent a local perturbation indicating a restricted-basin environment.

Co-author on manuscript by Clarkson *et al.* (in prep. for resubmission to *Science)*:

Ocean Acidification and the Permo-Triassic Mass Extinction

M.O. Clarkson[1], S.A. Kasemann[2], R. Wood[1], S. Richoz[3] F. Ohnemueller[2], S.W. Poulton[4] and E.T. Tipper[5]

[1] School of Geosciences, University of Edinburgh, West Mains Road, Edinburgh, UK
[2] Department of Geosciences and MARUM-Center for Marine Environmental Sciences, University of Bremen, 28359 Bremen, Germany
[3] Institute of Earth Sciences, University of Graz, Heinrichstraße 26, 8010 Graz, Austria
[4] School of Earth and Environment, University of Leeds, Leeds, LS2 9JT, UK
[5] Dept. of Earth Sciences, University of St Andrews, St Andrews, KY16, UK

Abstract

Ocean acidification has been implicated as a kill mechanism for the greatest mass extinction of the Phanerozoic, the Permo-Triassic event ~252.2 million years ago (Ma). The event occurred as two ecologically selective extinction phases separated by approximately 60 kyrs. Permo-Triassic ocean acidification hypotheses suggest that a massive, and rapid, CO_2 release from Siberian Trap volcanism acidified the ocean and so caused a biocalcification crisis. This CO_2 flux is inferred from the negative carbon isotope excursion recorded at the PTB. The evidence for a coeval ocean acidification event, however, remains debated. Here, we present the first boron isotope ($\delta^{11}B$) record for the Late Permian-Early Triassic in order to reconstruct seawater pH. Contrary to previous hypotheses, ocean pH appears to remain stable across the first phase of the mass extinction and the carbon isotope excursion. An acidification event is, however observed in the earliest Triassic and is coincident with the preferential loss of heavily calcified biota during the second phase of extinction. The decoupling of the acidification event from the carbon isotope record suggests that it was not simply a result of high CO_2 emissions. We hypothesize that the oceans' response to CO_2 emissions during the PTB reflects transitions in the buffering capacity, which were controlled by carbonate alkalinity availability.

Fermor Meeting 2012 (London, Poster):

Ocean-pH evolution during the upper Ediacaran: Insights from boron isotopes at the Gaojiashan section, Shaanxi Province, South China

Frank Ohnemueller [a,], Antonia Gamper [b], Quentin Scouflaire [c], Simone A. Kasemann [a]*

[a] *Department of Geosciences, University of Bremen, Leobener Str., D-28359 Bremen*
[b] *Museum für Naturkunde Berlin, Invalidenstr. 43, D-10115 Berlin*
[c] *Dept. of Geological Sciences, Freie Universität Berlin, D-12249 Berlin*

Abstract

The Ediacaran to Cambrian transition was a crucial time in Earth history. Substantial changes in ocean-atmosphere interactions, climate and biogeochemical processes catalyzed the advent and radiation of metazoa. In this study, we investigate the boron isotope records of the Algal Dolomite, Gaojiashan, and Beiwan Members (all Dengying Formation) at the Gaojiashan section (551-542 Ma) in south-western Shaanxi, South China to get detailed insights into changing ocean conditions and concomitant palaeo pH and atmospheric pCO_2 variations. The Gaojiashan section provides unique access to a widely undisturbed 80 m thick carbonate-siliciclastic succession located at the north-western margin of the Ediacaran Yangtze-platform. Sedimentary data suggest a near shore shallow water setting that is exceptionally well preserved and exclusively present in this part of the platform. Carbonate sedimentation is influenced by continuous detrital input presumably from a pro- and retrograding delta front. Whether the Gaojiashan Member records open ocean conditions or displays a more restricted environment remains unclear.

New $\delta^{13}C$ data unveil a sustained positive excursion (+6‰) followed by a distinct negative $\delta^{13}C$ anomaly with a nadir down to ~ -7‰ in the upper part of the Gaojiashan Member. These changing geochemical ocean conditions can be explained by enhanced nutrient supply from the continent followed by a time of anoxic shallow-water conditions. Owing to the associated variations in ocean alkalinity and ocean-atmosphere CO_2 exchange we also expect changes in ocean-pH documented in the boron isotope pattern preserved in carbonate succession.

Goldschmidt Conference 2013 (Florence, Poster):

Ocean-pH evolution and weathering conditions during the Ediacaran: Insights from B, Sr & Li isotopes at the Gaojiashan Section, South China

Frank Ohnemueller [a,], Anette Meixner [a], Antonia Gamper [b], Simone A. Kasemann [a]*

[a] *Department of Geosciences, University of Bremen, Leobener Str., D-28359 Bremen*
[b] *Museum für Naturkunde Berlin, Invalidenstr. 43, D-10115 Berlin*

Abstract

The Ediacaran to Cambrian transition was a decisive time in Earth history since substantial changes in ocean-atmosphere interactions, climate, tectonics and bio-geochemical processes catalyzed the advent and radiation of metazoa. In this study, we investigate the boron, strontium and lithium isotope records of the Algal Dolomite, Gaojiashan and Beiwan Members at the Gaojiashan section (551-542 Ma) in south-western Shaanxi, South China to gain detailed insights into changing ocean-pH and weathering conditions. The 65 m thick carbonate-siliciclastic Gaojiashan Section is located at the north-western margin of the Ediacaran Yangtze-platform. Sedimentary data suggest a near shore shallow water setting that is exceptionally well preserved and only present in this part of the platform. Carbonate sedimentation is influenced by continuous detrital input presumably from a pro- and retrograding delta front. In the upper part of the Gaojiashan Member, a negative $\delta^{13}C$ and $\delta^{11}B$ anomaly is unveiled with nadirs down to ~ -7‰ for carbonate carbon and -2‰ for boron, respectively. In total, the excursion comprises a shift of -13‰ for $\delta^{13}C$ and -12‰ for $\delta^{11}B$ which equals a decrease of ~ 1.5 pH units. At the same time, Sr isotopes display a positive excursion ($^{87}Sr/^{86}Sr$ 0.7085 to 0.7110) indicating a time of enhanced weathering through relative sea-level fall. To further assess the continental silicate weathering flux, Li isotopes have been analysed. If we accept that those changes in the isotope pattern and ocean geochemistry are of primary origin, it needs to be discussed whether a (temporarily) restricted environment or open-ocean conditions are recorded. In view of the pronounced negative $\delta^{13}C$ anomaly it must also be considered that the Precambrian-Cambrian boundary interval is recorded in the uppermost Gaojiashan Member and the overlying sediments already belong to early Cambrian strata.

GSA Annual Meeting 2013 (Denver, Poster):

Global ocean acidification in the aftermath of the Marinoan glaciation

Frank Ohnemueller [a,], Anthony R. Prave [b], Anthony E. Fallick [c], Simone A. Kasemann [a]*

[a] *Dept. of Geosciences/MARUM, University of Bremen, Leobener Str., D-28359 Bremen*
[b] *Earth Sciences, University of St Andrews, St Andrews KY16 9AL, UK*
[c] *Scottish Universities Environmental Research Centre, East Kilbride G75 OQF, UK*

Abstract

During the Cryogenian-Ediacaran transition the Earth underwent substantial changes in its climatic, tectonic and bio-geochemical cycles. Within the Cryogenian at least two global-scale ice ages led to profound modifications in the interplay between oceans, atmosphere and continents (e.g. Hoffman et al., 1998). In this study, we investigate boron and carbonate carbon isotope patterns recorded in cap dolostones deposited in the direct aftermath of the younger Cryogenian glaciation (~635 Ma) on four different cratons.

Cap dolomites of the Yangtze Platform (South China block), Kazakhstan and Namibia (Kalahari and Congo craton) show similar B isotope and hence similar ocean-pH pattern although the nadir in ocean acidification differs between the investigated cratons/blocks. Of all blocks, the most pronounced negative excursions of -12‰ in $\delta^{11}B$ and down to -6‰ in $\delta^{13}C$, occur in Namibia (Congo Craton, Kasemann et al., 2010) and South China whereas a drop from 8.0 to 1.8‰ in $\delta^{11}B$ and down to -3‰ in $\delta^{13}C$ is visible in Kazakhstan (Malyi Karatau range). Therefore, a transient decrease by >1 pH units down to a minimum ocean-pH of about 7 during deglaciation is indicated.

Our approach of a multi craton correlation provides evidence for a global ocean acidification event, potentially associated with enhanced atmospheric pCO_2 during time of deglaciation.

[1] Hoffman et al. (1998) Science 281, 1342–1346.

[2] Kasemann et al. (2010) Geology 38, 775-778.

GSA Annual Meeting 2014 (Vancouver, Talk, in October 2014):

Ediacaran to Cambrian ocean pH and continental weathering conditions: Implications from Southern Kazakhstan

Frank Ohnemueller [a,], Simone A. Kasemann [a]*

[a] *Department of Geosciences and MARUM - Center for Marine Environmental Sciences, University of Bremen, Leobener Str., D-28359 Bremen*

Abstract

From the aftermath of the late Cryogenian Marinoan glaciation (~635 Ma) to the Early Cambrian the Earth underwent major changes in (bio-)geochemical processes, climate and ocean-atmosphere interactions. This time period was intensely investigated within the last decades, yet the Karatau microcontinent (Kazakhstan, Central Asia) received little attention. The studied Kyrshabakty Section is located at the Malyi Karatau Range and hosts a >500 m succession of volcanics, siliciclastics and predominantly carbonates of Early Cryogenian to Ordovician age.

Here we present the first boron ($\delta^{11}B$) and strontium ($^{87}Sr/^{86}Sr$) isotope dataset for the Karatau microcontinent to elucidate long-term modifications to ocean pH and weathering fluxes from the Ediacaran until the Early Cambrian (Stage 3, ~520 Ma). Within the Marinoan-age cap dolomites an ocean acidification event is indicated by a transient negative $\delta^{11}B$ excursion of 7‰. Corresponding $^{87}Sr/^{86}Sr$ as low as 0.7083 are close to published primary post-glacial seawater values of ~0.707. The middle part of the section records the tremendous negative Shuram-Wonoka carbon anomaly with $\delta^{13}C_{carb}$ values down to -9.7‰ and radiogenic $^{87}Sr/^{86}Sr$ ratios scattering around 0.713. $\delta^{11}B$ data of this time period show a constant decline of ~9‰. Assuming a primary signal, a continuous decrease in ocean pH is indicated. At the Precambrian-Cambrian transition boron isotopes display a steady decrease in ocean pH by >0.7. Coeval strontium ratios show an increasing trend during the latest Ediacaran from 0.7086 to 0.7094 and decrease to 0.7092 within the Cambrian.

Overall, the Kyrshabakty Section provides valuable insights into changing ocean pH and weathering conditions over a time span of ~120 Ma: A general rise of seawater $^{87}Sr/^{86}Sr$ during the Ediacaran and several fluctuations in ocean pH until the Cambrian.

Appendix III: Curriculum vitae

Frank Patrick Ohnemüller

Bilsestr. 8, 28195 Bremen, Germany
(+49) 173 6750757, fohnemueller@marum.de

Personal information

Date of birth: 12.08.1983
Place of birth: Berlin, Germany
Nationality: German

PhD studies

07/2011 – 06/2014	University of Bremen (D) Department of Geosciences and MARUM Isotope Geochemistry Group DFG FOR 736

Education

10/2008 – 12/2010	Certificate: M.Sc. Geosciences Freie Universität Berlin (D) Institute of Geological Sciences
10/2004 – 09/2008	Certificate: B.Sc. Geosciences Freie Universität Berlin (D) Institute of Geological Sciences
09/1996 – 06/2003	Certificate: Abitur (A level) Lilienthal Gymnasium Berlin (D)